CIVIL ENGINEERING STUDIES
STRUCTURAL RESEARCH SERIES NO. 277

AN EXPERIMENTAL STUDY OF LIMIT DESIGN IN REINFORCED CONCRETE FLAT SLABS

By
MANUEL XANTHAKIS
and
M. A. SOZEN

UNIVERSITY OF ILLINOIS
URBANA, ILLINOIS
DECEMBER 1963

AN EXPERIMENTAL STUDY OF LIMIT DESIGN IN REINFORCED CONCRETE FLAT SLABS

by

Manuel Xanthakis

and

M. A. Sozen

University of Illinois
Urbana, Illinois
December 1963

TABLE OF CONTENTS

TABLE OF CONTENTS (Cont'd.)

LIST OF TABLES

LIST OF FIGURES

LIST OF FIGURES (Cont'd.)

LIST OF FIGURES (Cont'd.)

LIST OF FIGURES (Cont'd.)

LIST OF FIGURES (Cont'd.)

1. INTRODUCTION

1.1 Object and Scope

The investigation reported in this paper was undertaken in order to evaluate the effect of two major changes in the design procedure of flat slabs. The two major changes under study were: (a) the use of the full static moment rather than a fraction of it as is done in design according to the ACI Building Code (1)* and (b) distribution of the reinforcement in a manner independent of the elastic moment configuration. Other minor changes were introduced in an effort to investigate the effect of certain simplifications of the geometry of the structure. These changes were studied in an effort toward the simplification of flat slab design and construction.

Prior to the test on the structure reported in this paper, seven floor slabs had been tested at the University of Illinois. All the structures consisted of nine square panels of equal spans arranged three bays to a side. Four of these structures were flat slabs and their characteristics are tabulated below.

Structure No.	Mark	Scale	Reinforcement	Method of Design
2	F2	1/4	Intermediate Grade	ACI 318-56**
5	F3	1/4	Welded Wire Fabric	ACI 318-56
6	F4	1/16	Intermediate Grade	ACI 318-56
7	F5	1/16	Intermediate Grade	Reference 2

Slabs F2 and F3 were used to evaluate the differences in behavior with the change of reinforcement. Slab F4 was used to determine if very small scale

---

* Numbers in parentheses refer to entries in the list of references.

** Reference (1)

reinforced concrete models could be used to predict the behavior of larger size structures. Slab F5 compared the performance of the method proposed by Hatcher (2) with that of the ACI Building Code procedure. All the above mentioned structures have precise similitude of external dimensions.

The characteristics of the test structure described in this report, a flat slab, are:

Structure No.	Mark	Scale	Reinforcement	Method of Design
8	F6	1/16	Intermediate Grade	Limit Design

Sections 2.1, 2.2 and 2.3 present the design procedure for structure F6. Chapter 5 complements the above-mentioned sections. Chapter 6 compares the behavior of structure F6 with that of the other flat slabs. Chapter 7 closes with a summary and conclusions.

1.2 Acknowledgments

This project was conducted in the structural Research Laboratory of the Civil Engineering Department of the University of Illinois and was sponsored by the Department of Civil Engineering.

The report was prepared as a thesis for the degree of Master of Science in Civil Engineering under the direction of Dr. M. A. Sozen, Professor of Civil Engineering.

Acknowledgment is due to Mr. R. E. Shewmaker, former Graduate Student in Civil Engineering, for his aid in the preparation and testing of

the structure and to Mr. R. E. Pinckert, Graduate Student in Civil Engineering, for his help during the construction of the test structure.

2. DESCRIPTION OF THE TEST STRUCTURE

2.1 Geometry

Since four dimensionally similar flat slabs had been tested at the University of Illinois, it was deemed advantageous to try to compare the behavior of the test structure with the behavior of these structures. It was thus decided to keep the proportions of the test structure similar to those of structures F2, F3, F4, and F5. Changes were made where a desirable simplification of the design or construction procedure could be effected. The test would then serve to evaluate the behavior of a structure using a design method which deviates considerably from the traditional methods of design for flat slabs (1).

Figures 2.1 and 2.2 show the layout of the 1/16-scale models (structures F4 and F5). The layout of the 1/4-scale models (structures F2 and F3) is similar, but all the dimensions should be linearly increased by a factor of four. Detailed descriptions of the structures may be obtained from Reference (2) for F2, Reference (3) for F3, and Reference (4) for F4 and F5. The last reference contains a discussion on the use of small scale models to predict the behavior of full-size structures, and a brief discussion is included in Appendix B.

For structure F6, it was decided to eliminate the drop panels in order to simplify the formwork and simultaneously decrease the stiffness of the slab over the columns in an effort not to attract as much bending moment to the column strip.

The spandrel beams in structures F2, F3, F4, and F5 were designed for a load of 600 lb/ft. It has been pointed out in Reference (2), that it is

not correct to consider a beam and the adjoining slab as different elements, since in fact they are monolithic. An examination of the failures in structures F2, F3, and F4 indicated distress in the beam-column connections (due to excessive torsion) which was responsible for the initiation of the failure mechanism. The beams in structure F5 were spirally reinforced in the vicinity of the columns in order to add to the torsional capacity, and in this manner failure was avoided, and the formation of the failure mechanism was not precipitated as in the previous slabs. But whether the beams failed in torsion or not, the negative slab steel perpendicular to the face of the beam in the middle strip did not yield. Figure 2.3 shows the values of the steel stresses of the slab steel perpendicular to the face of the shallow edge beam in structure F2 during the test to failure. The stresses at the face of the deep beam are slightly larger. The same behavior was observed in structure F3. Structures F4 and F5 did not have strain gages at these particular locations, but the absence of cracks in the slab at the interior face of the beams showed that little negative moment restraint was provided by the beams. The reason for this may well be a combination of two factors: (a) the rotational rigidity of the beams is not sufficient to restrain the slab, and (b) the inward rotation of the columns as illustrated in Sketch A, particularly when the cracks are well developed, turns the beam inward.

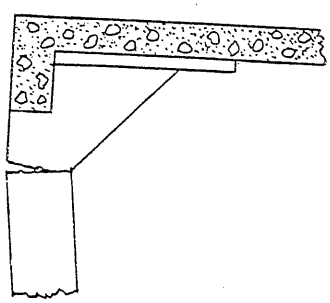

Sketch A

Since the spandrel beams did not enhance to a great extent the negative moment restraint on the slab periphery, and in view of the large number of buildings which do not sustain peripheral wall loads, it was decided to eliminate the edge beams altogether and study the behavior of the exterior slab-column connection.

Thus the geometry of the test structure was simplified in relation to the other slabs tested, in that the drop panels and the spandrel beams were removed. The design load remained the same with the exception that no wall load was assigned to the periphery. Figure 2.4 shows the layout of the test structure and the designation of the panels and columns. It may be noted that there exists symmetry about both diagonals as well as side center lines of the structure. The previous structures had symmetry only about one diagonal since two different spandrel beams were used. Figure 2.5 shows the column-to-slab connections and dimensions. As has been the case in the previous slabs tested, the columns are pinned at their base, and the column proportions are such as to simulate the stiffness of a column continuous from one story below to one story above the slab, which is the first story beneath the roof of the prototype building.

2.2 Basis of Design

The essence of the design of the test structure was the combination of (a) the use of the full static moment with (b) complete reliance on moment redistribution, in order to simplify the design and construction of floor slabs.

The first of the two criteria mentioned above has already been used in the design of structure F5 (4). Essentially it consists of designing for the full static moment, based on Nichols' method (5), instead of reducing

it by 28 percent as the ACI Building Code suggests (1). Reference 6 explains to greater detail the reasons why the full static moment must be used, instead of the reduced static moment, if only flexural resistance is to be provided.

The second criterion has been used extensively in plastic design of steel, and to some extent in reinforced concrete structures. The criterion of moment redistribution is used to a limited extent in every indeterminate structure that has been built, since the supplied moment capacity of every section is never strictly in proportion to the actual elastic moment distribution. In the present structure, it was decided that moment redistribution would be used to the fullest extent in order to simplify the reinforcement layout and design calculations involved in slab construction. It was thus decided to rely on the development of fully plastic hinges, and on the redistribution of moments from negative to positive regions, as well as from regions of high initial moment to adjacent regions of low initial moment. On this basis it was concluded that only two spacings of steel would be sufficient to reinforce most continuous flat slabs of constant bay lengths.

The static moment values for the different panels in the test structure are shown in Fig. 2.6. These values were obtained by assuming no shears and twisting moments acting on the column and panel center lines. The above assumption is not strictly correct in any of the panels, but the values of static moment obtained with this assumption have agreed closely with the measured values in the previous slabs tested. Thus, within the tolerances allowed for design, it is assumed that the values for the static moments are accurate if the position of the column reaction can be ascertained for each panel. This introduces another doubtful parameter, namely the

distribution of shear on the slab at the face of the columns. The values shown in Fig. 2.6 are for two extreme cases of shear distribution: (a) uniformly distributed around the periphery of the column and (b) concentrated at the interior corners of the capitals. The first of these cases gives larger static moments, because the effective span is greater. The correct value lies somewhere between the two extreme cases. For the test structure, the largest value of the static moment for each panel (given by case "a") was conservatively chosen as the design moment.

A quick examination of possible failure mechanisms, according to the yield line theory, (see Chapter 5) points out that the most likely mode of failure involves a structural mechanism (Fig. 5.3). Since each panel can not fail by itself and since there are some uncertainties concerning the accuracy of the third significant figure of the moment values given, it was felt that using the average of the static moment for each of the two sets of spans would greatly simplify the reinforcement layout. The static moments are therefore taken as follows:

SPAN	STATIC MOMENT PER PANEL (M_o)
Interior (continuous at both ends)	0.094 WL
Exterior (discontinuous at one end)	0.097 WL

Where: W = total load on each panel

L = distance between column center lines in the direction of the moment desired.

The design load was chosen as 285 psf. This gives the following design moments for the 1/16-scale-model test structure:

SPAN	STATIC MOMENT PER PANEL (M_o)
Interior	0.626 kip-in.
Exterior	0.650 kip-in.

Since separate mechanisms are possible involving both static moments, averaging these values would decrease the strength of this structure by 1.8 percent. Of course, this is within the uncertainty of the calculations and the average could be used, but if the exterior spans were different from the interior, the error could be large. Therefore the discussion will be continued using different moments for the two spans.

Once the total design moments have been determined, the problem of their distribution arises. As stated at the beginning of this section, the simplification of the construction was one of the goals to be achieved. For this reason, moment redistribution should be used to the fullest extent. The epitome of steel-layout simplification would be to have a constant spacing between bars, while supplying no more steel area than required by an "elastic" moment distribution. The method of proportioning the steel throughout the structure can best be explained through a simple plastic design example.

The elastic moment distribution in a three-span continuous beam is as follows:

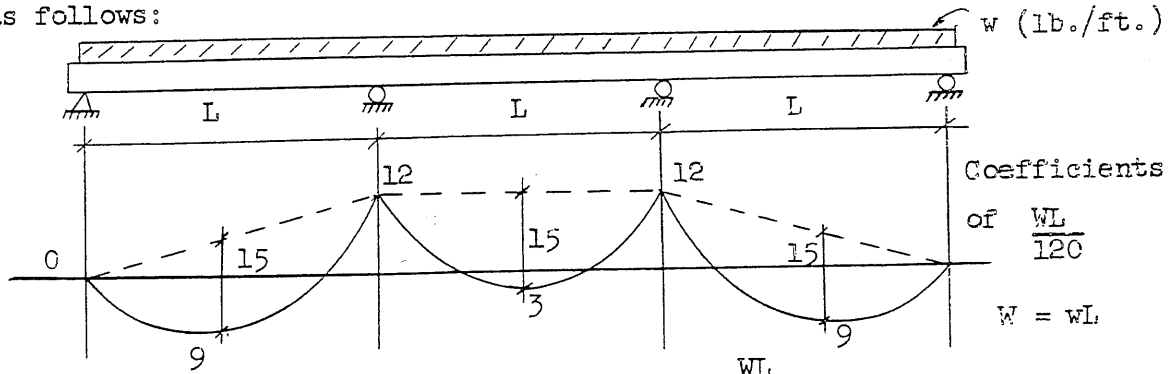

Static moment in all spans = $\frac{WL}{8}$

Design No. 1

But the beam may be designed by considering collapse mechanisms, fully plastic hinges and moment redistribution, with the following result:

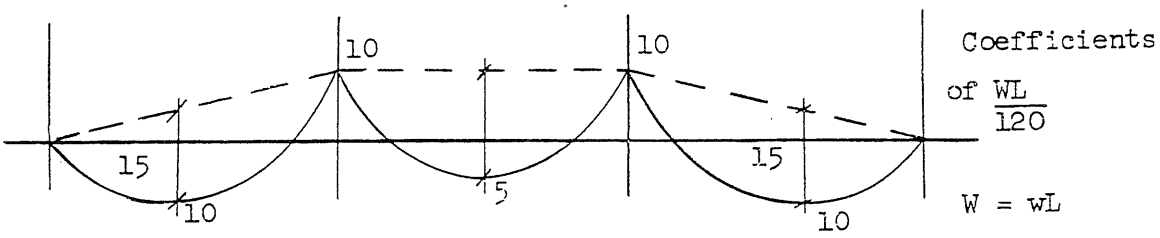

Static moment in all spans = $\frac{WL}{8}$

Design No. 2

It may be seen that in both cases and for all spans, the static moment M_o (or simple beam moment) remains WL/8. Design No. 2 is valid and both beams have the same factor of safety against collapse, as long as there is enough ductility in the plastic hinges that will be formed in Design No. 2. It should be noted that Design No. 1 has three different values of moment, while Design No. 2 has only two different values of moment. The total steel cross sectional area of the critical regions in both cases is the same, if the moment is assumed directly proportional to the steel area.

The same procedure may be followed in assigning moments to design sections of the slab. It is certain that enough ductility exists in a slab since the reinforcement will not exceed 1.5 percent in most cases.

As stated previously, the spandrel beams did not provide enough restraint to develop the yield stress of the negative slab reinforcement framing into them. For the test structure, the spandrel beams have been omitted; therefore it was decided not to assign any design moment to the free edge. Thus, essentially, a pinned, zero-moment end condition was assumed, similar to that of the end of the beam in the sketch above. The

positive moment in the middle of the end span was assigned a value of 2/3 M_o or 0.433 kip-in. In order to satisfy the requirement of full static moment, the negative moment over the support must also be 2/3 M_o , thus giving a total supplied moment of:

$$M = \frac{2}{3} M_o + (\frac{1}{2}) \frac{2}{3} M_o = 0.65 \text{ kip-in.} = M_o$$

Since the negative moment capacity at the ends of the center span is 0.433 kip-in., in order to supply enough moment capacity, the positive moment at the center of the middle span must be

$$M^+ = M_o - 0.433 = 0.626 - 0.433 = 0.193 \text{ kip-in.}$$

These values are for each panel, and it is evident that the sum of the elastic moment distributions over the negative and positive moment regions are not in the same proportion as the values assigned, but the static moments will be closely the same. In the test structure, the positive moment regions of the exterior spans have been assigned a larger proportion of the static moment than an elastic analysis would give. This indicates that the negative moment regions will develop a plastic hinge first. Consequently, subsequent load will be carried by the positive moment regions until these yield and the slab becomes a mechanism.

The distribution of the negative and positive moments across the panel must now be determined. Since it was previously stated that failure would occur in the manner illustrated in Fig. 5.3, it may be argued that a uniform distribution of moment across a section will give the same strength as a distribution of elastic configuration. Furthermore the uniform moment distribution will greatly simplify the steel layout. Thus the regions of high elastic moment will crack first, transferring the load through shears

and twisting moments to adjacent regions which have not cracked yet. Subsequently, the high elastic moment regions will yield first and transfer the load to adjacent regions until yield lines are completely formed. Simultaneously, there will be transfer of load from the negative moment regions to less stressed positive moment regions.

Thus the moment in the test structure has been distributed tentatively as shown in Fig. 2.7. Figure 2.8 shows the distribution in structure F2 which was designed according to ACI 318-56 code. A visual comparison of these two figures shows how the use of plastic design in slabs can simplify the reinforcement layout. In structure F2, there are 14 different moment coefficients in the slab itself while in structure F6 there are only two different moment coefficients.

2.3 Final Design of Structure F6

In the previous section, the basis of the over-all design of the test structure was explained. So far the design has presented the method used to consider the flexural proportioning of the structure from the point of view of statics. There was no mention of the factor of safety, and no effort was made to insure against other possible manners of failure or to consider the actual layout of the steel.

(a) Factor of Safety

The first thing that must be considered is the factor of safety of the structure against flexural collapse. In the previous section, conservative values of the moments necessary to withstand the design load were chosen, and moments assigned to the sections were thus design-load moments. In order to compare this structure with the previous structures

tested, it was decided to proportion the sections according to working stress design as it had been done for the previous slabs. Thus with an allowable steel stress of 20 ksi and an allowable concrete stress of 1350 psi, the result was a total of 69 bars of 0.0355 in. diameter across exterior positive and interior negative moment lines, and 31 bars across interior positive moment lines in each panel. This satisfied the working load moments of 0.433 kip-in. and 0.193 kip-in. respectively for the two critical sections in the test structure. The average depth of reinforcement was taken as 3/8 in.

Since at low percentages of steel, and by using the straight line theory, the moment calculated at a section is closely directly proportional to the steel stress, the factor of safety against yield and ultimate moment of the sections designed is:

$$\text{Factor of Safety} = \frac{f_y}{f_s} = \frac{f_y}{20 \text{ ksi}}$$

Past experience has indicated that the yield stress of the wires used is on the order of 45 ksi, thus giving a factor of safety of 2.25 against yielding of the sections considered. This, nevertheless, is not the factor of safety of the structure against flexural collapse since in Section 2.2 it was pointed out that a conservative value was chosen for the static moment. The factor of safety is thus expected to be around 2.5. To determine the factor of safety with greater certainty, a yield line analysis should be made after the final design and if desired, modifications of the design can be made on the basis of such analysis. Chapter 5 shows the results of the strength analysis of the test structure.

(b) Slab-to-Column Connections

Assuming the factor of safety to be 2.5, the total ultimate load to be carried by each panel is about 1,200 lb. From this it may be deduced that the approximate values for the ultimate shear around the face of the supports are:

Corner	Side	Center
300 lb.	600 lb.	1200 lb.

These values are obtained by dividing each panel in four equal sections and assigning the load on each section to a corner of the panel. A more sophisticated manner of finding the reactions would be to use values from the yield line analysis, but the refinement is not warranted or compatible with the uncertainties in determining the shear capacity of the slab.

As was pointed out earlier, the ACI 318-56 Building Code design of the previous slabs required drop panels over the capitals. Also there were peripheral edge beams. All these factors added up to give satisfactory punching shear capacity of all the slab-column connections. But when the decision to remove the drop panels and edge beams was made, there remained the question of the adequacy of these connections in sustaining the collapse load without a shearing failure.

According to the working stress design of the ACI 318-56 Building Code, the allowable shear stress of the center and side columns would not be exceeded when the design load acts on the structure. But the corner column shear stress at design load would exceed the value allowed by the Code. If the ultimate load is considered, the column reactions given by the table above give shear stresses which exceed the ultimate allowable

stresses of ACI 318-63 (7). Since the purpose of this test structure was to try out a manner of simplifying the design of slabs, it was decided that a closer and less conservative look would be appropriate in this case in order to be able to test the innovations to be investigated. For this reason, the concept of shear at the slab-to-column connection was experimentally examined by performing pilot punching tests on slab sections. The tests are described in Appendix B.

Essentially, tests were performed on a square slab section 7/16 inches deep and reinforced with the same steel percentage as the slab negative moment sections. The test specimens were made of a concrete mixture similar to that used in the previous 1/16 scale slabs. The punching tests to failure indicated that for the concrete used the shear strength was at least $7.5\ f'_c$. On the basis of this value, which applied for a section reinforced in a specific manner, it was decided that the shear strength of all the slab-to-column connections was adequate to carry the column reactions at the ultimate load. The above statement implies that there is negative reinforcement of a certain percentage over all the columns in this structure. This is not the case, since so far the assumption of no steel perpendicular to the discontinuous edge has been adhered to. Nevertheless, to insure the continuity of the slab-to-column connections, as well as sufficient shear capacity, it becomes necessary to have steel perpendicular to the discontinuous edge at least over the column. It was then decided to have a steel percentage equal to the one over the interior columns. In this manner the same spacing of steel could be used, in line with the spirit of simplification stated at the beginning of Section 2.2. Furthermore, the results of the punching tests could thus be applied to all the columns.

The spacing of the steel over the side and corner columns has been determined largely as a matter of convenience and efficiency. It now remains to determine how far the reinforcement should extend on either side of the column center line. An examination of the crack pattern over the side and corner columns of previous slabs indicated that at worst the negative moment cracks spread out at 45 degree angles from the inside corners of the support to the free edges of the structure, as illustrated in sketch B (see Fig. 6.22)

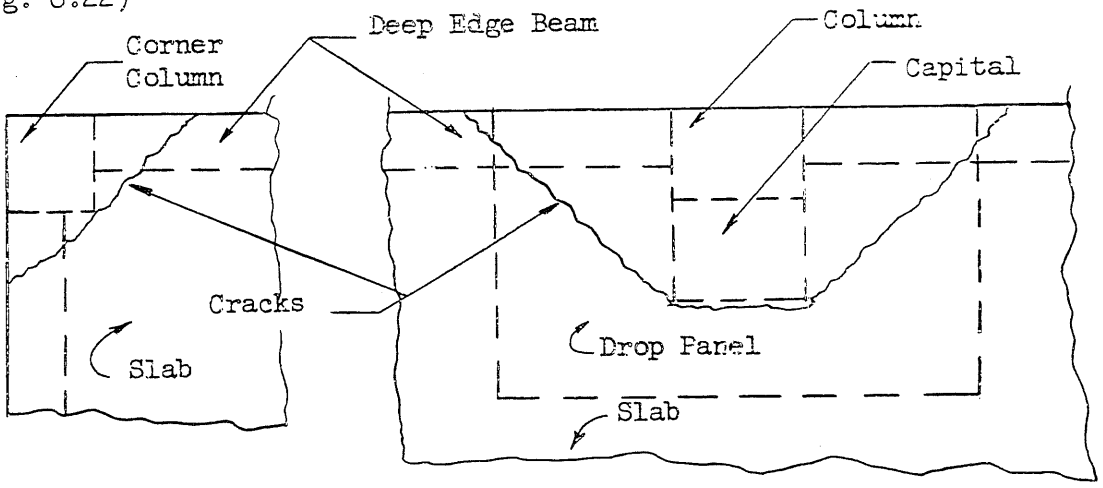

Sketch B

It was thus decided to extend the reinforcement far enough to cover these cracks. Thus negative reinforcement perpendicular to the edge of the structure was assigned as far as two inches on either side of the center of the side columns, and one inch on either side of the center of the corner columns. The steel should be bent into the column behind the column reinforcement cage, and spot welded to the column longitudinal steel, whenever possible. Other bars should be hooked. The above procedure would avoid failure due to the slab tearing away from the column (Fig. 7.30, Reference 3).

(c) Reinforcement of the Test Structure

Previously in this section it was stated that 69 bars per panel were necessary to reinforce the interior negative moment section and the exterior positive moment section. Over a span of 15 in., the spacing between bar center lines is 7/32 in. For the interior positive sections, the spacing should be 0.485 in. Nevertheless, at this point it was deemed convenient to increase the number of these bars to 34 per panel so as to have a spacing double the spacing of the other critical sections in the slab.

Thus the final result was a slab with only two different spacings of steel: 7/16 and 7/32 in. Figures 2.9 and 2.10 show the top and bottom steel layout of the test structure. A comparison can be made with Figs. 2.11 and 2.12 which show the arrangement of a slab reinforced according to the ACI 318-56 Building Code. The simplification of the steel layout is evident.

It must be noted that the positive bars are 15 in. long and span across the panel. This is not a strict requirement, since shorter bars could have been used in alternate spaces, especially near the columns. Again, it was thought a matter of convenience to have all bars of equal lengths. The negative reinforcement extends 5 in. from the critical section in all cases, making the interior bars 10 in. long, and the bars perpendicular to the edge 5 in. long. Thus ample anchorage has been provided and no section is without reinforcement.

(d) Effect of the Additional Reinforcement over the Exterior Columns

The addition of the negative reinforcement perpendicular to the edge of the structure over the column increases the moment supplied above the static requirements for the design load. Thus the factor of safety

of the exterior spans is increased. If all the extra steel supplied were to yield, the collapse load would be 8 percent greater than what it would have been if the extra steel were not there. Furthermore, the addition of 10 bars to the middle three panels increases the moment capacity supplied, making the collapse load of the interior spans 3 percent greater than it would have been.

At this point, a revision of the design sections could be carried out to reduce the supplied moment by removing some bars from the critical sections. The economy of steel was weighed against the advantage of having a convenient spacing which would ease the construction procedure. It was decided to keep the design unchanged, since there is an uncertainty regarding the efficiency of the steel perpendicular to the edge. Thus the structure has been proportioned for at least 103 percent of the conservative static moment.

(e) Quantity of Reinforcement

It should be interesting to compare the number of reinforcing bars in the test slab with that for slab F4, designed according to ACI 318-56.

	No. of Bars Used in the Slab	
	F4	F6
Positive reinforcement	536	1035
Negative reinforcement	832	828
Total	1368	1863
Total/F6	0.73	1.0

The number of bars in structure F6 does not include the negative bars added over the exterior columns. A greater number of bars were used in F6 as slab reinforcement since the slab was provided with reinforcement to resist the full static moment. Table 2.1 shows the distribution of steel in all the slabs considered.

(f) Column Design

The columns in structure F6 are essentially reinforced in the same manner as those of structure F5. The sole change was the removal of two bars from the compression region of the side columns. This was done in order to reduce the rigidity of the column at high stages of loading and allow an increased rotation which would diminish the possibility of having the slab tear out of the column. The column reinforcement is shown in Fig. 2.13.

2.4 Material Properties

A small scale model can predict directly the behavior of a full scale structure if the material properties of the model are the same as those of the larger structure. When the size of the reinforcement and the aggregate particles of the concrete is decreased, some changes may occur which slightly alter the resulting material properties from those used in full scale structures.

(a) Steel

The steel used in the test structure consisted of annealed bright basic wire of 0.0355 in. diameter. The process used in straightening and annealing the wire is described in Appendix A. The stress-strain curve of the reinforcement showed an elasto-plastic behavior with a modulus

$E_s = 30 \times 10^6$ psi, and a yield stress of 43,000 psi. This stress-strain curve will be assumed to govern for the steel in the structure. Different batches vary slightly, and the variation will be taken in consideration whenever it is of importance, since the location of the batches in the structure was recorded. The standard deviation for 60 samples tested was: $\sigma = 2,000$ psi. The column steel had a yield stress of 39,000 psi.

(b) Concrete

The detailed proportions of the mix used in structure F6 are presented in Appendix A. Generally, the concrete used had a maximum aggregate size of 1/16 in. and a water/cement ratio of 0.74 by weight.

Figure 2.14 shows a typical concrete stress-strain curve. The average modulus of elasticity, using the initial tangent as a criterion, was 3,000,000 psi with a high value of 3,400,000 psi and a low value of 2,750,000 psi, while the average strength was 4,000 psi. The low modulus-to-strength ratio is believed to be a consequence of the high porosity of the concrete. The above values were obtained from tests of 4-in. by 8-in. and 2-in. by 4-in. cylinders, both sizes showing the same range of values.

Split cylinder tests were made on 4-in. by 8-in. and 2-in. by 4-in. cylinders. The former gave 360 psi and the latter 410 psi as average tensile strength of the concrete.

All the tests were performed within two days after testing the structure, which was 80 days after the casting operation.

Flexure tests performed on sample beams cast as companion specimens of the structure gave an average modulus of rupture of 780 psi. The beam tests were performed 40 days after the slab was tested.

2.5 The Structure After Form Removal

The procedure of form removal is explained in Appendix A. It is important, nevertheless, to point out at this stage that the self weight of the structure is on the order of 5 psf. This weight is not large enough to produce a sizeable negative moment over the columns, so since the slab-to-column connections were not reinforced for a reversal of moment, extreme care had to be exercised during the removal of the plastic forms from the columns in order not to introduce a positive moment. For example, in the corner column a horizontal load of 3 lb. outward applied at the base would be sufficient to crack the slab at the face of the column. The situation of the side columns was not so severe because of the presence of the bracket. Figure 2.13 shows the steel arrangement over the columns and illustrates the above reasoning.

Even though extreme care was exercised, the slab around Column 4 was damaged in the above-described fashion, developing a positive crack at the face of the column. The crack initiated at the bottom surface of the slab and extended upward to the level of the negative reinforcement. If the positive reinforcement had been anchored into the column, the above-mentioned crack would have been efficiently restrained. This was not done because the structure had been designed only for vertical loads, without reinforcing against a frailness only particular to the handling problems of a very small scale model.

Since the presence of the crack, shown in Fig. 2.15b would nullify the shear-carrying capacity of the section unless the crack were perfectly closed, it was judged essential to supply a capital in order to force the critical section away from the column face. The solution chosen

was to precast a capital which could in turn be post-stressed against the column while grouted against the slab. In this fashion the slab would be resting on the capital and the capital would in turn be held against the column through friction. Figures 2.15a and 2.15b show the plan and profile of the arrangement. Figure 2.15c shows the arrangement of the slab negative steel over the support. Even though the steel area remained the same, more concrete is expected to be in compression at the face of the capital, thus enhancing the shear-carrying capacity. On the other hand, the question arises as to the adequacy of the anchorage of the reinforcement, since no detailed investigation had been made of bonding properties of these materials. Figure 2.15d shows the capital of Column 4 in place. To preserve symmetry, and insure against other accidental cracking of the corner columns, similar capitals were provided for Columns 1, 13 and 16.

Except for the beveled shape the dimensions of the corner capitals were the same as those of the center capitals. It is obvious that the static moment in the exterior spans has thus been decreased, since the effective span was reduced. Assuming the reaction concentrated at the corners the static moment is reduced by 7 percent, and assuming uniformly distributed reaction the static moment is reduced by 4 percent. The factor of safety of the exterior panels is thus increased by the same amounts for each assumption of reaction distribution.

3. LOADING SYSTEM, INSTRUMENTATION AND TEST PROCEDURE

3.1 Loading System and Dynamometers

Figure 3.1 shows the test frame layout. The locations marked with an "O" were the column reaction points and the locations marked with an "X" were the load points. The load was applied at 16 points per panel by means of 2 by 2 by 1/4-in. steel bearing plates with a layer of 1/8-in. cork between the slab and the bearing plate. The load was transmitted to the bearing plates by high strength 3/64-in. cables which passed through 1/8-in. holes cast in the slab (Appendix A). All 16 cables in a panel were pulled down by means of a "loading tree" connected to one jack. Figure 3.2 illustrates the loading system. As it may be seen, the loading system is determinate and thus eliminates any possibility of arching.

The pressure was applied to the wires by 10-ton, Blackhawk R78 jacks through one hand pump and a system of valves at a control manifold.

The slab was supported at each column (marked "O" in Fig. 3.1) by means of an adjustable column reaction base, illustrated in Fig. 3.3. The necessity of the adjustable support was dictated by shrinkage movements which took place during the preparation of the slab for testing. One day before testing, the column reaction bases were carefully adjusted so that the ball upon which the columns rested was snugly in place. To test the accuracy of contact, the columns were manually pushed down with a 50 lb. force and the deflection dials checked to make sure no movement occurred. Thus the columns were judged to be accurately "pinned" at their base.

The load was measured by means of dynamometers fixed at the end of the jack plunger. At the other end the dynamometers pushed against a 1/2-in. ball which rested on the main beam of the "loading tree." Thus since the "loading tree" was suspended from the slab by 3-ft. flexible cables a moment-free action of the dynamometer was possible. To obtain a calibration curve that could indicate the load applied on the slab accurately, the dynamometers were calibrated using an apparatus similar to the loading system, which insured no eccentric loads due to slight misalignments (see Appendix B).

The dynamometers were constructed from 2-in. lengths of aluminum alloy tubing on which type A-7, SR-4 strain gages were mounted in a four-arm bridge pattern. Two opposite gages were in a vertical position, while the other two opposite gages were in a horizontal position. The dynamometers were judged to be accurate to within a load of ± 5 psf on the slab.

3.2 Strain Gages

The test structure was equipped with 28 strain gages attached to the reinforcement at key locations. The major purpose of the gages was to study the feasibility of using this type of instrumentation in small scale models.

Since the use of strain gages on wire of such small diameter (0.0355 in.) was still in the experimental stage, it was decided, for the sake of economy, to use the four lines of symmetry of the structure to the fullest advantage, and not have repetitive gage locations. The gage arrangement is shown in Fig. 3.4.

It should be mentioned at this point that during form removal the leads of gages N2, N3, N8 and N9 were severed. Furthermore, gage N1 was nullified by the addition of the postensioned corner-column capitals since the gage was no longer in the slab but over the support. Nevertheless, it will be shown in Section 6.4 that this gage gave clues as to the effectiveness of the added capitals in supporting the slab.

In order to keep a measure of the stability of the strain measuring system, a drift check gage was read after each set of strain readings. This gage was placed on a reinforcing wire which was cast in one of the test beams described in Appendix B thus being in environment identical to the gages in the slab, but under no stress. The gage used was from the same batch and mounted in exactly the same fashion as the gages in the slab.

3.3 Deflection Dials

The deflection measuring system of the test structure consisted of 49 dials which measured the vertical deflections at all the intersections of the column and panel center lines. All dials measured to 0.001 in. per division, with a 1 or 1/2-in. stroke. Figure 3.5 shows the location at which the deflections of the slab were measured. Dials were also placed over all the columns in order that any column movement could be detected and an appropriate correction could be made on the slab deflections.

The dials were fixed to 3-in. steel angles spanning the width of the slab. The angles were bolted to 4-in. steel channels which were fastened to channel columns that were in turn bolted to the loading frame.

The plunger of the dials was 3 in. above the surface of the slab and connected to the slab by means of high strength, flexible steel wire. At the dial end, the wire was fastened to the plunger by winding around the bearing screw and tightening the latter. At the slab end, the wire was tied to a lug which was in turn fastened to the slab by means of an Epoxy adhesive. Thus, the deflections of the slab were recorded by pulling the dial plunger. Figure 3.6 shows a photograph of the assembly after the slab was tested.

The entire assembly was tested for rigidity by severe jarring. The dial plungers were depressed and released suddenly permitting the dial spring to act dynamically against the wire. The angles supporting the dials were depressed and slowly allowed to regain their initial position. Throughout the above tests, the dials repeated their readings within 0.0005 in. The deflection system was thus capable of accurate reading reproduction and was free from disturbances arising from direct contact of the dials on the slab.

3.4 Test Procedure

The procedure followed in testing the structure was similar to that used in structures F4 and F5. The load was applied in continually increasing stages until failure occurred, approximately six hours after the beginning of the test.

The load was applied by monitoring the dynamometer corresponding to panel F while all the hydraulic system was pumped simultaneously. Once the desired load increment was reached, the pump valve was closed

and all the dynamometer readings were recorded in alphabetical order, from panel A to panel J. No adjustments were made to equalize the loads on individual panels, since the variations in load were small.

As soon as the load was applied, the deflection and strain readings were recorded. The reading of each dynamometer was then recorded again before the next load increment was applied. In most cases the drop in load between initial and final readings was less than 10 psf.

The structure was checked for cracks after each load increment. This operation could not be performed very efficiently since the top surface was covered by loading plates and deflection wires, and the bottom surface was inaccessible due to the loading cables, as may be seen in Fig. 3.6.

Testing chronology, load numbers and their corresponding incremental and total loads are presented in Table 3.1.

4. BEHAVIOR OF THE TEST STRUCTURE

4.1 Introductory Remarks

As described in Section 3.4 the test structure was loaded continually to failure. The load was applied in 23 increments, and the intensity of each increment is shown in Table 3.1. Testing of the structure took six hours for completion. Deflection and strain readings were taken at each load increment and the results are presented in Sections 4.2 and 4.3, respectively. Section 4.4 describes the cracking and observed mode of failure.

4.2 Deflections

As explained in Section 3.3 dials were placed on top of the columns. The slab deflections are presented as deflections relative to the column tops by performing the following corrections: (a) For mid-panel values, the deflections of the four column dials at each corner of the panel in question were averaged and added algebraically to the mid-panel deflections. (b) For column center line values, the average of the deflection of the two columns at the end of the span were added algebraically to the column center line deflection. The corrected results are presented for two stages of loading:

(a) Load-Deflection Curves at Initial Stages of Loading

Figures 4.1 and 4.2 provide information about the measured load-deflection curves at loads below 300 psf. These figures are presented in order to show in detail the response of the structure at working loads. The design load was 285 psf including dead and live loads.

The curves for the corner panel are plotted in Fig. 4.1a. Visual examination of these curves shows that the initial "elastic" slopes have the same value for all the corner panels, except for a slightly decreased slope for panel J due to a small overload in this panel.

Figure 4.1b shows the deflection of the side and interior panels. The slope for the side panel curves is obviously steeper than that of the corner panel, due to the larger number of sides restrained. The side panel curves are also very consistent in their initial slope except panel H which seems a little stiffer. This is due to a slight underloading of this panel. Panel E, being restrained on four sides is evidently stiffer than all the other panels.

In general, all the curves of Fig. 4.1 show that the load-deflection relation for the mid-panels is linear up to an applied load of 200 psf. Over the load, the corner panel deflections increase at a faster rate, while the deflections for the other panels still increase nearly linearly.

The performance of the structure at the design load may be judged from mid-panel deflections:

	CORNER PANELS	SIDE PANELS	INTERIOR PANEL
Δ @ Design load	L/700	L/1000	L/1900

where L = bay span

Figure 4.2a shows typical curves for the exterior span column center lines (discontinuous at one end and continuous on the other, as labeled in Fig. 2.4). Seemingly, there are two conditions for these

center lines: (a) the center line at the peripheral edge of the structure, and (b) the center line between two panels. Nevertheless, since this structure does not have any edge beams, if we neglect deflections due to torsion and Poisson's effect, the load-deflection relationship of the inside column center lines should be very similar to that of the outside column center lines. This is shown by the comparison of dials A1 and C4 with dials D1 and J2.

Figure 4.2b shows typical curves for the deflection of interior span column center lines (continuous at both ends). Again, it may be seen that there is little difference between inside and outside center line deflections.

The deflection of the interior spans is considerably less than that of the exterior spans, as may be expected. The deflections for the column center lines are as follows:

	EXTERIOR SPAN	INTERIOR SPAN
Δ @ design load	L/1200	L/2200

To avoid repetition, the readings of only 8 of the 24 column center line dials were presented. Due to symmetry only four need have been shown, but the number was doubled so as to illustrate the consistency of the data. A schematic deflection diagram is shown in Fig. 4.3, illustrating all the deflections of the structure measured at the design load. At this load, inelastic action had taken place in some regions, while others still remained elastic (seemingly uncracked). This accounts for some lack of symmetry in the column center line deflections.

(b) Load-Deflection Curves to Failure

The maximum load on the structure was reached at the nineteenth load increment corresponding to an applied load of 867 psf (total load 890 psf). After this load was reached, any attempt to increase the load resulted in temporary increases which dropped rapidly below the previous load level. The test was continued, nevertheless, in order to form easily distinguishable yield line patterns. At the twenty second load increment the test was discontinued due to a combined bond-shear failure near Column 16. This failure is explained in Section 4.4.

Figure 4.4 shows the deflections of the mid-panels up to the end of the test. It may be seen that all panels showed large ductility, irrespective of their position in the structure. This means that failure mechanisms extended throughout the structure (i.e., the load was not prevented from rising by a local failure in a group of panels, which would have restrained the inter-connected hydraulic system from increasing the load).

Comparison of the three groups of curves shows that the corner panels are initially softer than the side panels, and these in turn are initially softer than the interior panel. As the load is increased to the vicinity of 800 psf the deflection rate of all the panels seems to be equal, again indicating a simultaneous yielding of all panels.

Figure 4.5 is a plot of the deflections of the same column center line dials shown in Fig. 4.2. The readings in these locations for symmetrical positions are not as consistent as the mid-panel deflections, since they are more directly susceptible to differences in the load at which

they initially cracked, while the mid-panel deflections tend to average the four column center line deflections that bound the panel.

Figure 4.6 shows a schematic diagram of the slab deflections when the limit load of 867 psf was applied. A comparison with Fig. 4.3 will show the extent of moment redistribution since some of the inner spans of the column center lines deflected more than the outer spans, which is not the trend of the elastic deflections. The reason for this is that structural type mechanisms are beginning to form, involving the center cross arrangement of panels. Even at this stage of high loading, the deflections of symmetrically located points do not vary more than 20 percent from the average. This is very good considering that the values are measured from yielded sections (i.e., at the "flat top" of the load-deflection curves).

Figure 4.7 shows the schematic deflection diagram at the last load increment applied. The load is 20 psf less than for the diagram of Fig. 4.6, but the yield lines have developed considerably more than the ones shown in Fig. 4.6. It should be noted that the interior panel has deflected more than two corner panels (G and C) and more than one side panel (D). This indicates a definite formation of a yield mechanism in the interior panel.

In summary, it may be concluded that the load-deflection curves for the structure indicate a favorable behavior insofar as serviceability and utilization of all structural components to the fullest degree is concerned. Furthermore, it is seen that the response of the structure was symmetrical about the axes of geometrical symmetry so that it is justifiable to average deflections at comparable locations in further discussion.

4.3 Strains

It was mentioned in Section 3.2 that only enough gages were used in the test structure to give an idea of the strain profile. The gages were 1/4 span away from adjacent gages and no duplicates were provided. Due to the breaking of some leads during form removal gages P6, N2, N3, N8 and N9 did not function during the test. The locations of these gages and of the 23 functioning are shown in Fig. 3.4. The stability of the strain gages was checked, during each reading, against the drift check gage. Corrections were made by algebraically subtracting the incremental reading of the drift check gage from the incremental readings of the gages in the test structure. Strain data are presented for two stages of loading, as was done for the deflection data.

(a) Load-Strain Curves at Initial Stages of Loading

The load-strain curves for the positive moment region gages (P-gages) are shown in Fig. 4.8. The response of these gages is essentially linear up to 200 psf, indicating that the positive moment regions have not cracked yet. After passing the design load, there appears to be a slight increase in the strain rate, which indicates that cracking has started. This compares very well with the results shown by the deflection dials, which generally indicated nonlinear behavior only after 200 psf. It may be seen, nevertheless, that the strain at which the curves become nonlinear varies from gage to gage.

Figure 4.9 shows the load-strain curves for gages in the negative moment regions (N-gages). Again in these gages, nonlinearity begins at low strains, and in most cases at a load of about 150 psf. The initiation

of local cracking at the negative moment sections did not affect the over-all response of the structure as indicated by the fact that the load-deflection curves were essentially linear up to an applied load of 200 psf.

The distribution of the measured strains across various sections at an applied load of 100 psf may be seen in Fig. 4.10. These distributions refer to an uncracked "elastic" structure.

The positive moment strain distributions (P-gages) seem reasonable, with the possibliity that the measurements by gages P5 and P11 are a little low. The relative magnitude of the strains of gages P1 through P7 are plausible, since the gages nearer the column center lines show higher readings than the gages located at mid-panel. The same can be said for gages P8 through P14. It may further be noticed that the strains indicated by P1 through P7 in the exterior span are higher than the strains of the interior section at comparable gage locations. This is to be expected since the interior spans are restrained (continuous) at both ends, while the exterior spans are restrained on one end only.

The negative moment region gages (N-gages) also seem to show a reasonable distribution of elastic strains. In this section, nevertheless, there were not enough gages to define the strain profile completely. Since there were no gages close to the capital and parallel to its side, the distribution can not be ascertained. Notwithstanding the above disadvantages, the relative magnitudes of the strains across the N4-N14 section seem reasonable since they indicate that the moment is increasing toward the column center lines and decreasing toward the middle strip.

Figure 4.11 shows the strain distribution across the same location of Fig. 4.10 at design load (265 psf applied). It was mentioned earlier that some cracking had occurred, especially in the negative gages, before the design load was reached. It may be seen by comparing Figs. 4.10 and 4.11 that the strains of the negative section increased at a faster rate than those of the positive sections. This was due to the reduction in stiffness of the negative moment sections which cracked before the positive moment sections.

Figure 4.11 is of particular importance because it shows the performance of the structure at design load. It may be seen that the maximum steel strain occurred at the corner of the capital. This strain corresponds to a stress of 9,500 psi.

Further discussion and comparisons with theory and other test results are given in Section 6.3.

(b) Load-Strain Curves to Failure

During the test, the gages in operation seemed to function properly at low stages of loading. However, when higher stages of loading occurred, it was evident that some of the P-gages showed signs of malfunction. Thus, a quantitative presentation of strain profiles does not seem warranted in this case. Some of the strain readings, nevertheless, do not seem erratic. So a qualitative and limited "observed behavior of the structure" at loads above the design quantity will be presented in terms of strains.

In Fig. 4.12 the gages shown indicate the type of load-strain behavior that may be expected in a slab strip. Gage P1 was located at the column center line in a region of high elastic stresses. The shape

of the load-strain curve indicates that yielding of the steel occurred in this location before the maximum load was applied to the structure (about 85 percent of the peak load). The steel then proceeded to strain at a very fast rate with each successive load increment, finally reaching a strain of 0.0060 (about four times that of the proportional limit). This behavior compares very well with the readings shown by the deflection dial on the same point. The behavior of gage P13 is very similar to that of gage P1. Although gage P13 was one fourth of the span away from the column center line, in a region of lower elastic stress as seen in Fig. 4.10, the strain rate increased very rapidly after cracking had occurred. Yielding of the reinforcement occurred at an applied load of about 750 psf. After this load the strain rate increased considerably with further load increments, to reach a final strain of 0.0075 (about five times the proportional limit strain). Once more, this behavior is comparable with the deflections in that region (see Fig. 4.6 and Fig. 4.7). The higher strains of gage P13 versus gage P1 are also evident in the relative deflection close to those positions.

Gage N14 in Fig. 4.12 ceased to give readings at the point indicated by the cross. This gage is located at the corner of the capital. Notwithstanding the fact that this gage ceased to function, it indicates that the reinforcement yielded in this region at an applied load of 600 psf (70 percent of the peak load). Cracking occurred at a lower load in this gage location than in the positive gage locations since this is the region of severest moment concentration in the structure.

4.4 Cracking and Observed Mode of Failure

The first indication of cracking was noticed in the slab at a load of 354 psf. As mentioned in Section 3.4, the loading and deflection measuring systems did not allow efficient use of magnifying tools for crack detection on the surface of the slab. The cracking detected at the above-mentioned load occurred in the slab at negative moment regions located directly above the side columns (same location as shown in Fig. 4.16b). These cracks were visible without magnification, which indicated that cracking had occurred at lower loads.

The next increment raised the applied load to 506 psf and more cracking was visible, coupled with a noticeable increase in the rate of deflections.

After three more increments, a load of 667 psf was applied and by this time the cracks were plainly visible and were on the order of 0.005 in. Cracking was observed at the negative moment regions of the slab over the corner columns and over the interior columns. A careful but distant examination of the bottom surface of the slab revealed no cracks. Positive moment cracks could not be seen even at the edge of the slab. No cracking could be discovered on the sides of the column.

When an applied load of 758 psf was reached, positive moment cracks were discerned at the edge of the slab. In Panel J the crack extended halfway up the thickness of the slab. Smaller cracks could be seen at other positive moment regions at the edge of the slab, but no cracks could be discerned in the middle of the panels. This crack formation is consistent with the initiation of yielding at these regions, as illustrated by the strain values shown in Fig. 4.12. Most of the

exterior columns showed fine cracks about 1/4 inch below the end of the capital. Some of the negative moment regions of the slab above the columns showed definite signs of yield line initiation.

At an applied load of 850 psf, failure seemed imminent. There appeared to be as much of a chance of having a failure of the interior strip of three panels as having a failure of the exterior strip of three panels. As the load was increased to 867 psf, which was the maximum load the structure could withstand, the positive yield line of the interior strip of panels extended considerably and was visible even at the middle of the panel. The cracks in the edge columns were, at this point, on the order of 0.05 in. Further jacking served only to increase the deflections while the load remained unchanged. The structure seemed to fail in all the panels simultaneously, with slight preference of the interior span failure. The negative moment yield lines in the slab could be seen to extend from column to column. Looking at the slab profile from different sides, three well-defined troughs could be discerned, each corresponding to a bay. At this stage, a trace of tensile membrane cracking could be seen in the middle of the interior span of panel F.

Further pumping increased the deflections with a drop in load to 848 psf. During the increase of deflections, tensile membrane cracks developed in all the interior spans as may be seen in Fig. 4.13b. Loading was stopped when Column 16 punched through the slab as illustrated in Fig. 4.14.

Subsequently, the structure was unloaded and the instrumentation and loading apparatus were removed in order to permit the marking of cracks. It is recognized that some cracks closed after the removal of the load,

but enough remained open to give a good idea of the mode of failure and regions of distress. Figure 4.13 shows photographs of the top and bottom surfaces of the slab. Figure 4.14a shows a profile of the structure, while Figs. 4.14b and 4.14c show the details of the punching failure. This set of figures illustrates that failure of the slab was not due to one particular cause but rather to general distress throughout the structure (complete formation of yield lines throughout the structure, punching of the columns through the slab and yielding of the side columns). The latter distress is pictured in Figs. 4.14a and 4.15c. Punching of the columns through the slab was not restricted to Column 16, but also seemed imminent in some center and side columns as may be seen in Figs. 4.15b and 4.15c indicated by the hatched lines. The hatched lines in Fig. 4.13a indicate that Columns 3, 7, 11, 12, and 15 were almost ready to punch through. Figure 4.16a shows the top of Column 7 and the region where "punching" had started.

Figure 4.16 shows a detail of the yield lines that developed above each of the three types of columns of the structure.

No evidence of torsional distress could be detected in the exterior slab-column connections.

5. STRENGTH ANALYSIS

5.1 Introductory Remarks

As mentioned in Sections 2.2 and 2.3, the flexural strength of the structure can best be estimated through a yield line analysis (6, 9, 10) after the reinforcement has been proportioned. On the basis of such analysis, modifications may be made on the moment capacity of the design sections to increase or decrease the expected factor of safety against the flexural collapse mechanisms investigated.

This chapter presents the results of yield line analyses of the test structure (with due consideration of the increased support width at the corners). It should be remarked that the results of a yield line analysis divided by WL (total load times span) should give a value equal to M_o (static moment) as long as the assumptions involved in both calculations are the same. Theoretically the yield line analysis will produce the upper limit on the strength of a structure for a given yield pattern. The method relies on the selection of arbitrary plastic hinge lines (yield lines) which are sufficient to form a collapse mechanism. Each collapse mechanism gives a value for the failure load. The set of yield lines which produces the lowest computed failure load will be the lower bound.

Since the yield lines that form the actual collapse mechanism do not form at the same load (especially in this test structure whose design moments are not in proportion to the elastic moments) consideration should be given to the rotational capacity of the yielding section. In a reinforced concrete slab the rotational capacity is more than necessary because of low percentages of reinforcement.

As implied above, a yield line analysis assumes that the structure collapses due to the formation of a flexural mechanism, and not from "weak links" such as shear, bond, torsion or local flexural distress.

5.2 Moment Capacity of Critical Sections

The resisting moment across slab sections at which the plastic hinge or yield line formed was computed using the formula for ultimate moment,

$$M_u = A_s f_{su} d (1-0.4 k_u) \qquad 5.1$$

where

$$k_u = \frac{A_s f_{su}}{bd f_{cu}} \qquad 5.2$$

Moments could have also been computed using the straight line formula,

$$M_y = A_s f_y j d \qquad 5.3$$

where

M_y = resisting moment capacity of the section

M_u = ultimate moment capacity of the section

A_s = area of tension reinforcement

f_{su} = steel stress at ultimate

d = effective depth

b = width of the section

f'_c = concrete strength in compression

$f_{cu} = 0.7\, f'_c$

jd = effective internal moment arm

However equations 5.1 and 5.3 give closely the same results since the slab sections are underreinforced and since the flat-top portion of the stress-strain curve is used. Strain hardening in the reinforcement was neglected.

The value of "d" was taken as the measured slab thickness minus the average cover of the reinforcement in orthogonal directions.

A comparison of this method of computation with the results of the companion beam specimens tested and reported in Appendix B showed good agreement between the computed and measured moments.

5.3 Failure Mechanisms

Several collapse mechanisms are possible in slabs of shape similar to the test structure. However, the low bound mechanisms of flexural collapse are usually associated with two basic mechanisms: (a) "slab failure" and (b) "structural failure."

The "slab failure" is illustrated in Figs. 5.1 and 5.2. This type of failure involves diagonal yield lines from the columns to or near the middle of the panel. Except for the diagonal lines, the location of the negative moment yield lines is near the column center lines, and the location of the positive moment yield lines is near the center of the panel but depends on the manner of load application and magnitude of the moments developed.

The "structural failure" is illustrated in Fig. 5.3. This type of failure can best be described as having yield lines extending across the entire structure. The negative moment yield lines occur near the column center lines, and the location of positive moment yield lines is near the center of the panel but again depends on the load application and magnitude of the moments developed.

For structures F2, F3, F4 and F5 the "slab mechanism" of the exterior panels was found to give the low bound value of the collapse load.* This was due mainly to the fact that in order to produce a "structural mechanism," the peripheral beams had to be yielded, which added a large resisting moment. The test structure, nevertheless, has been designed without edge beams and it may easily be shown that the "structural failure" gives a lower collapse load than the "slab failure" for the particular reinforcement arrangement of the slab.

In order to calculate the collapse load of any possible mechanism, the location of the centroid of the vertical reaction must be known. Any uncertainty in the position of this reaction directly affects the effective span of the bays, and thus affects the ultimate load calculations.

To illustrate the expected range of variation, two extreme positions of the reaction were assumed. The longest effective span (lowest limit load) is produced when the reaction is assumed uniformly distributed around the periphery of the support. The shortest effective span (highest limit load) is obtained when the reaction is assumed concentrated at the interior corners of the support.

---

* See References (2, 3, 4).

5.4 Comparison of Computed and Observed Strengths

The results of yield line analysis for a "structural failure" mechanism using the two reaction distributions described above are presented in the following table:

Spans	Reaction Distribution	
	Uniform	Concentrated
Exterior Strip	700 psf	900 psf
Interior Strip	740 psf	820 psf

These values were computed by considering the loads as they were actually applied on the structure (16 points, 2 x 2 in. each). The table points out that the failure should initiate in the row of panels B-E-H or D-E-F, termed as interior spans in Fig. 2.4. The range of values showed that at an applied load equivalent to about 800 psf, yielding of the interior spans would prevent further increase of load.

The actual maximum load carried by the test structure was 890 psf, including the dead load. This is about 10 percent greater than the computed capacity of the interior spans. The difference between the computed and measured loads in the interior spans may be due to several factors which were disregarded by the particular application of the yield line theory such as torsional moments, warping of the slab section, and planar forces.

The load carrying carrying capacity of the exterior spans, as computed and shown in the table above, has a larger spread in extreme values. The average computed value is about 6 percent less than the actual

load carried by the structure, but the load carried is within the computed range of values.

Since the load carrying capacity of the interior spans was boosted to the level of the exterior spans, the structure should evidence yielding simultaneously at all the panels, which is what actually happened as may be appraised from Figs. 4.6, 4.13 and 4.14a.

6. COMPARISON OF THE BEHAVIOR OF STRUCTURE F6 WITH THE BEHAVIOR OF STRUCTURES F2, F3, F4, AND F5

6.1 Introductory Remarks

As it was mentioned in Section 1.1, the object of this project was to investigate the behavior of a flat slab designed in a manner which deviated considerably from the accepted design practice (1). The basis of the design of the test structure was explained in Section 2.2. In order to evaluate the performance of the design, the behavior of the test structure must be compared with that of other similar structures designed by approved and established methods.

In Chapter 5 it was shown that the observed strength of the structure compared favorably with the values predicted by the yield line analysis, so with respect to strength the performance of the structure was satisfactory.

In this chapter, the behavior of the test structure will be evaluated in terms of deflection and strain readings. Comparison will be made with other flat slabs tested* and with results of theoretical analyses.

6.2 Deflections

As stated in Section 4.2, the average load-deflection curves will be used for Structure F6 since the agreement between symmetrically located points is very good. For comparison, the curves have been

---

* A discussion of the use of very small scale models to predict the behavior of full size structures is presented in Reference (4), and briefly discussed in the Appendices (Sections A.1 and B.1).

interpolated to "total load" scale (including dead load). Table 6.1 shows the material properties of the structures. As in Section 2.2 the discussion will refer to two stages of loading:

(a) Load-Deflection Relationships at Initial Stages of Loading

Figure 6.1 shows load-deflection curves measured at the mid-panel for loads up to 300 psf total. In this figure the deflections of the test structure (F6) are compared with those of the four other slabs of similar geometry (see Section 2.1). Slabs F2, F3 and F4 were designed according to the 1956 ACI Building Code, while structure F5 was designed for the full static moment according to the procedure recommended by Hatcher (2). The curves for locations AO, JO, CO and GO are identical as far as structure F6 is concerned. But for the other structures, due to the presence of two different edge beams, symmetry exists only about one diagonal. The same may be said for locations BO, DO, FO and HO.

Thus, it may be concluded from Fig. 6.1 that the behavior of the test structure at working loads, in terms of mid-panel deflections does not differ appreciably from what could be expected of a slab designed by the 1956 ACI Building Code.

Figure 6.2 shows deflections of the mid-span of the column center lines at working loads. For structure F6 the deflections of four locations have been chosen as being representative of all the column center line mid-span deflections because symmetry exists about both diagonals of the slab. Since the other structures had two different kinds of edge beams, the behavior of the test slab can be compared with that of flat slabs having deep or shallow peripheral beams.

It may be seen from the values at position E2 that the deflections of points located away from the edge of the structure are obviously not affected by the dimension of the edge beam, even if the points are only one span away from the edge. For points located half a span away from the edge the effect of beam size is very slight. But, as may be expected, if the points in question are located at the periphery of the structure, the size of the edge beam has considerable effect on the deflections. This effect may be seen in the load-deflection curves of locations A1 and D2. It may also be noticed that the test structure, which had no edge beams, is only slightly "softer" at these locations than a structure with shallow beams (depth of shallow beam = 1.43 x slab thickness).

It may be concluded then that, excepting points located in the immediate vicinity of the deep edge beams (i.e., 1/4 span away), the changes in geometry introduced in the test structure have not affected appreciably its load-deflection response at working loads.

The deflections of the test structure may also be compared with theoretical deflections obtained by the method proposed by Vanderbilt (11). Figure 6.3 shows the actual and computed load deflection curves at seven locations which from symmetry are representative of all the measurements taken in the test structure. Vanderbilt's method predicts accurately the deflection of the corner panel and the peripheral column center line. The method is off by about fifty percent at location E0, but the values are small, and the error is of low absolute magnitude (L/3000). It must be noted that the slope of the computed lines is directly proportional to the modulus of elasticity of the concrete, and thus the uncertainty in

the values is proportional to the uncertainty in E_c . Vanderbilt's method then, provides a reasonable measure of the deflections at initial stages of loading.

(b) Load-Deflection Curves to Failure

Figures 6.4 through 6.9 show the mid-panel load-deflection curves for all the flat slabs tested. It should be pointed out that for locations F0, J0 and E0 the load applied to structure F5 is greater than its collapse load because additional load was applied to these panels (together with panel H) while the load was maintained on the yielded panels.

An over-all examination of these six figures indicates that the deflections of the test structure are certainly within the realm of response of structures designed by the ACI Building Code.

If structure F4 is considered a typical example of a design based on the ACI Building Code (f'_c = 3,700 psi, f_y = 46,000 psi), it may be seen that the behavior of structure F6 (f'_c = 4,000 psi, f_y = 43,000 psi) is somewhat "stiffer" than that of a "typical structure." The increase in stiffness is more evident in the corner panel bounded by shallow beams (Fig. 6.4) while in the interior panel (Fig. 6.9) the load-deflection curves for the two structures are almost identical. The reason for this is that the structures designed by the ACI code have low amounts of steel in the positive regions relative to those in the test structure. As was shown in Section 2.3d the steel in the test structure in excess of that required by the ACI code was placed in the positive moment regions. This more than doubled the amount of positive steel in the exterior spans. Thus, the load required for the formation of the positive moment yield lines in the exterior spans of the test structure was increased in relation to the load

required for the formation of the same yield lines in structure F4. The early formation of the positive, exterior-span yield lines precipitates the exterior column rotations because additional load must be resisted through negative moments which must be developed perpendicular to the edge of the structure. These additional moments are responsible for flexural and torsional distress in the beam-column connections. On the other hand, if the formation of the exterior positive moment yield line is delayed by the shifting of reinforcement (as was done for the test structure) to the extent that this yield line is the last one to be formed, the exterior slab-column connection will not be subjected to distress at relatively low loads. The above statement is backed by the observed behavior of the exterior columns. In structure F6 these columns showed signs of flexural cracking at much higher loads than for the other slabs. This discussion is pertinent to loads under 600 psf since that is almost the limit of structure F4.

If the load-deflection curves for structures F2 (f'_c = 2,700 psi, f_y = 42,000 psi) and F6 (f'_c = 4,000 psi, f_y = 43,000 psi) given in Figs. 6.4 - 6.9 are compared, it may be seen that structure F6 shows consistently better behavior in that it is stiffer and develops greater load and ductility at ultimate. Part of the "softness" of structure F2 at lower loads is due to the weaker concrete. At higher loads the columns cracked, and since the column reinforcement yielded, excessive column rotations contributed to the large deflections. The effect of the exterior columns, nevertheless, is not appreciably felt in the interior panel which showed considerably larger deflections than the same location in slab F6, as may be seen in Fig. 6.9. It may also be noted from this figure that the center

panel of structure F2 has not formed a mechanism, as evidenced by the slope of the curve, but the deflection at the maximum load is as large as that of structure F6 when the latter reaches maximum load.

An examination of the curves of structure F3 (f'_c = 4,000 psi, f_y = 70,000 psi) which was also designed according to the working stress method (1) illustrates that an increase in collapse load can stiffen the structure. Slabs F3 and F4 had very nearly the same concrete strength, but F3 was consistently stiffer, due to the higher yield moment capacity of its sections. A comparison of the curves of structure F3 with those of structure F6 shows a much closer agreement than that of the curves for F6 with the curves for F2 and F4. The large deflections of the exterior panels of structure F3 is again due to the initiation of the positive yield line at lower stages of loading. The agreement is very good in the interior panel.

So far, the test structure has been compared with three flat slabs designed according to the ACI Building Code. Slab F5 (f'_c = 3,100 psi, f_y = 48,000 psi) was designed for 100 percent of the static moment and consequently its cracked sections have an average moment of inertia 42 percent larger than that of the structures designed by the Code. The effect of the increased moment of inertia may be evaluated by comparing the load-deflection curves of slab F5 with those of slabs F2, F3 and F4 (Figs. 6.4 to 6.9). It is evident that the increase of the cracked moment of inertia improved the behavior of slab F5 to the extent that it made it stiffer than structure F3 which in fact has stronger concrete, higher factor of safety, but similar geometry and roughly similar steel distribution. The test structure was also designed for the full static

moment which is the reason for the stiffer load-deflection curves of structure F6 compared with those of structure F3.

A comparison of the load-deflection curves of the corner panel bounded by shallow beams (Fig. 6.4) shows that the design of the test structure combined (a) a larger factor of safety, (b) larger cracked moment of inertia and (c) delaying the formation of the exterior span positive yield lines, to give a structure of stiffer behavior at higher stages of loading than that of the structures designed by the ACI Building Code. The above statement is made with respect to the panel bounded by the shallow beams, since it offers the closest similitude between the test structure, which had no edge beams, and the other slabs. The effect of the beam stiffness may be evaluated by comparing the curves of Figs. 6.4 and 6.6, remembering that the solid curve (slab F6) is identical in both figures. Finally, it may be concluded that for interior panels, the design method of the test structure gives results which compare favorably with those of structures designed by the ACI Building Code (Fig. 6.9).

Again, the deflections at higher loads may be compared with the theoretical deflections obtained by the method proposed by Vanderbilt (11). The computed deflections at the three typical mid-panels of the test structure are shown in Fig. 6.10. In general, the calculated deflections give a conservative estimate of the deflections of F6. The agreement is quite good at the vicinity of the computed collapse load (800 psf) while at lower loads the test structure is somewhat stiffer than predicted. If the predicted collapse load were as high as the actual collapse load, the agreement between calculated and actual deflections would improve. It must be pointed out that Vanderbilt's method does not take in consideration the

order of formation of the yield lines. It may be shown through a simple example a beam fixed at one end and simply supported at the other, that the order of formation of the yield lines will in fact affect the deflections. When the positive moment yield line forms last, the deflections at higher stages of loading are smaller. This is the case for the exterior spans in the test structure.

The computed deflections of the column center lines compare slightly better with the actual deflections of F6 than the deflections of the mid-panel locations. In spite of the uncertainties mentioned above and the uncertainty in E_c, Vanderbilt's method can be considered as giving reasonable, though slightly larger deflections than the ones measured in the test structure.

6.3 Strains

In the previous section it was shown that the performance of the test structure was satisfactory from the point of view of deflections. In this section an evaluation of stresses and moment distributions will be made using the strain data presented in Section 4.3. Figure 6.11 shows the typical moment-strain relationship used to obtain moments from the measured strains. The discussion will be made for two stages of loading:

(a) Comparison of Behavior at Initial Stages of Loading

The moments calculated for the interior panel of the test structure at a load of 100 psf (uncracked slab) are compared with the moments for structure F3 and the results of theoretical analysis in Figs. 6.12 and 6.13. In Fig. 6.12 the comparison is made with Nielsen's solution for an interior panel of an infinite array (12). The moments are

presented as a function of the load in dimensionless coefficients which are equal to M/W, where M is the unit moment (e.g. lb.-in./in.) and W is the total load on the panel (e.g. lb.). The sum of the areas under each curve for both sections taken should give a coefficient close to the static moment. It may be seen that the values for F6 seem a little low when they are compared with the theoretical values. The values for F3 are lower than those for F6 in the positive region but higher in the negative region. This is consistent with the fact stated previously, that the removal of the drop panels would tend to lessen the concentration of moment in the negative moment regions. Figure 6.13 shows the comparison of measured moment with the solution obtained by Corley (13). This solution considers the torsional restraint at the face of the columns. The moments measured in F6 compare more favorably with this solution than with Nielsen's.

The above comparison was made to determine whether the values of strain obtained by the gages can be used to obtain reasonable values for the unit moment at a given section. The answer is affirmative, but the clarification should be made that for gages N13 and N14, which are located at the corner of the capital, the depth of the section is uncertain.

Figure 6.14 shows the moments at 100 psf throughout the representative quarter of F6 compared with the moments of F3 at the shallow beam quarter. As it may be seen, the agreement between the two slabs is generally good, except near the edge at the positive sections, where the unit moment in slab F3 is less, due to the presence of the spandrel beams. This good agreement is to be expected since the slab sections are essentially uncracked at this stage. The moments in this figure are again given in terms of the dimensionless coefficient M/W. The use of this

coefficient makes a comparison apply to any scale of slab, since the moment is then directly proportional to the total uniform load applied on the structure.

Figure 6.15 shows the moment distributions of both slabs at the design load of 285 psf. As may be noted, the relative distributions of moment have not changed much, since cracking was not extensive in either structure at this load. Thus, the conclusion may be drawn that the changes in geometry of structure F6 did not change the moment distribution in the slab substantially, with the exception of increasing the applied moment at the positive regions of the wall strip. This increase does not bring the moments at the edge to excessive values, but tends to smooth out the moment distribution across the positive sections 1-1 and 3-3. Furthermore, the increase in reinforcement area and the change in its distribution do not seem to affect the behavior of the structure at design load. The effect on behavior might have been larger if concrete of lower tensile strength had been used.

The steel stresses corresponding to the design load are shown in Fig. 6.16. It may be seen that the largest stress in F6 was on the order of 10 ksi. For F3 the largest stress was about 11 ksi. Both these values occurred in the negative moment region directly above the corner of the capital. The stresses in F2, which had weaker concrete, are considerably larger than those of F3 and F6, since less moment was resisted by the tension in the concrete.

Thus it may be stated that the behavior of the test structure up to working loads does not differ appreciably from that of comparable structures designed according to the ACI Building Code.

(b) Comparison of Behavior to Failure

As the load is increased further, cracking in the structure becomes more pronounced and the distribution and quantity of reinforcement with the respective effects on the cracked moment of inertia becomes noticeable. Moments and steel stresses across a section at a given load are functions of the moment-strain curve shown in Fig. 6.11 which in turn varies with the parameters tabulated in the figure. Furthermore, the applied moment at a section is a function of the relative stiffness of the slab sections at a given load. Thus an attempt to explain thoroughly the mechanics of moment redistribution in two directions simultaneously would lead to extremely complex presentation, and will be avoided in favor of presenting an objective view of the results of the strain data.

Figure 6.17 shows the stresses in F2, F3 and F6 at a load equal to one dead load plus one and half live loads. The low percentage of steel area in section 1-1 is responsible for the higher stresses in F3 as compared with those in F6. The high stresses in F2 correlate very well with the larger deflections shown by this structure.

Figure 6.18 shows the stresses at one dead load plus three live loads. The stresses in section 3-3 of F6 are larger than those of F3 because of the proximity of a failure in the interior spans of F6.

Figure 6.19 has been prepared to illustrate the extent of moment redistribution in structure F6. It shows the measured distribution of bending moments (in terms of M/W) at failure for F6 and F3. The distribution for F3 is included to provide a measure of what would be expected in a slab designed in accordance with the elastic moment distribution (ACI Building Code).

Further illustration of moment redistribution after yielding of certain reinforcing bars is illustrated by Fig. 4.12. These measurements show clearly the extent of moment redistribution in structure F6. At gage location N14 the maximum moment capacity was reached at 70 percent of the failure load. From then on, further load resistance must be provided by other sections which have not yielded. (i.e. positive or adjacent negative regions). Gages P1 and P13 showed that the yield moment of their respective sections was reached at 85 percent of the failure load. Thus any added load carrying capacity had to be supplied by other sections which had not yielded.

6.4 Cracking and Failure

A comparison in terms of cracking and mode of failure of the behavior of the test structure with that of the structures designed according to the ACI Building Code can give another measure for the evaluation of the results of the principles used in the design of the test structure.

The manner of observation of cracks in the test structure (Section 3.4) was not suited for a step by step analysis of crack formation. However, the observation of the formation of yield lines can give a measure for comparison. Figure 6.21 shows the yield lines on the bottom of the test structure. These yield lines were observed very shortly before the maximum load was applied to the structure. Thus they were the final contributing factor to the formation of the failure mechanism. On the other hand, positive yield lines occurred in the exterior spans of structures F2, F3 and F4 at loads 20 percent lower than the failure load. The earlier formation of the exterior span positive yield lines in these

structures was discussed in Section 6.2. It was stated that their formation was related to rotation of the exterior columns and that both these factors caused an increase in the deflection rate, which is responsible for the "softer" behavior of Panel A (Fig. 6.4) of slab F3. The added amount of steel at the location of the exterior-span positive yield line in structure F6 (see Table 2.1) retarded the formation of the outer positive moment hinge of the mechanism, thus helping the test structure withstand the applied load with much less distress and deflection in the exterior spans at higher stages of loading.

An examination of the cracks over the side columns in Fig. 6.20 shows the absence of 45° cracks present in the slabs with edge beams (Section 2.3b). In Column 2 for example, all the negative cracks over the column are flush with the faces of the capital. Similar behavior was evidenced by the side columns supporting the shallow beam side of the other slabs. Thus yielding of the reinforcement at a 45° angle with the edge of the slab was limited to the deep beam side where the torsional moments were presumably greater. Evidently, in designing the reinforcement perpendicular to the edge of the slab, it is sufficient to assume that such reinforcement is required over a distance x,

$$x = c + \frac{b}{2}$$

Where:

x = distance parallel to slab edge measured from column center line.

c = dimension of capital in the direction perpendicular to the free edge.

b = dimension of capital in the direction parallel to the free edge.

It should be noted that the moment restraint which the columns can impose on the slab cannot be greater than the moment capacity of the column under the applied axial load. In the case of the test structure, the flexural capacity of the column was not enough to develop the steel perpendicular to the edge of the structure. With the column reinforcement as designed, there was very little reason to increase the amount of slab steel perpendicular to the edges. The behavior of the test structure justified this approach assumed in design; the side columns yielded before all of the slab negative moment reinforcement in the vicinity of these columns yielded.

Since the corner column had about the same moment capacity as the side columns but less than half the slab steel over it, all the slab steel yielded over the corner columns. In this case, biaxial bending causes a yield line (Fig. 6.20) which crosses the edges of the slab at a 45° angle through the tip of the post-tensioned capital. This behavior is comparable to that of the other slabs, but it is caused partly by the fact that the reinforcement does not extend past the capital, as may be seen in Fig. 2.15. The presence of some negative cracks parallel to the discontinuous edge of the slab near the corner column further points to the necessity of placing negative steel perpendicular to the edge of the slab beyond the area covered by the support. This was the original intent, but the addition of the capitals changed the configuration.

The comment should be made that the crack pattern in the vicinity of the corner columns and the fact that the strain gage N1 (Fig. 3.4) did not record more than 0.000170 strain, showed that the post-tensioned capitals proved efficient in supporting the slab.

Figures 6.20 and 6.21 indicate the type of mechanism that was responsible for the collapse of slab F6. It may be seen that it is a "structural mechanism" (Fig. 5.3) which developed in every direction and panel of the test structure. On the other hand, Figs. 6.22 and 6.23 show that the failure mechanism of the slabs with edge beams (represented by slab F4) were of the "slab mechanism" type involving only exterior spans (Fig. 5.1). The relative advantages and disadvantages of the two types of failure depend on the particular conditions of design. However, the fact that F6 failed almost simultaneously in all panels while the failure in F4 was isolated in panels ADG is a point decisively in favor of F6.

7. SUMMARY AND CONCLUSIONS

7.1 Basis for the Design of the Test Structure

A nine-panel flat slab was designed and built in order to study the effect of certain deviations in the amount and distribution of flexural reinforcement from the recommendations made in the ACI Building Code (1). These deviations were made in an effort to simplify the design and construction of flat slabs. They were:

(1) Flexural reinforcement was provided for the full static moment.

(2) The distribution of the reinforcement was not made in strict accordance with the distribution of moments in the elastic uncracked structure: (a) the reinforcement spacing was the same at all strips of a given design section as indicated in Figs. 2.9 and 2.10, (b) the ratio of the positive and negative design moments was modified arbitrarily to make the use of only two different steel spacings throughout the structure possible, and (c) no design moment was assigned to the peripheral negative moment sections.

The assumed design loads were 200 psf LL and 85 psf DL.

7.2 Description of the Test Structure

A plan view and section of the test structure are shown in Figs. 2.4 and 2.5. The arrangement of the reinforcement is shown in Figs. 2.9 and 2.10. Key material properties were a concrete strength of 4,000 psi and steel yield stress of 43,000 psi.

The structure was loaded through a hydraulic system at sixteen points per panel, the load being applied to each panel by a determinate "loading tree" controlled by one jack. At each load increment, steel strains were recorded and deflections were measured at mid-panel and mid-span of column center lines by means of dials sensitive to 0.001 in. The load was applied in continually increasing increments until failure occurred about six hours after testing began. The maximum total load sustained by the structure was 890 psf.

7.3 Working Loads

(a) Stresses at Working Loads

The steel stresses at working load levels are an important parameter in the evaluation of the effects produced on the behavior of the test structure by the changes introduced in the design procedure. The maximum steel stress in the test structure at design load was on the order of 10,000 psi. The reason for this is that at the design load level, the slab is relatively uncracked and the applied moments were resisted primarily by tension in the concrete. If the concrete were of lower strength the maximum steel stress could have been on the order of 20,000 psi as was the case in structure F2 (Fig. 6.16, f'_c = 2,800 psi). The steel area of the test structure at the region where this maximum stress occurs is about 25 percent greater than the area provided by the ACI Building Code. However the test structure was designed for the full static moment rather than a fraction of it, which is what the Code recommends. The uniform distribution of steel across the design sections can not be recommended if the definition of the static moment adopted by the ACI Building Code is used.

An approximate estimate can be made of the steel stresses to be expected in any design if it is recognized that the magnitude of the steel stress is a function of three factors: (a) the static moment assumed in the design, (b) the steel distribution and (c) the concrete strength. The first two factors define the steel quantity, thus the yield moment at any particular section in the slab. The last factor defines the cracking moment of the same section. Once these two moments are known a curve similar to that shown in Fig. 6.11 may be used to approximate the steel stress if an estimate of the moment applied at the section in question can be made.

(b) Moments at Working Loads

The moment distribution in the test structure at design load was essentially elastic since the slab was not cracked to any appreciable extent. In this respect the moment distribution in F6 is very similar to any slab designed by the ACI Building Code, and the comparison has been made with slab F3 in Figs. 6.14 and 6.15. However, since the test structure had no edge beams the positive moments at the edge were higher than for the slabs with edge beams.

(c) Deflection and Cracking

Figures 6.1 and 6.2 show the load-deflection relationships for the test structure as well as those for structures F2, F3, F4 and F5. For the test structure deflections at design load were on the order of L/600 for the center of a corner panel and L/1600 for the center of the interior panel.

Insofar as the load-deflection relationships at the mid-panel are concerned there was little difference between the behavior of the

test structure and that of the structures designed by the ACI Building Code. Any variation can be ascribed to the difference in concrete properties.

The measured edge deflections are interesting since no spandrel beams were used. A comparison of the edge deflections of the test structure with the deflections of the edge beams of the other structures is made in Fig. 6.2 (A1: Shallow, Deep; and D2: Shallow, Deep). The deflections of F6 at the edge are about three times as large as the deflections of the deep beams and about 50 percent larger than the deflections of the shallow beams of the other structures of comparable concrete strength. However the absolute differences of deflection at the mentioned locations are of small magnitude and on the order of L/1500 and L/4000, respectively.

Cracking could not be discerned on the test structure at design load, but some strain gages indicated that cracks had developed in negative moment regions (Fig. 4.9).

Long term loading and/or weaker concrete strength would have increased the deflections of structure F6. However the deflections of this structure under these conditions would have been less than those of a similar structure designed by the ACI Building Code since larger quantities of steel were placed in the high moment areas of the test structure.

7.4 Performance of the Test Structure During Loading to Failure

The difference in the design of the test structure from the design of the other structures becomes rather important at higher stages of loading.

(a) Mode of Failure

The test structure failed by simultaneous flexural yielding of all the panels. Its failure load was closely predicted by a yield line analysis which was the main criterion in the proportioning of the reinforcement. There was no evidence of torsional distress and although shearing distress occurred at some columns, it was connected with the compressive crushing of the concrete which occurred at large deflections. The results of this test showed that it is possible to design a well-balanced structure with an explicit factor of safety by considering the mode of failure in the design procedure.

The structures designed by the ACI Building Code (F2, F3 and F4) showed signs of severe torsional distress in the beam-column connections and failed by the formation of localized failure mechanisms. Another structure investigated at the University of Illinois, a flat plate (F1), designed according to the ACI Building Code failed in shear at an interior column. Structure F5 which was designed for the full static moment without considering the mode of failure also failed through the formation of a localized yield line mechanism.

(b) Moment Redistribution

As mentioned in Section 7.1 the steel in the test structure was distributed independently of the elastic moment configuration in the slab. At working loads, the moment configuration in the slab was essentially elastic. However, the ratio of the assigned moment (the moment for which reinforcement was provided) to the elastic moment, was as high as two, e.g. at the exterior span positive moment design sections. The formation of yield lines throughout the slab showed that the strength of the steel

supplied in excess of the elastic moment proportions was developed in full. This is possible when the percentages of steel in the slab are low and the sections are ductile. In these cases the strength of the structure can be developed regardless of the sequence of yield line formation. It should be noted that negative moment yield lines will not form along the periphery of a slab unless provisions are made to transmit this moment to the supports.

(c) Deflections

The deflections at higher stages of loading in the exterior spans of the test structure were relatively lower than those of the other structures (Fig. 6.4). This was due to the higher moment capacity of the positive moment section in those spans. Since the positive moment yield line was prevented from forming until the limit load had been reached, the deflections of the structure up to the limit load were lower than what they would have been had the positive moment yield line developed well before the limit load was reached. Since in the structures designed by the ACI Building Code, the exterior span positive moment capacity was low and the negative moment restraint at the discontinuous edge was very small (Fig. 2.3), the exterior-span positive moment yield line formed at loads lower than the limit load, thus resulting in an increase of the deflection rate.

(d) Edge Beams

The lack of edge beams in the test structure simplified the formwork and increased the architectural pliability of the structure. From the engineering viewpoint, the torsional problem was eliminated at the expense of flexural stiffness along the edges. However, the edge deflections were tolerable.

REFERENCES

1. American Concrete Institute, Building Code Requirements for Reinforced Concrete, (ACI 318-56), 1956.

2. Hatcher, D. S., M. A. Sozen, and C. P. Siess, "A Study of Tests on a Flat Plate and a Flat Slab," Structural Research Series No. 217, Department of Civil Engineering, University of Illinois, July 1961.

3. Jirsa, J. O., M. A. Sozen, and C. P. Siess, "An Experimental Study of a Flat Slab Floor Reinforced with Welded Wire Fabric," Structural Research Series No. 249, Department of Civil Engineering, University of Illinois, June 1962.

4. Shewmaker, R. E., M. Xanthakis, and M. A Sozen, "Very Small Scale Reinforced Concrete Multi-Panel Flat Slabs," Structural Research Series No. 265, Department of Civil Engineering, University of Illinois, June 1963.

5. Nichols, J. R., "Statical Limitations upon the Steel Requirement in Reinforced Concrete Flat Slab Floors," Transactions, ASCE, Vol. 77, 1914, pp. 1670-1681 and discussion pp. 1682-1736.

6. Sozen, M. A., and C. P. Siess, "Investigation of Multi-Panel Reinforced Concrete Floor Slabs: Design Methods - Their Evolution and Comparison," Journal of the American Concrete Institute, Proceedings V. 60, No. 8, 1963, pp. 999-1028.

7. American Concrete Institute, Building Code Requirements for Reinforced Concrete, (ACI 318-63).

8. Wood, R. H., "Plastic and Elastic Design of Slabs and Plates," Ronald, N. Y., 1961.

9. Ingerslev, A., "The Strength of Rectangular Slabs," Journal of the Institute of Structural Engineers, Vol. 1, p. 3, London, 1923.

10. Johansen, K. W., "Beregnin af krydsarmerede Jarenbetonpladers Brudmoment," Bygningsstatike Meddelonsen (Copenhagen), Vol. 3, 1931. (See also: Hognestad, E., "Yield-Line Theory for the Ultimate Flexural Strength of Reinforced Concrete Slabs," Proc. ACI, Vol. 49, 1953, p. 637; Ferguson, P. M., "Reinforced Concrete Fundamentals," John Wiley and Sons, N. Y., 1958, p. 251.)

11. Vanderbilt, M. D., M. A. Sozen, and C. P. Siess, "Deflections of Reinforced Concrete Floor Slabs," Structural Research Series No. 263, Department of Civil Engineering, University of Illinois, April 1963.

12. Nielsen, N. J., "Bestemmelse af Spaendinger i Plader ved Anvendelse af Differensligninger," Copenhagen, 1920.

13. Corley, W. G., M. A. Sozen, and C. P. Siess, "The Equivalent Frame Analysis for Reinforced Concrete Slabs," Structural Research Series No. 218, Department of Civil Engineering, University of Illinois, June 1961.

TABLE 2.1

COMPARISON OF STEEL AREAS AT VARIOUS DESIGN SECTIONS

Design Location	Area of Steel in Square Inches				
	Structure F_2	Structure F_3	Structure F_4	Structure F_5	Structure F_6
Interior Middle Strip	A_s	A_s	$16A_s$	$16A_s$	$16A_s$
Interior Positive	0.172	0.182	0.170	0.262	0.270
Exterior Positive	0.234	0.228	0.232	0.370	0.530
Interior Negative	0.203	0.184	0.200	0.262	0.530
Exterior Negative (SB)	0.141	0.135	0.139	0.170	0
Exterior Negative (DB)	0.234	0.231	0.232	0.170	0
Exterior Middle Strip					
Interior Positive	0.172	0.192	0.170	0.278	0.270
Exterior Positive	0.234	0.238	0.232	0.401	0.530
Interior Negative	0.203	0.184	0.200	0.293	0.530
Exterior Negative (SB)	0.141	0.135	0.139	0.170	0
Exterior Negative (DB)	0.234	0.231	0.232	0.170	0
Column Strip					
Interior Positive	0.234	0.231	0.232	0.262	0.270
Exterior Positive	0.281	0.262	0.278	0.370	0.530
Interior Negative	0.422	0.429	0.417	0.509	0.530
Exterior Negative (SB)	0.328	0.303	0.324	0.278	0.290
Exterior Negative (DB)	0.265	0.231	0.262	0.278	0.290

continued on next page

TABLE 2.1 (continued)

COMPARISON OF STEEL AREAS AT VARIOUS DESIGN SECTIONS

Design Location	Area of Steel in Square Inches				
	Structure F_2	Structure F_3	Structure F_4	Structure F_5	Structure F_6
Wall Strip	A_s	A_s	$16A_s$	$16A_s$	$16A_s$
Shallow Beam Side					
Interior Positive	0.125	0.122	0.123	0.077	0.135
Exterior Positive	0.156	0.141	0.154	0.108	0.265
Interior Negative	0.234	0.215	0.232	0.139	0.265
Exterior Negative (SB)	0.218	0.200	0.216	0.108	0.107
Exterior Negative (DB)	0.234	0.221	0.232	0.108	0.107
Deep Beam Side					
Interior Positive	0.078	0.080	0.077	0.046	0.135
Exterior Positive	0.078	0.080	0.077	0.046	0.265
Interior Negative	0.109	0.140	0.108	0.046	0.265
Exterior Negative (SB)	0.123	0.122	0.123	0.046	0.107
Exterior Negative (DB)	0.094	0.091	0.093	0.046	0.107

TABLE 3.1

LOADING SCHEDULE

Note: Throughout the entire test all the panels were equally loaded.

All values of nominal uniform load include the weight of the slab and the load distributing system, total 23 psf.

Load No.	Time	Load (psf)	Increment (psf)
0	-	23	
			27
1	10:05	50	
			25
2	10:25	75	
			32
3	10:37	107	
			20
4	10:58	127	
			26
5	11:13	153	
			23
6	11:28	176	
			49
7	11:43	225	
			51
8	12:02	276	
			51
9	12:31	327	
			50
10	12:54	377	
			152
11	13:12	529	
			48
12	13:35	577	
			59
13	13:52	636	
			54
14	14:04	690	
			40
15	14:19	730	
			50
16	14:44	780	
			40
17	15:07	820	
			55
18	15:24	875	
			15
19	15:45	890	
			-2
20	16:00	888	
			-9
21	16:12	879	
			-9
22	16:26	870	
			-847
23	16:36	23	

TABLE 6.1

MATERIAL PROPERTIES OF COMPARED SLABS

Structure	Reinforcement	f_y (ksi)	f'_c (psi)	E_c (10^6 psi)	f_t (psi)	f_r (psi)
F2	1/8" Square plain bars	42	2800	3.1	-	600
F3	Welded Wire Fabric	70*	4000	3.7	-	750
F4	0.0355 ø Annealed Wire	46	3700	3.7	460	-
F5	0.0355 ø Annealed Wire	48	3100	3.1**	-	-
F6	0.0355 ø Annealed Wire	43	4000	3.0	400	780

* At 0.002% offset.

** Estimated at 3.1 since it was not directly measured.

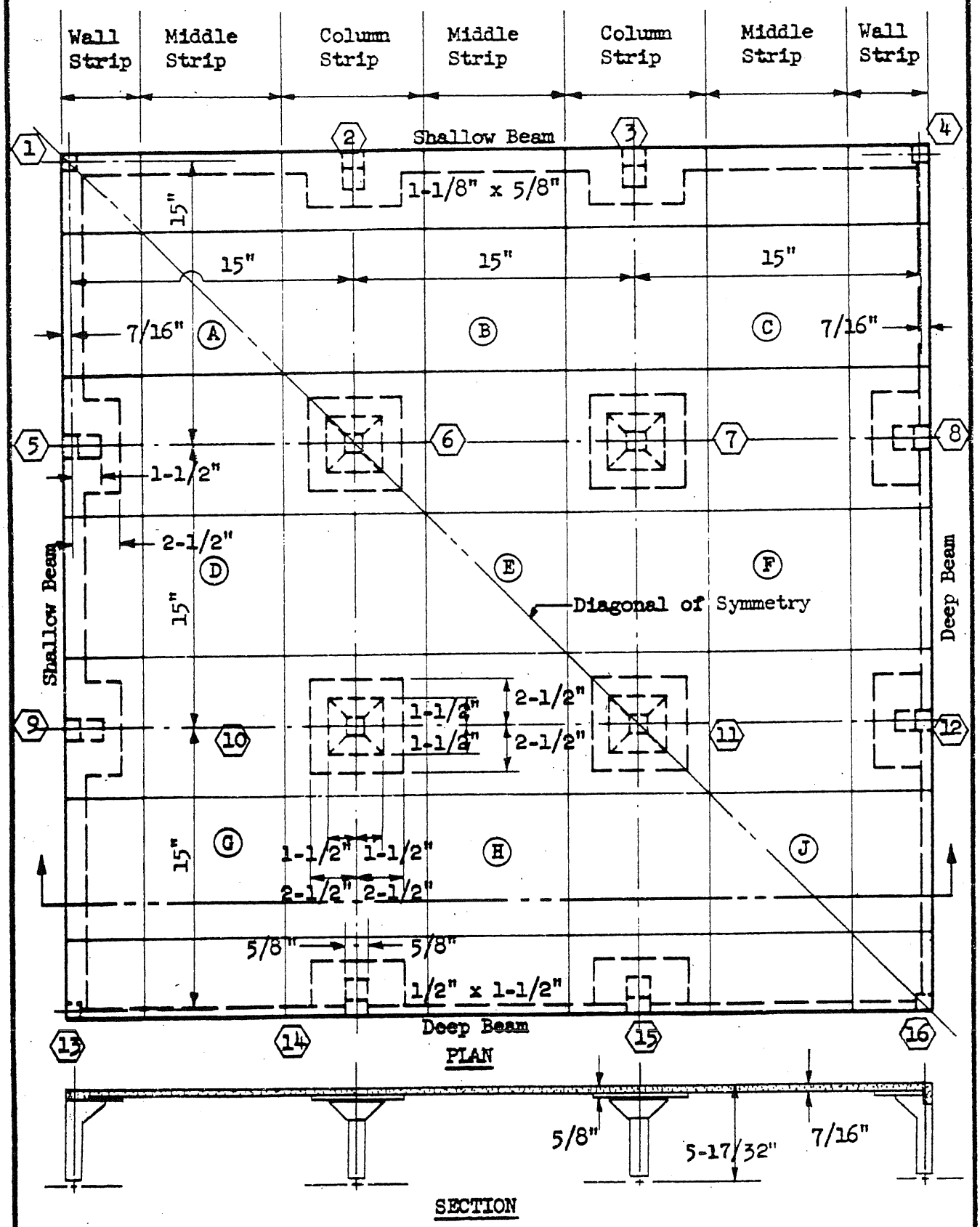

FIG. 2.1 LAYOUT OF STRUCTURES F4 AND F5

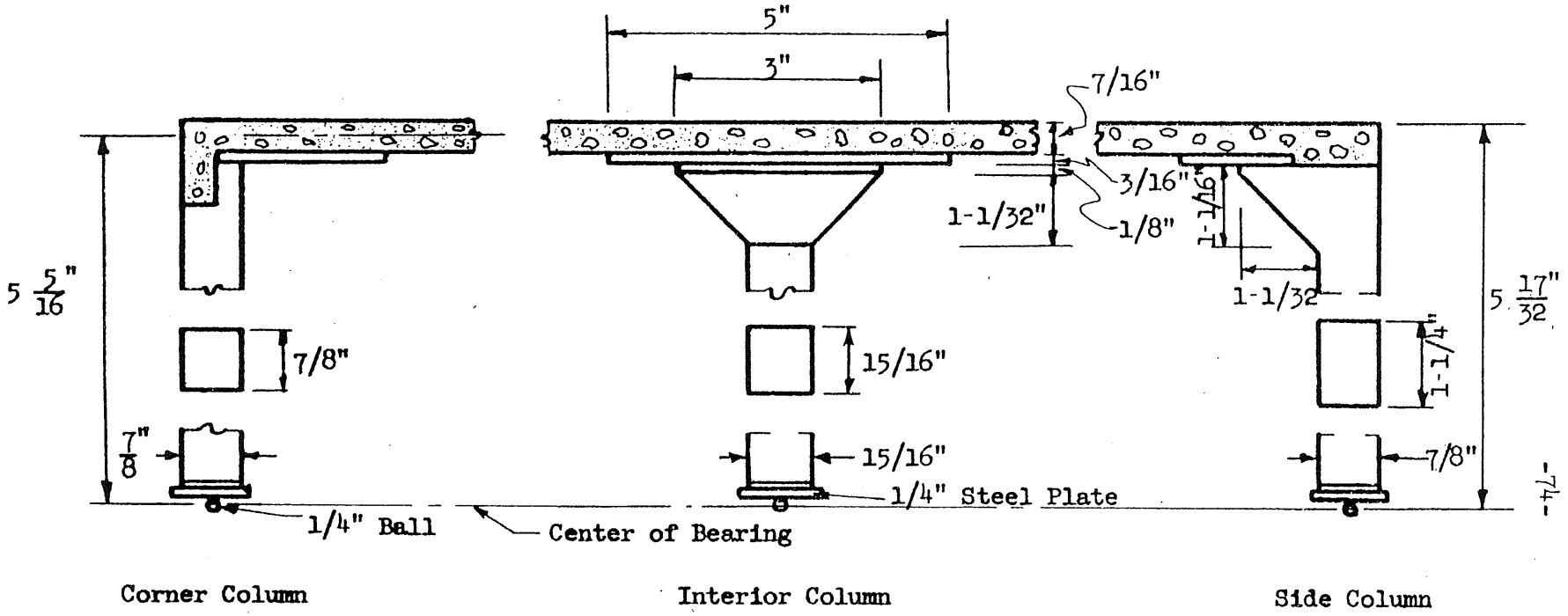

FIG. 2.2 COLUMN DETAIL, STRUCTURES F4 AND F5

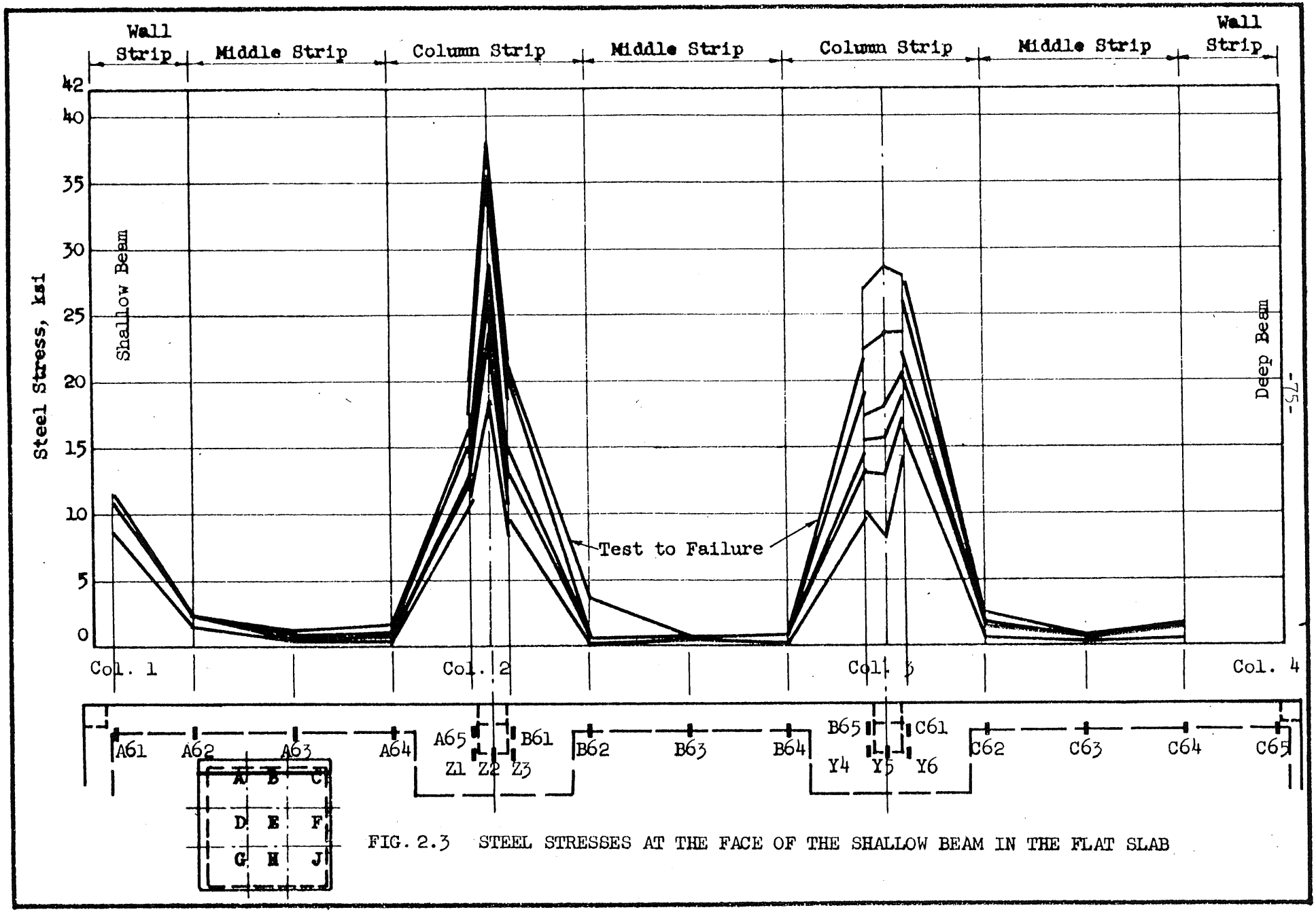

FIG. 2.3 STEEL STRESSES AT THE FACE OF THE SHALLOW BEAM IN THE FLAT SLAB

Note:

Columns labeled by numbers 1 to 16

Panels labeled by letters A, B, C, D, E, F, G, H, J

Symmetry about both diagonals and side center lines

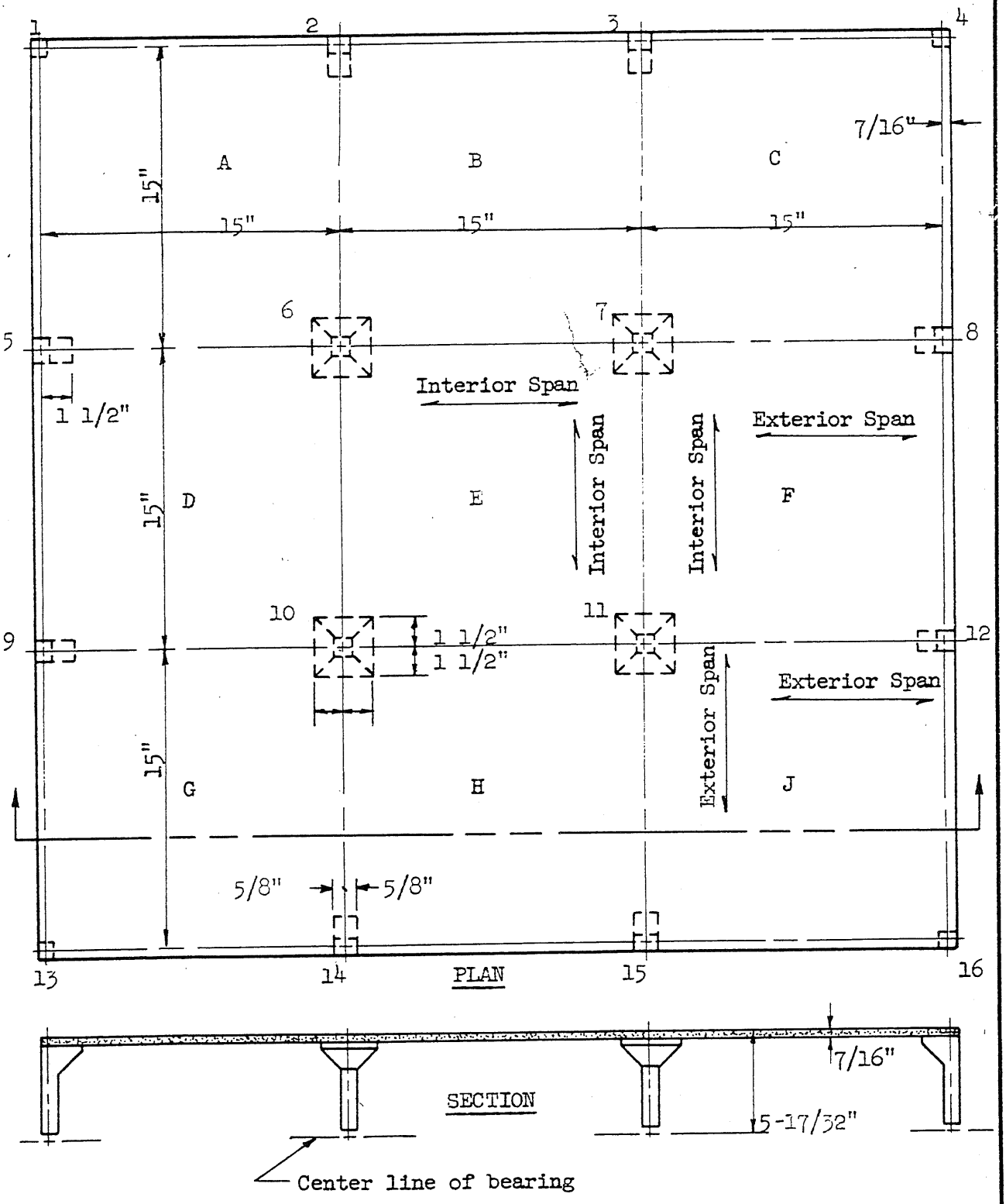

FIG. 2.4 TEST STRUCTURE LAYOUT

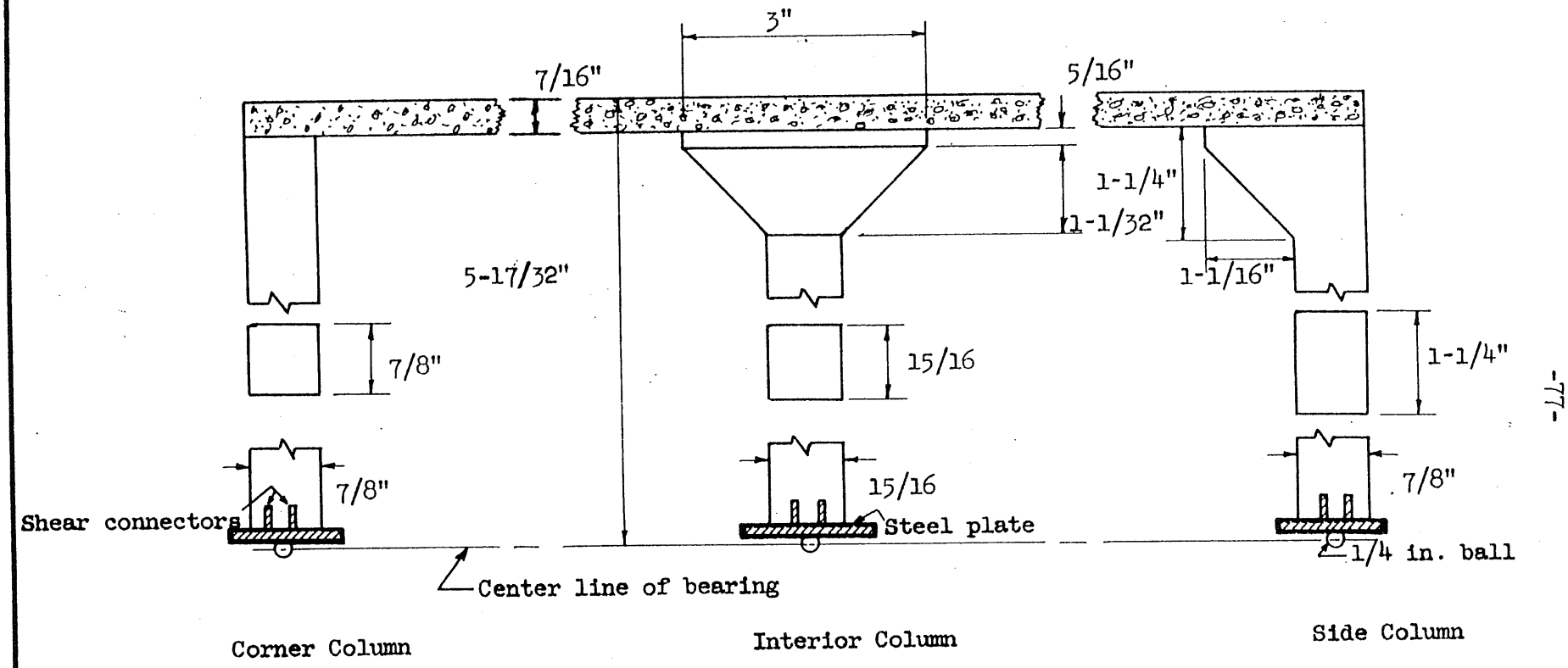

FIG. 2.5 TEST STRUCTURE COLUMN DETAIL

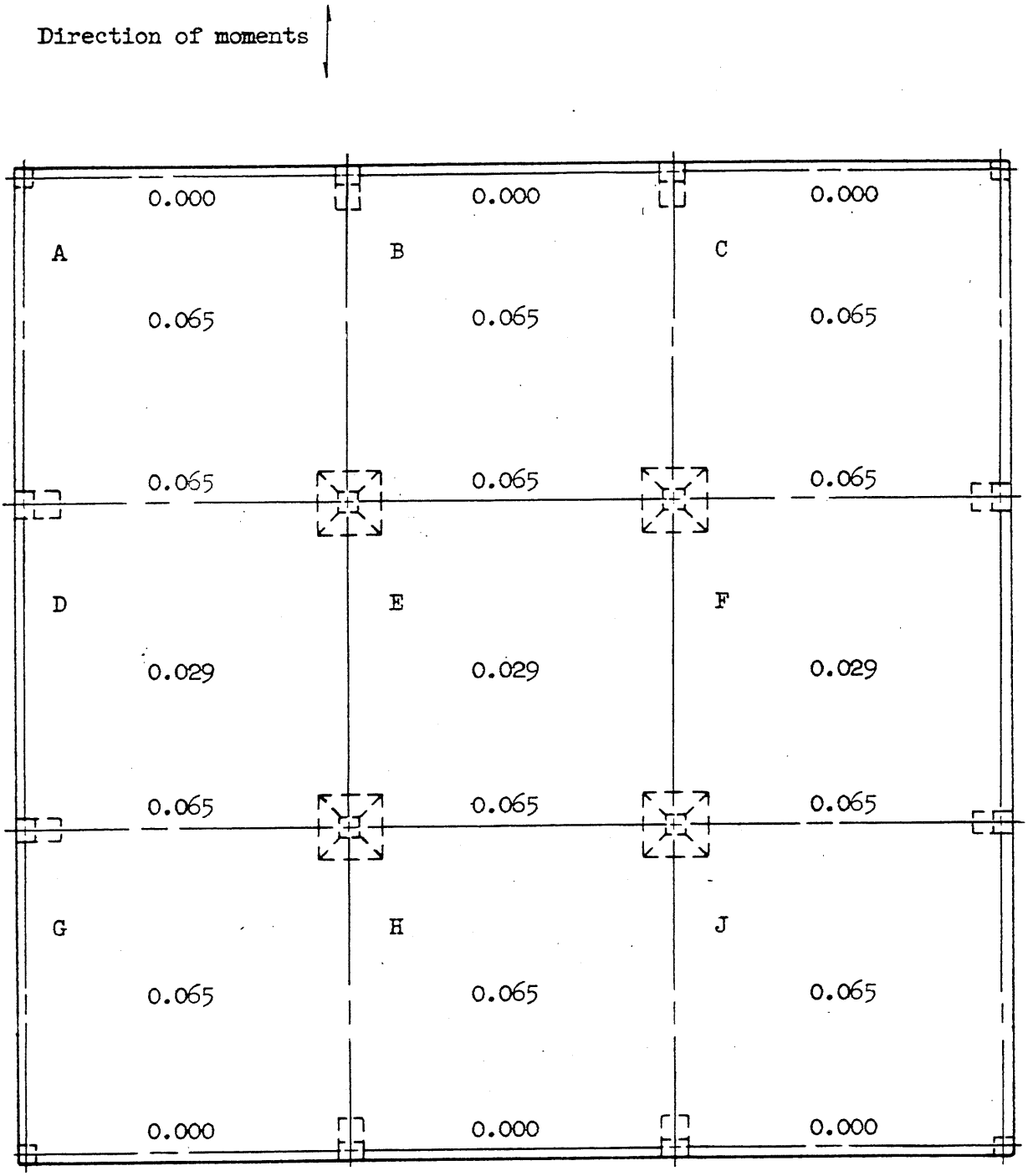

Note: Moments are given in coefficients of M/WL
Moments extend across full width of panel

FIG. 2.7 DESIGN MOMENT COEFFICIENTS IN STRUCTURE F6

Direction of moments ↕

Coefficients of structures F2, F3 and F4

Shallow Beam	Wall Strip	Middle Strip	Column Strip	Middle Strip	Column Strip	Middle Strip	Wall Strip	Deep Beam
0.012	0.013	0.007	0.028	0.007	0.028	0.007	0.006	0.022
0.016	0.009	A 0.013	0.016	B 0.013	0.016	C 0.013	0.004	0.025
0.019	0.018 / 0.018	0.011	0.037 / 0.033	0.011	0.037 / 0.033	0.011	0.009	0.035
0.012	0.007	0.010 D	0.013	0.010 E	0.013	0.010 F	0.003	0.017
0.019	0.018	0.011	0.033 / 0.037	0.011	0.033 / 0.037	0.011	0.009	0.035
0.016	0.009	0.013 G	0.016	0.013 H	0.016	0.013 J	0.004	0.025
0.012	0.014	0.013	0.016	0.013	0.016	0.013	0.004	0.025

NOTE: Moments are given as coefficients of M/WL
Moments extend across the width of design strips

FIG. 2.8 DESIGN MOMENT COEFFICIENTS IN THE FLAT SLAB ACCORDING TO ACI 318-56

NOTE: All bars 0.0355 in. diameter
Symmetry along both diagonals and side center lines

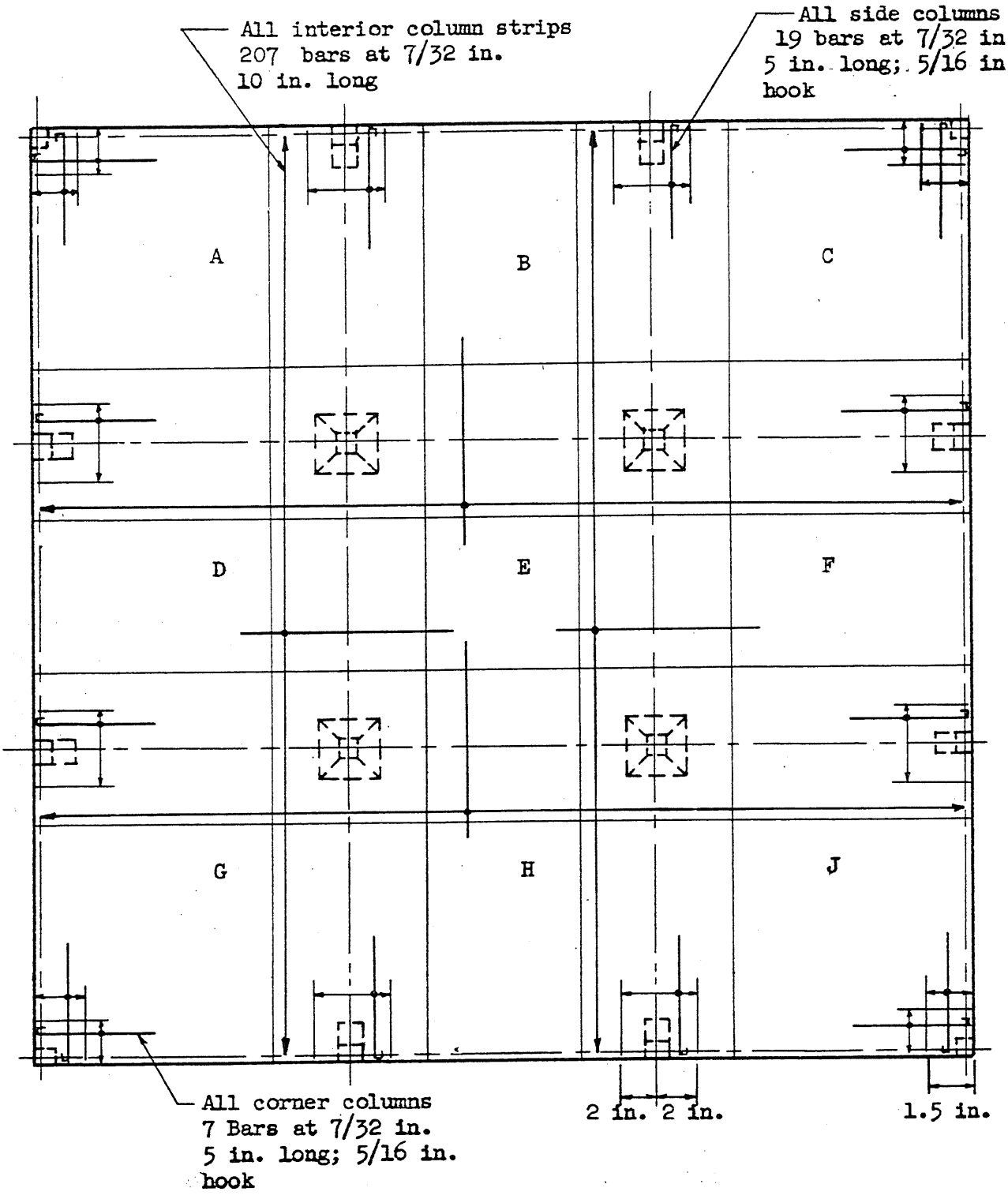

FIG. 2.9 TEST SLAB TOP STEEL

NOTE: All bars 0.0355 in. diameter
Symmetry along both diagonals and side center lines

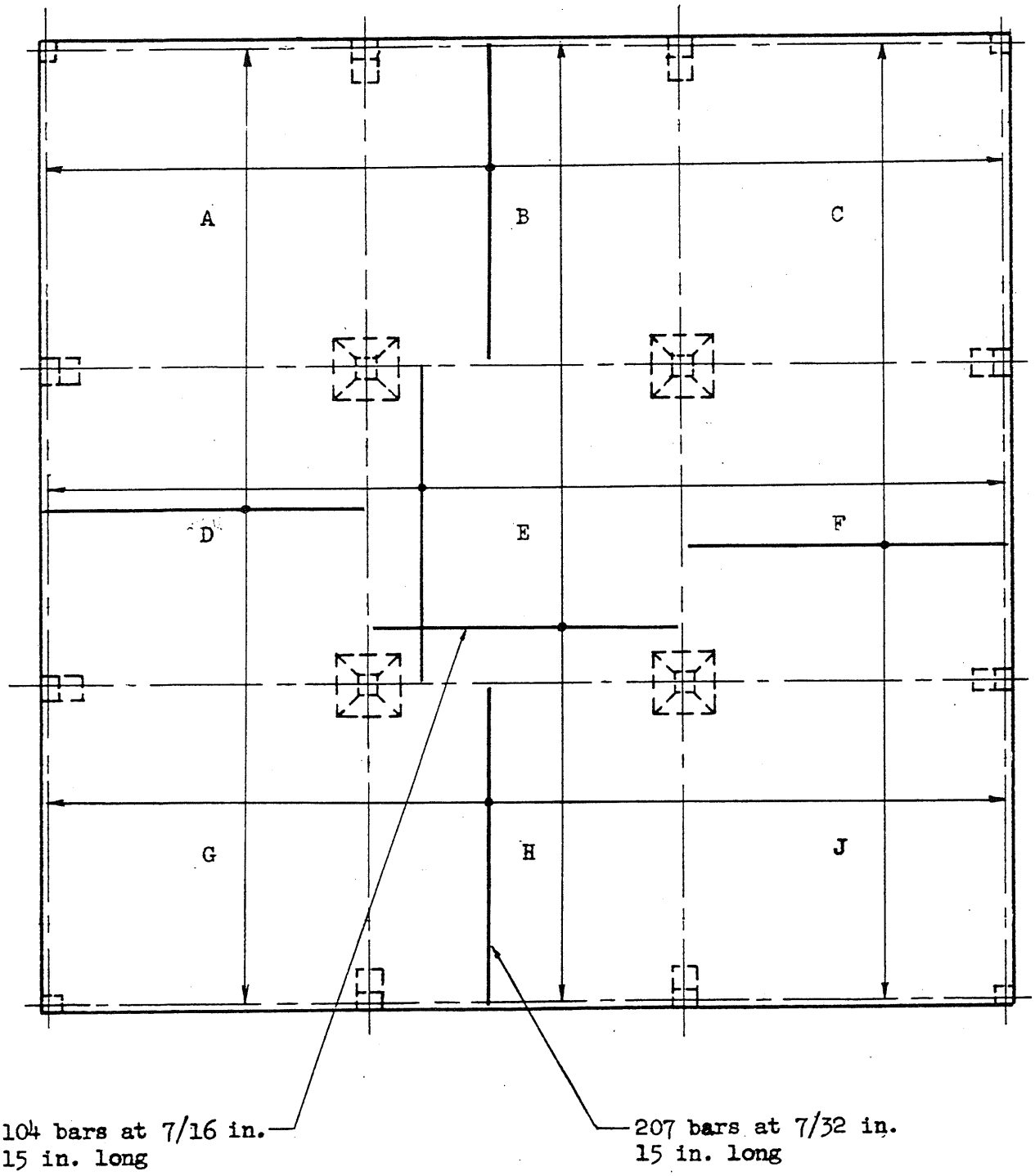

Fig. 2.10 TEST SLAB BOTTOM STEEL

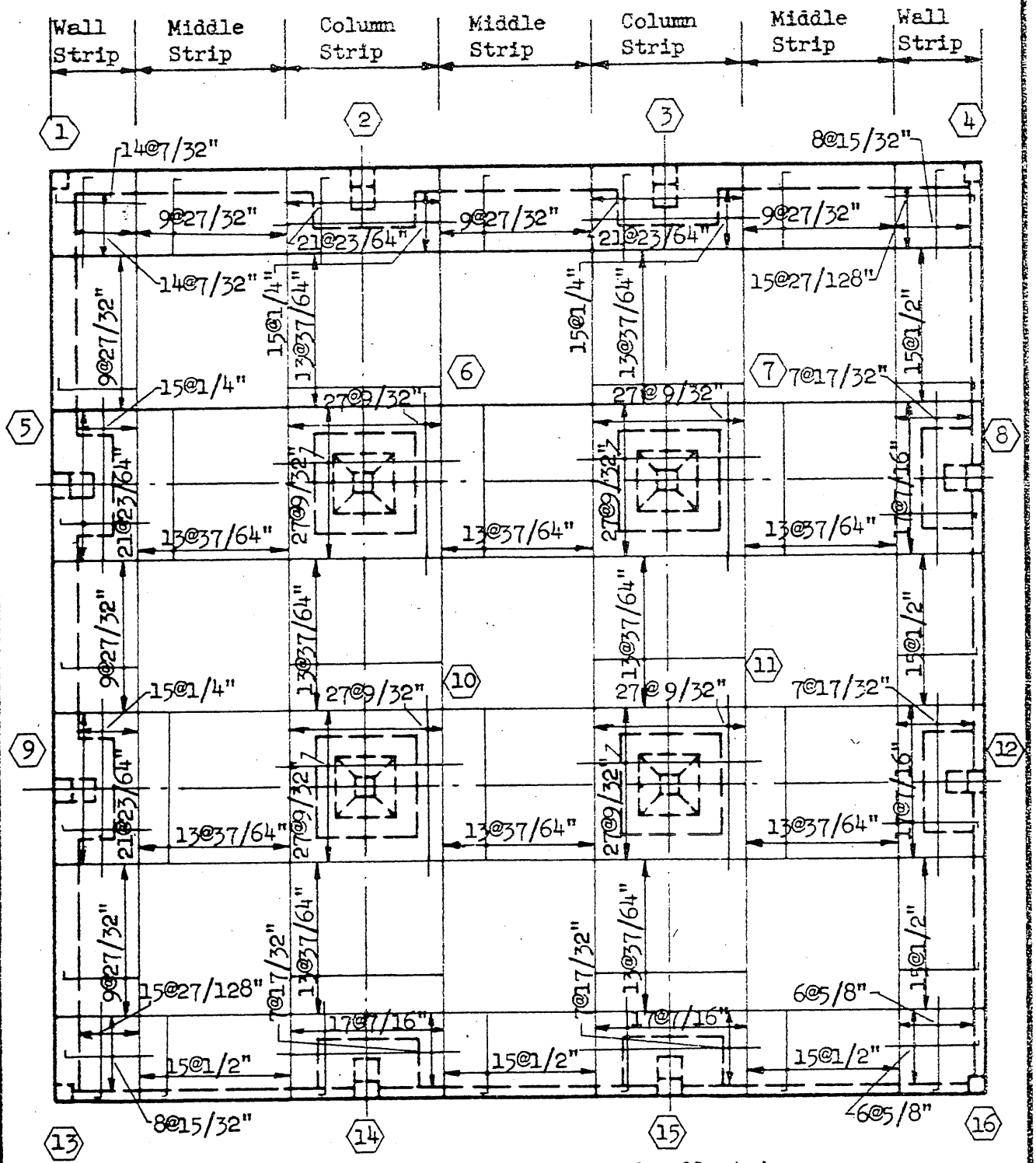

Note: Bars over interior columns of column and wall strips were alternately 7-1/2 and 9-15/16" in length. Bars over exterior columns of column strip were alternately 5-11/16 and 4-7/16" in length with a 1/2" hook. Bars in interior of middle strip were 7-1/2" in length. Bars at the end of the middle strip were 4-7/16" in length with a 1/2" hook. Bars over exterior columns of wall strip were alternately 5-3/16 and 4-7/16" in length with a 1/2" hook. Bar diameter 0.0355".

FIG. 2.11 STRUCTURE F4, NEGATIVE MOMENT REINFORCEMENT

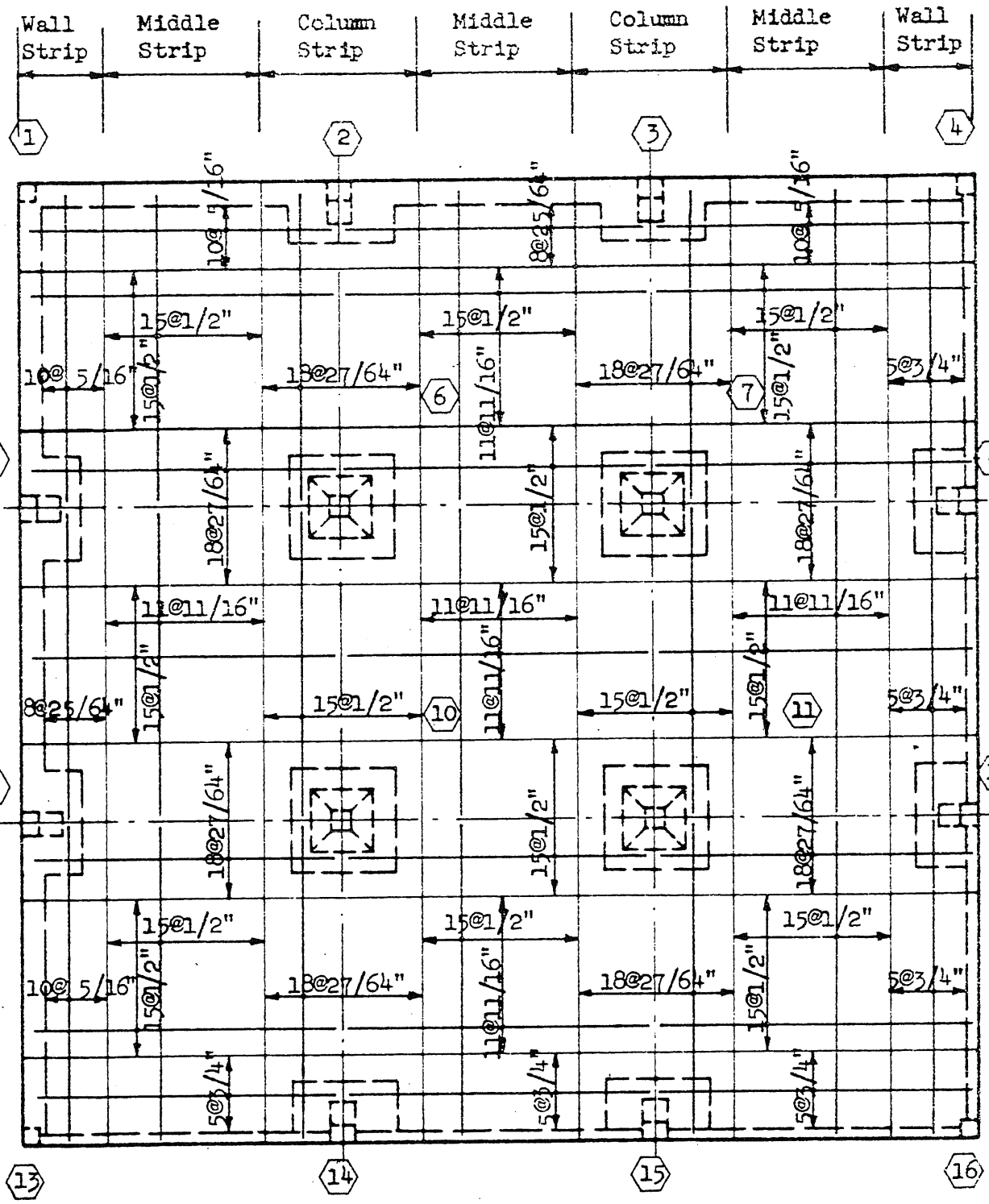

Note: All bars in column strips were 11-1/4" in length. All bars in middle were 15-1/8" and 13-1/16" in length and were placed alternately. All bars in wall strips were 13" in length. All bar diameters were 0.0355".

FIG. 2.12 STRUCTURE F4, POSITIVE MOMENT REINFORCEMENT

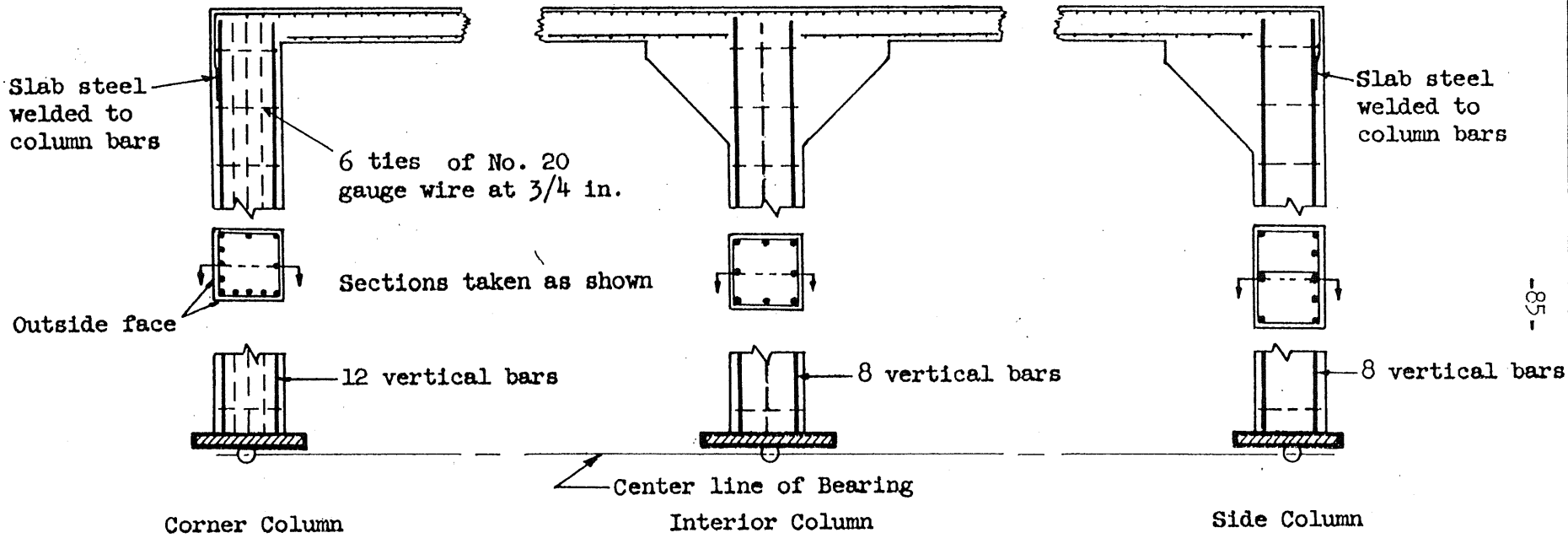

Note: All vertical column reinforcement of 16 gauge wire of f_y = 42 ksi
(0.063 in Φ and 0.00312 sq. in. cross sectional area)
Cover of 1/16 in.

FIG. 2.13 COLUMN REINFORCEMENT AND CONNECTION DETAIL

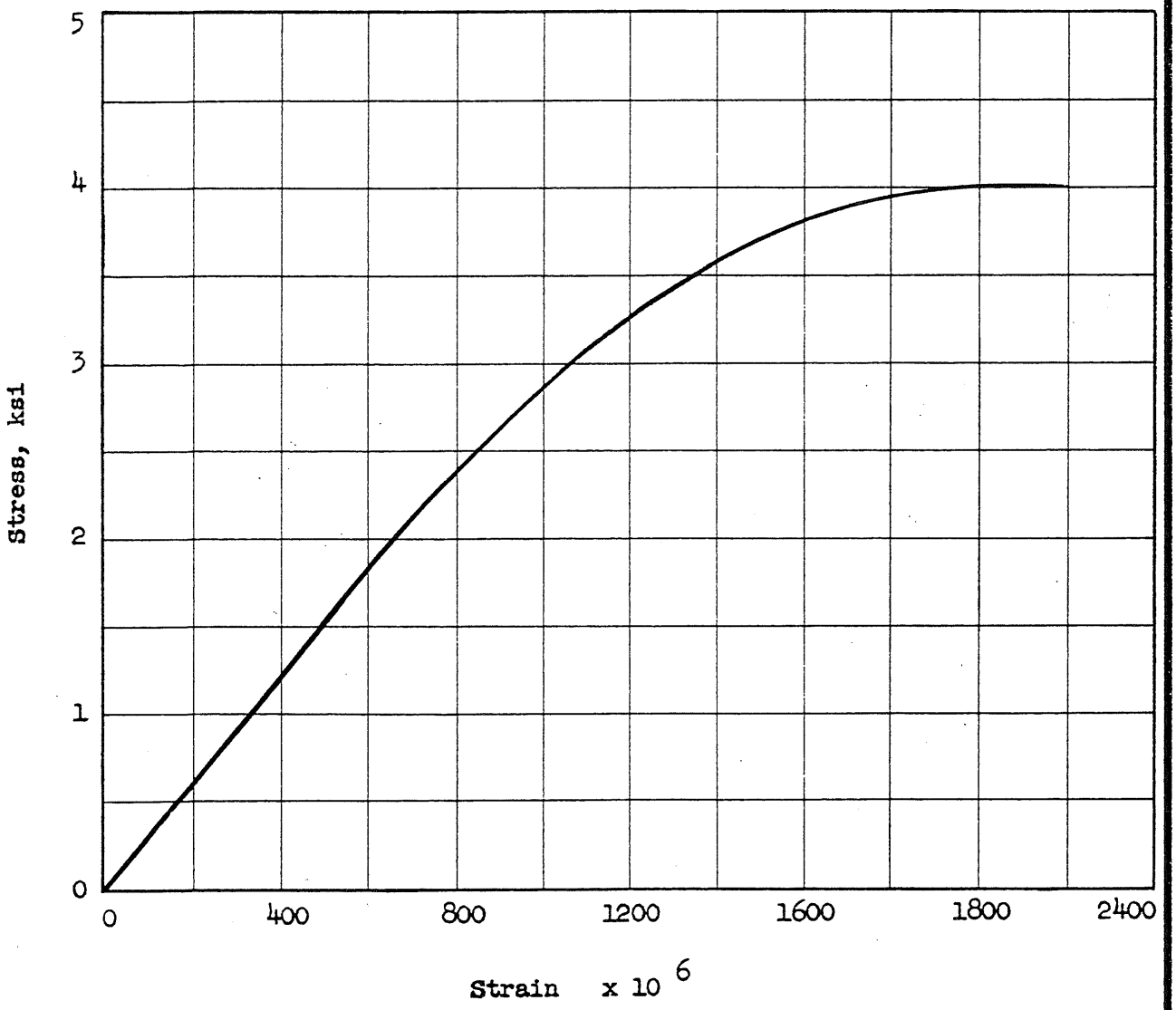

Typical values:

E_c = 3,000,000 psi

f_c = 4,000 psi

f_t = 400 psi (split cylinder)

f_r = 780 psi (beams)

FIG. 2.14 CONCRETE STRESS-STRAIN RELATIONSHIP

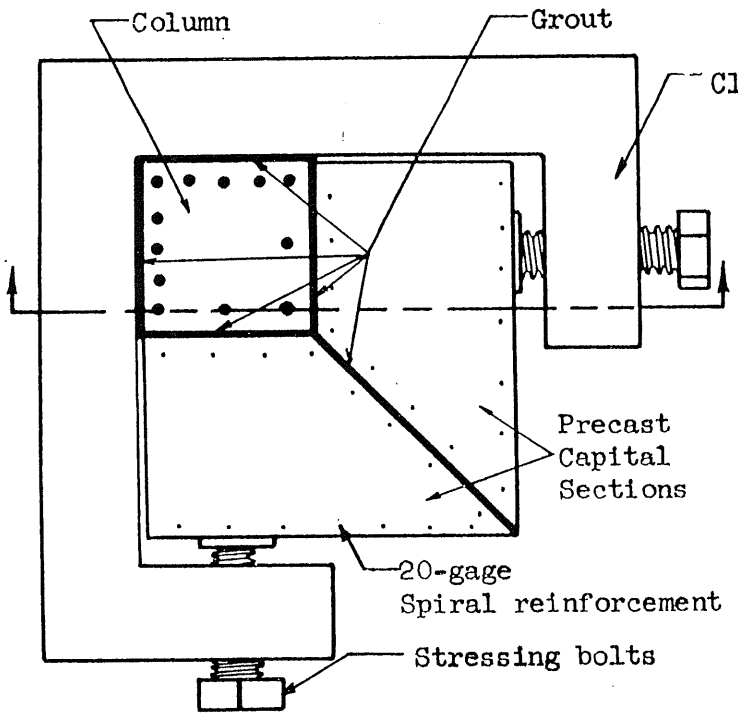

(a) Plan of precast capital in place

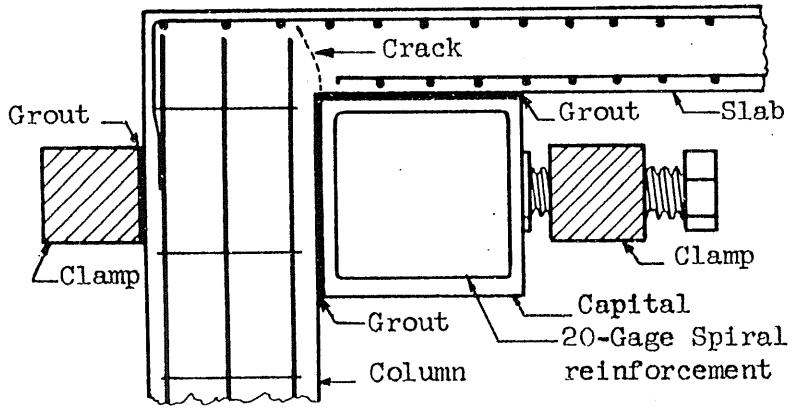

(b) Profile of capital in place

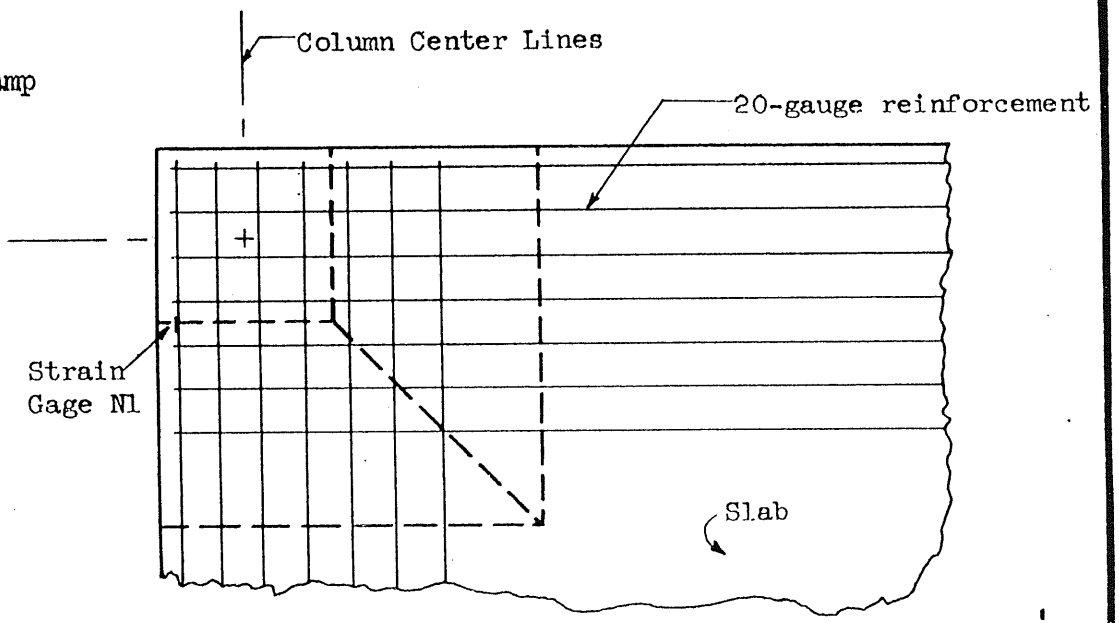

(c) Reinforcement layout over corner column

(d) View of clamp and capital of Column 4 in place.

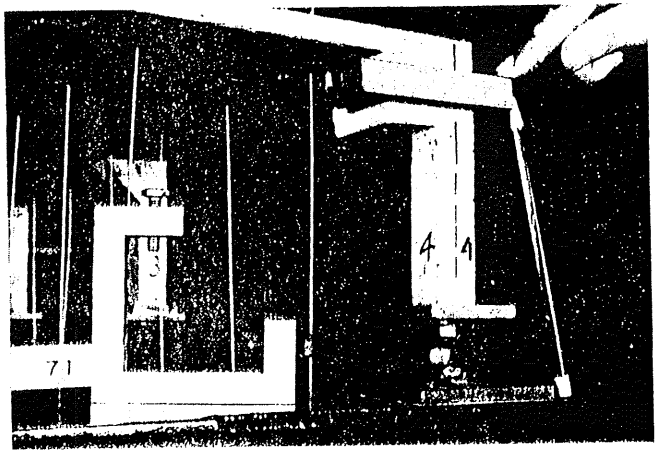

FIG. 2.15 PRECAST CORNER-COLUMN CAPITALS

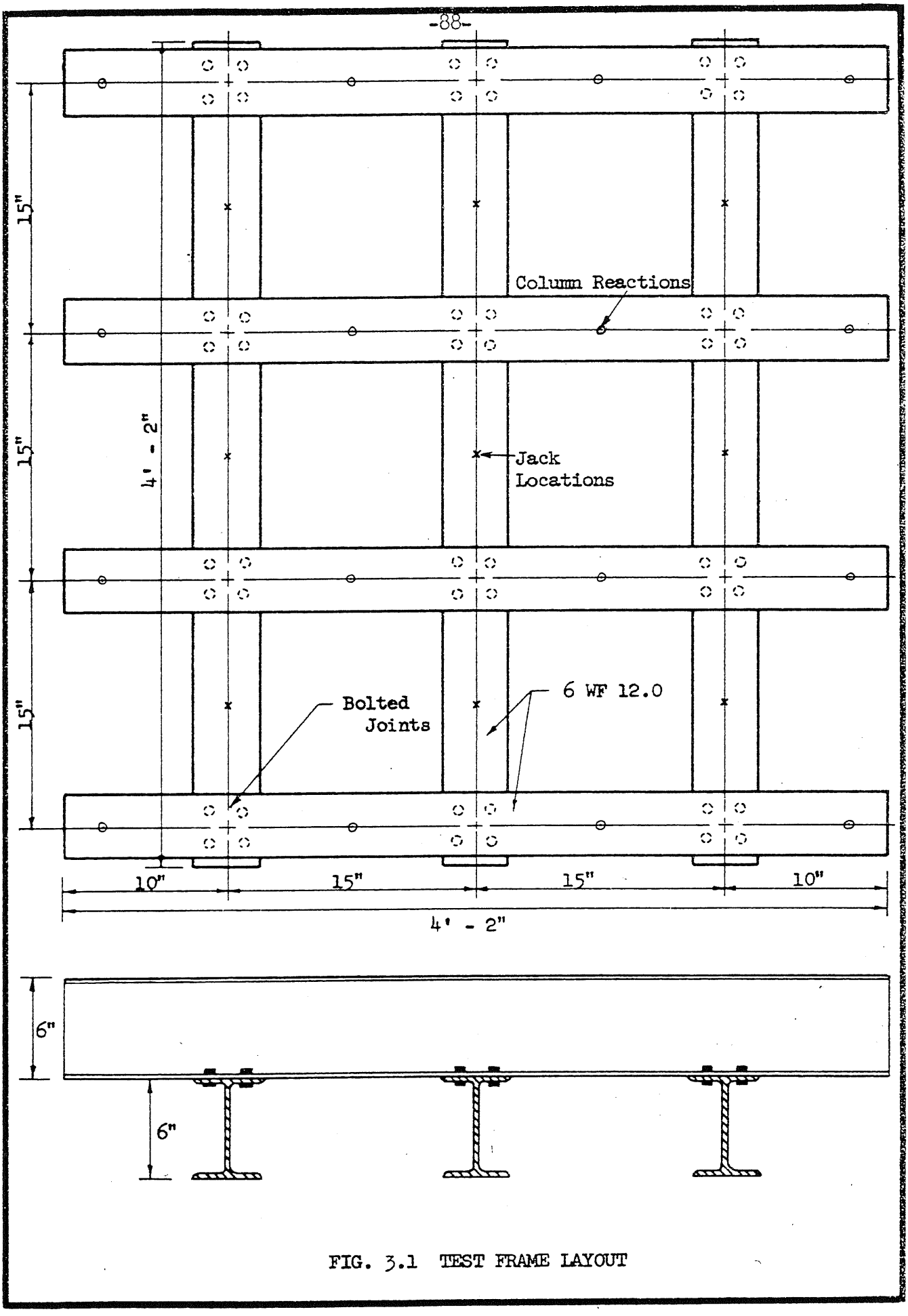

FIG. 3.1 TEST FRAME LAYOUT

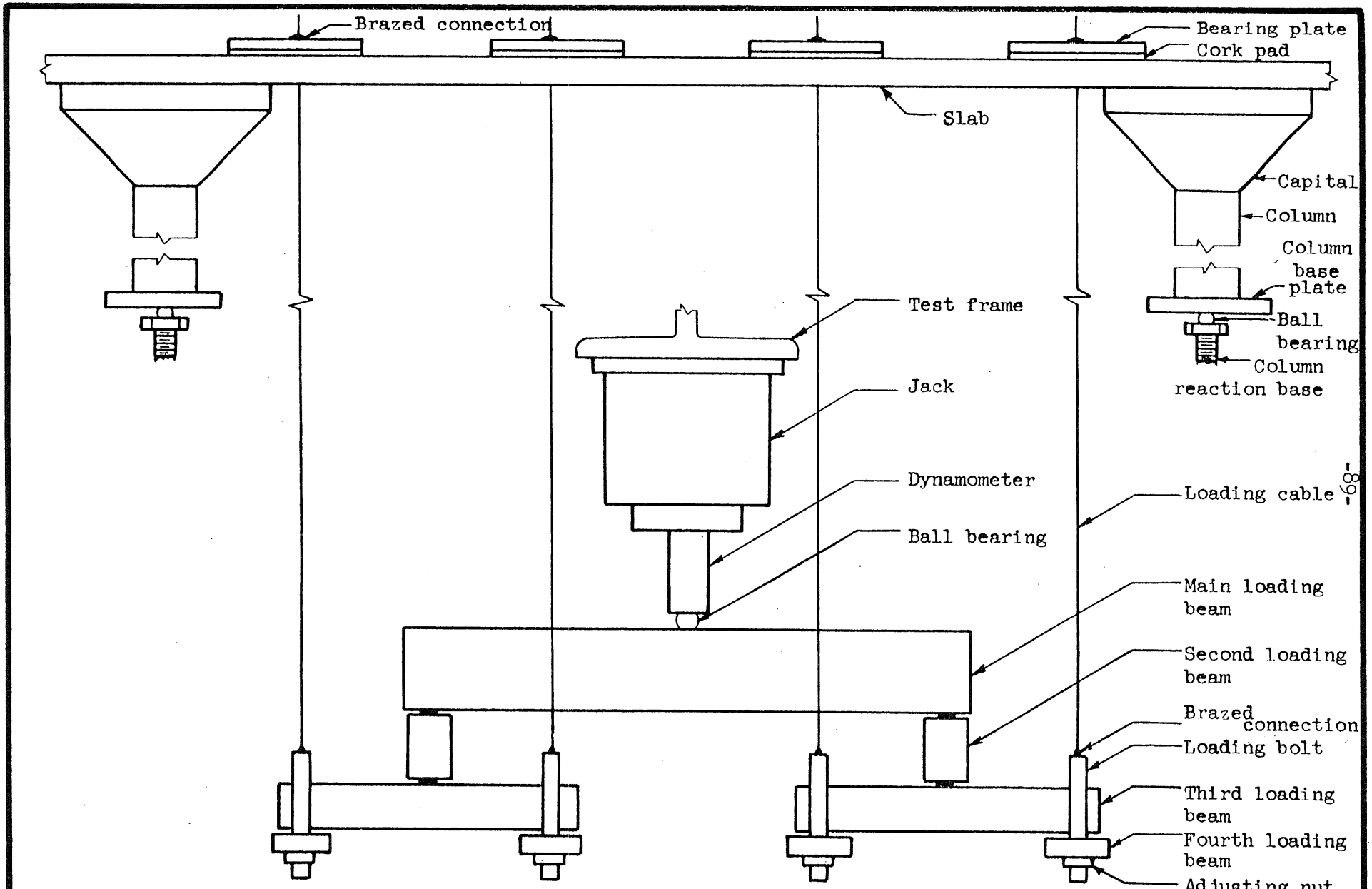

FIG. 3.2 LOADING SYSTEM FOR ONE PANEL

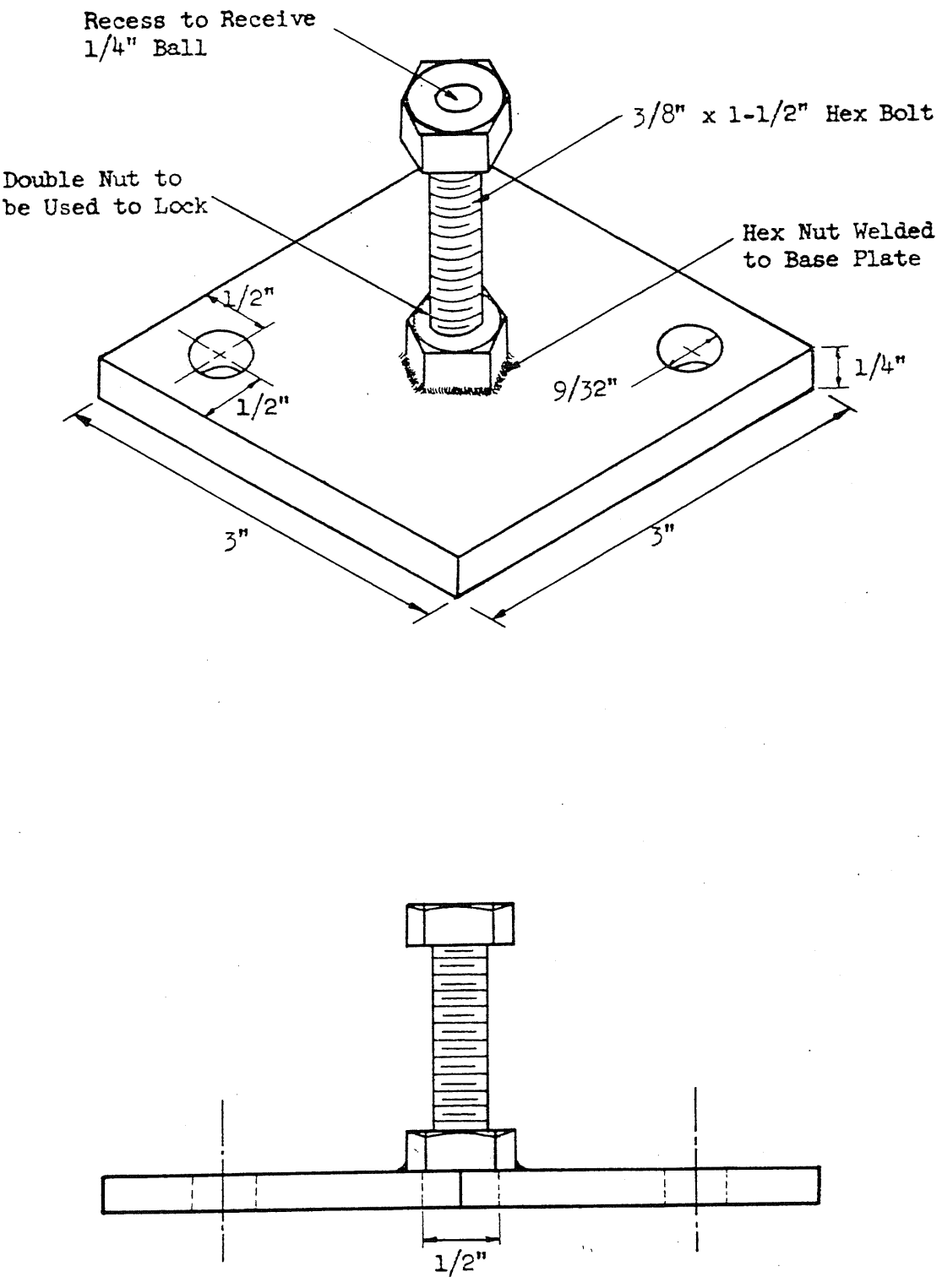

FIG. 3.3 ADJUSTABLE COLUMN REACTION BASE

All gages: Budd Metalfilm
Type C6 - 1 x 1 - 32A

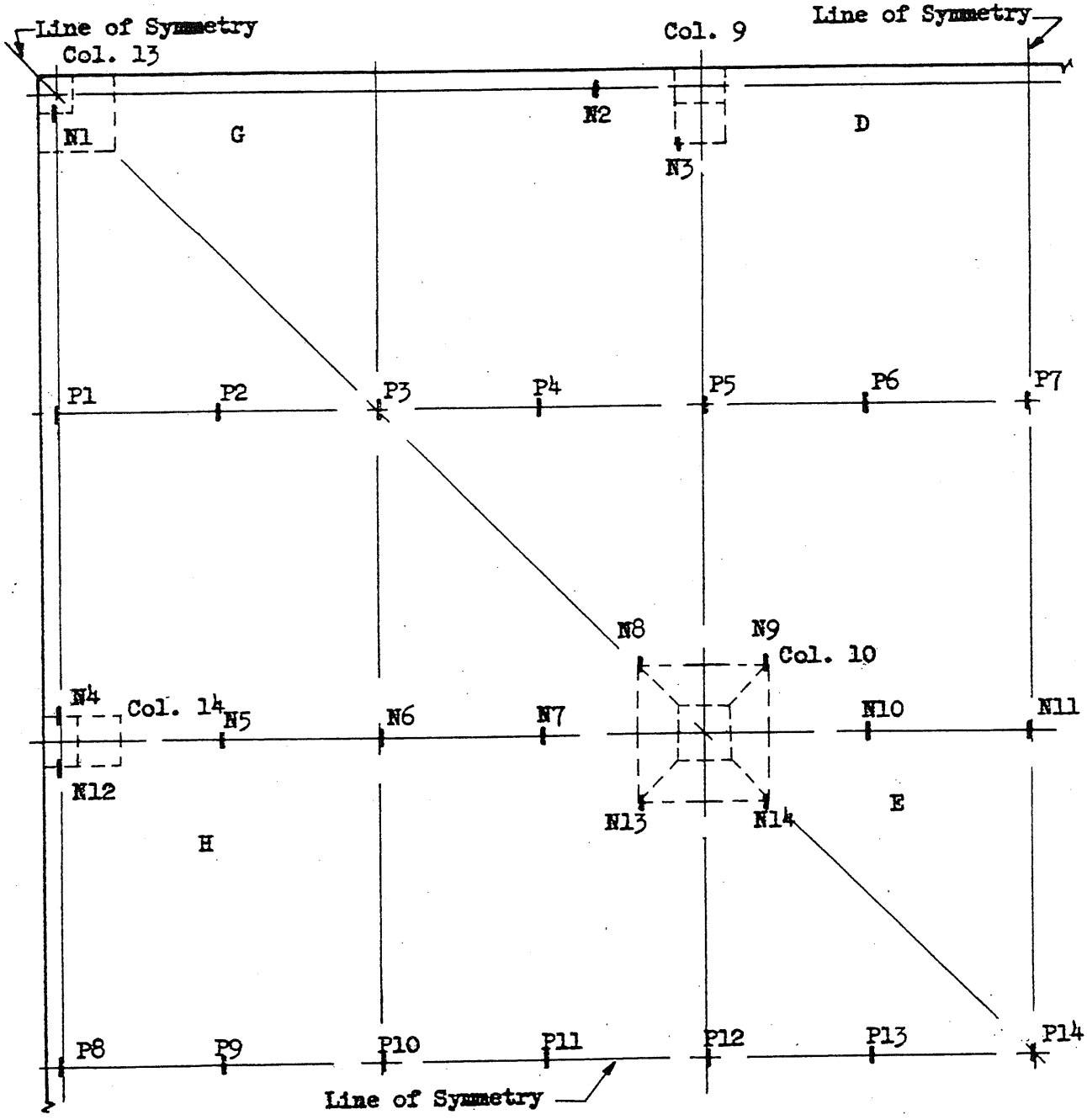

Note: "P" means gage applied to positive moment reinforcement
"N" means gage applied to negative moment reinforcement

FIG. 3.4 STEEL STRAIN GAGE LOCATIONS

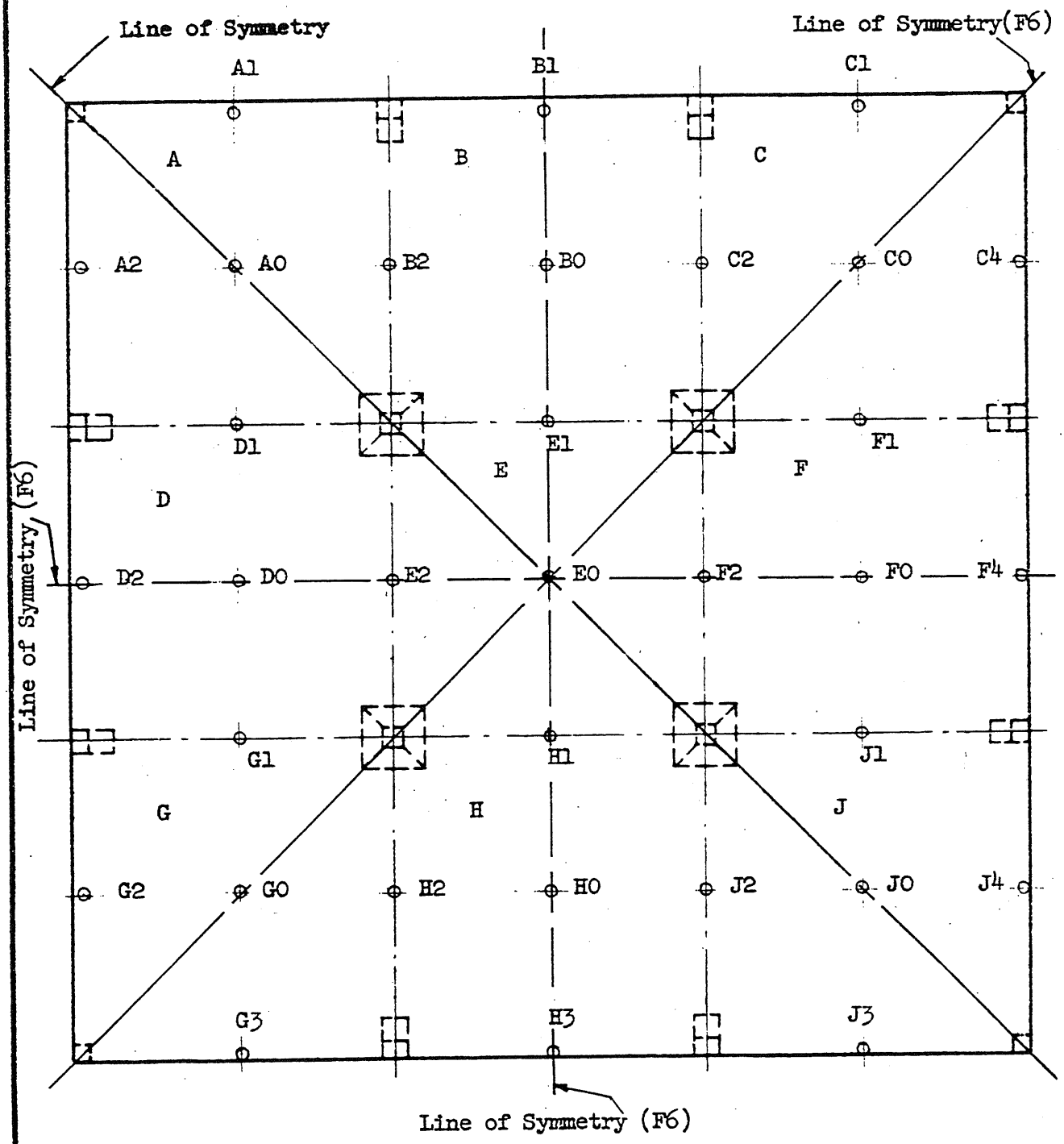

FIG. 3.5 LOCATION AND DESIGNATION OF DEFLECTION DIALS FOR ALL THE STRUCTURES

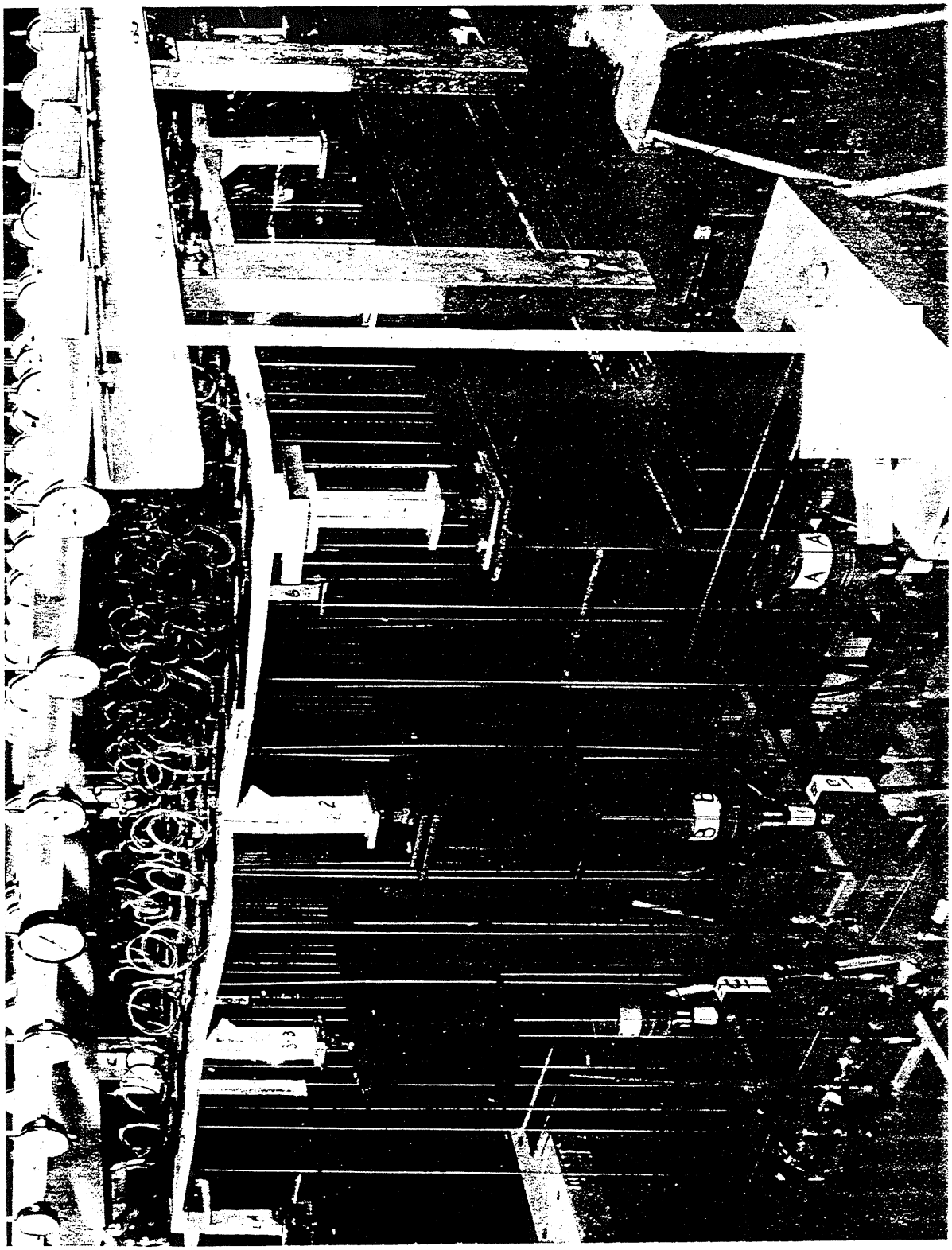

FIG. 3.6 VIEW OF TEST STRUCTURE F6 AFTER TEST TO FAILURE

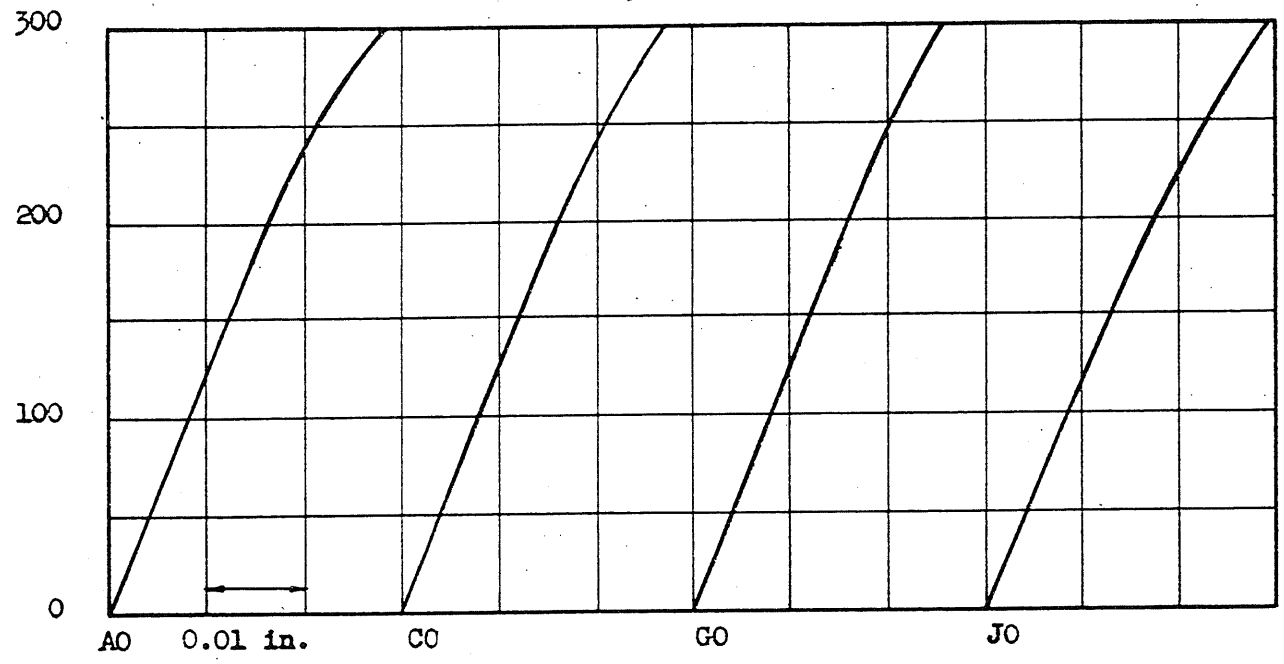

a. Above: deflection of corner panels.

Deflection at midpanel at early stages of loading. Design load = 263 psf applied.

Dial location shown by sketch

b. Below: deflection of side and interior panels

AO	BO	CO
DO	EO	FO
GO	HO	JO

Applied Load, psf

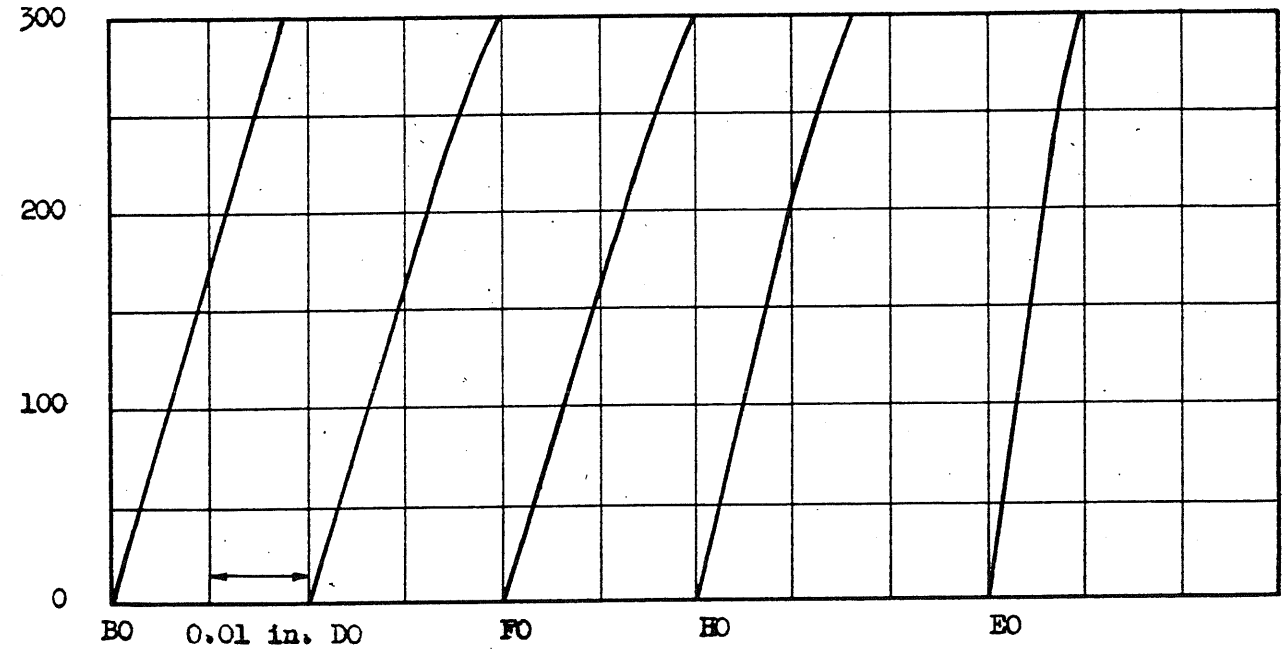

FIG. 4.1 LOAD-DEFLECTION RELATIONSHIPS FOR STRUCTURE F6

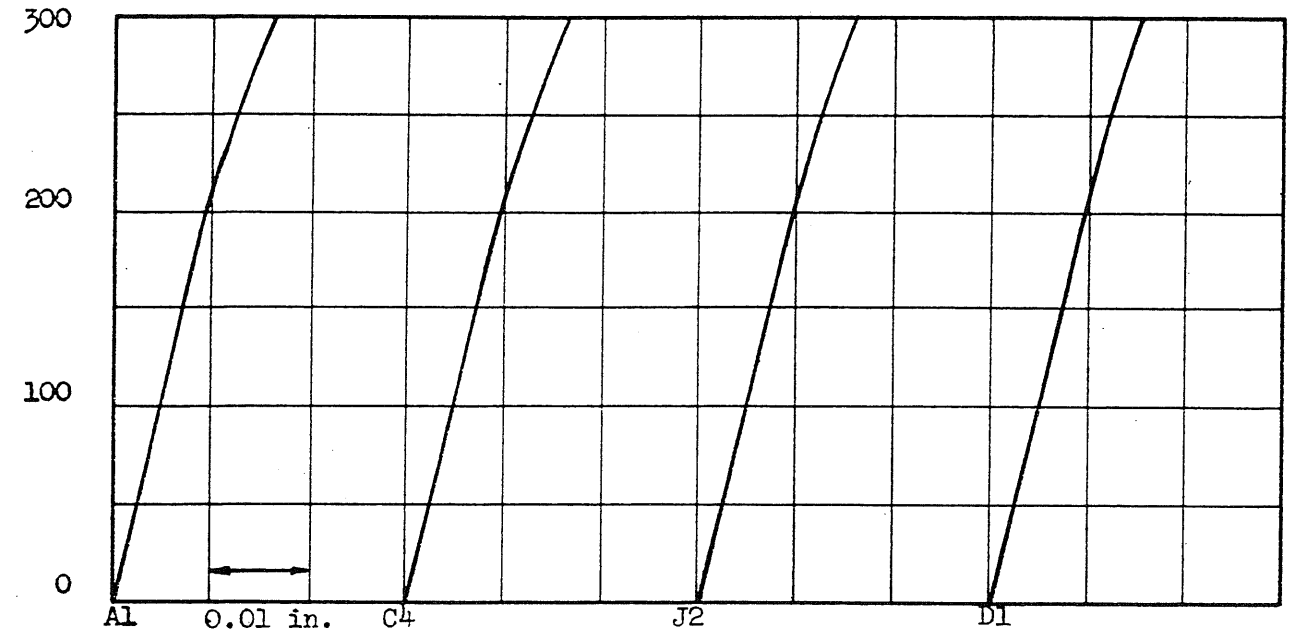

a. Above: deflection of outer span inside and outside column center line

Deflection at midspan of the column center line at early stages of loading. Design load = 263 psf applied

Dial location shown by sketch

b. Below: deflection of inner span inside and outside column center line

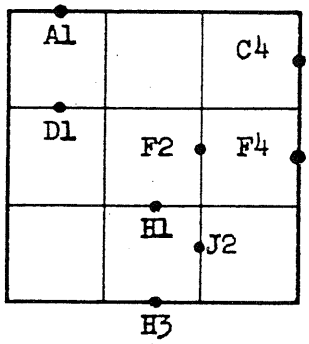

Applied Load, psf

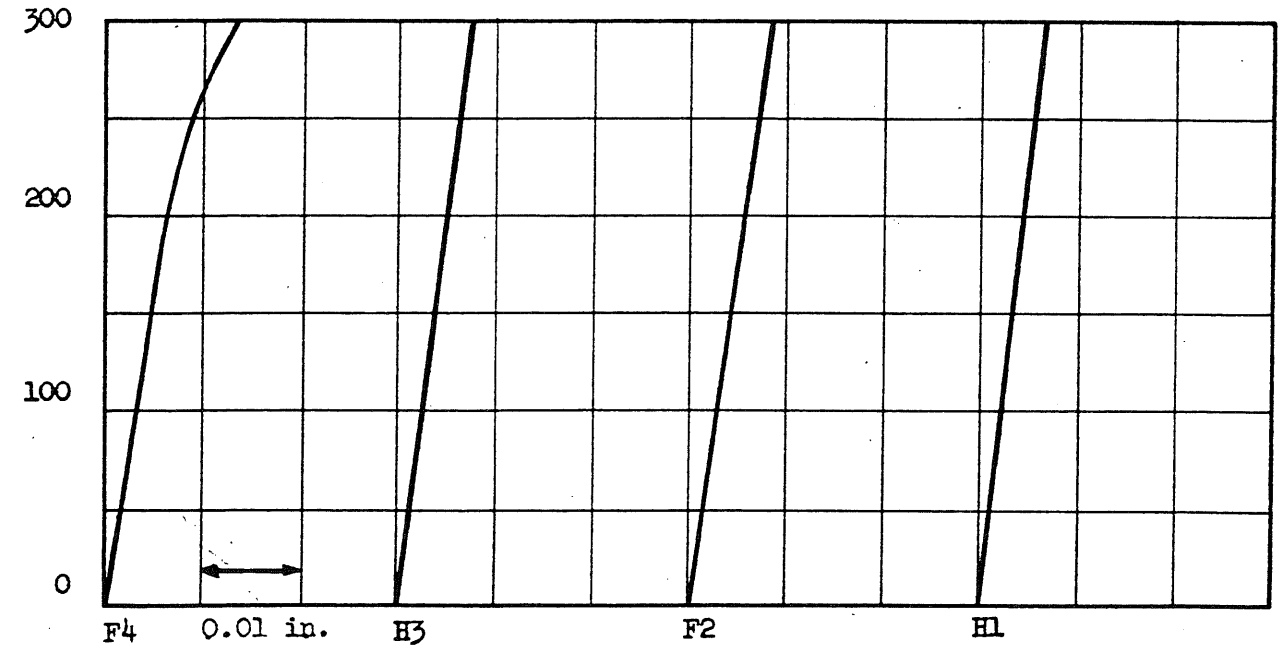

FIG. 4.2 LOAD-DEFLECTION RELATIONSHIPS FOR STRUCTURE F6

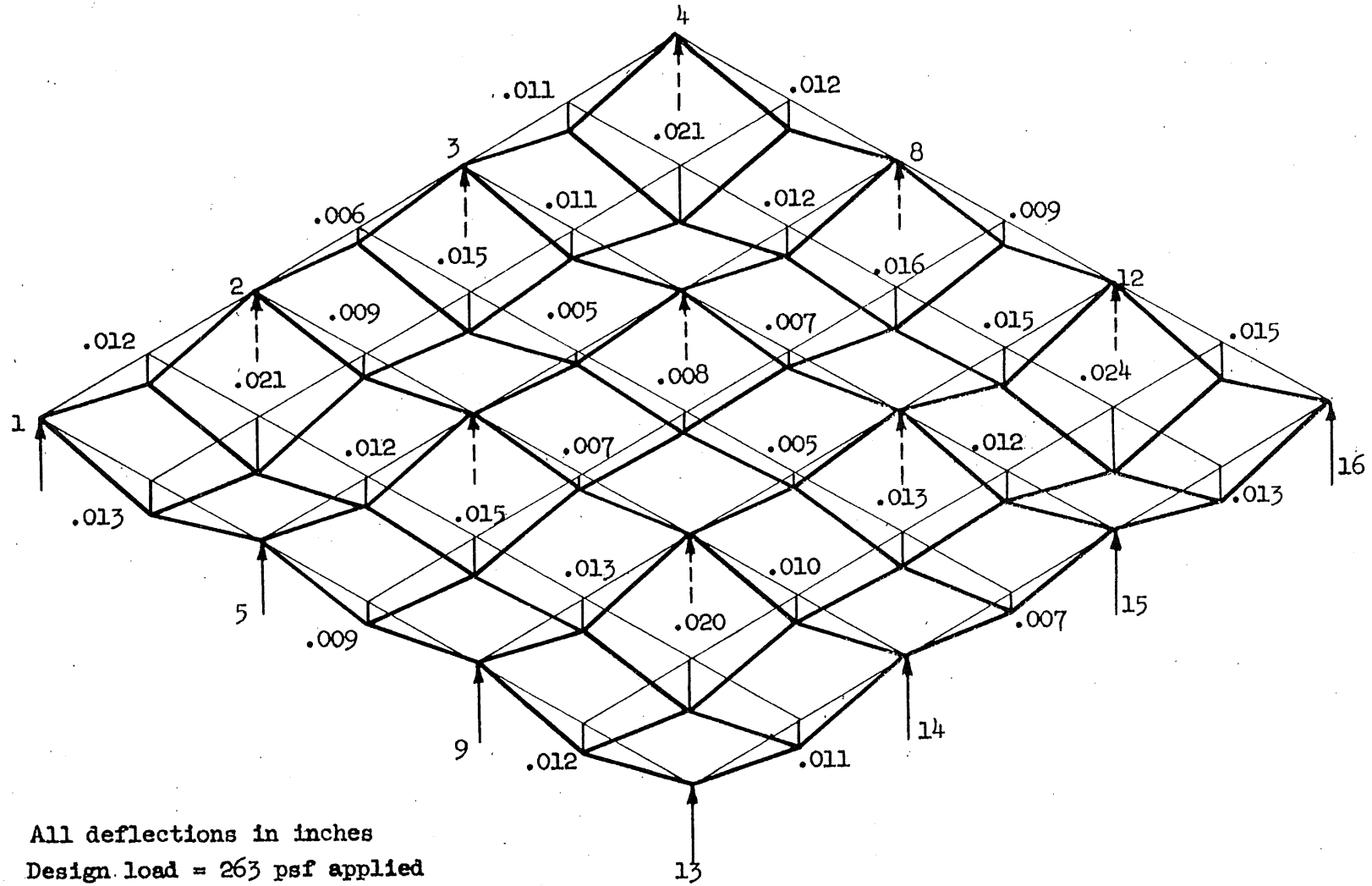

All deflections in inches
Design load = 263 psf applied

FIG. 4.3 SCHEMATIC DEFLECTION DIAGRAM AT DESIGN LOAD OF STRUCTURE F6

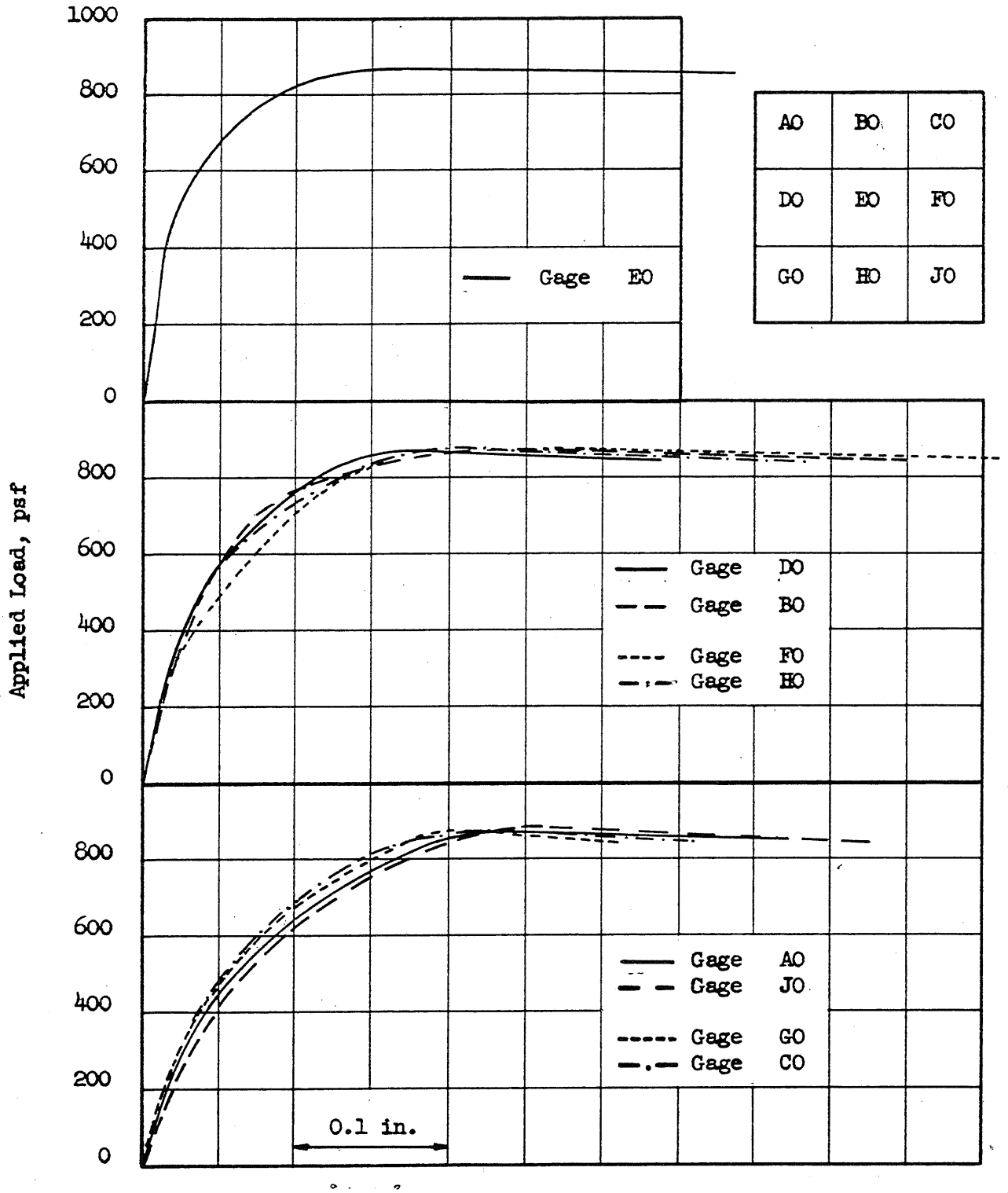

Midpanel deflections up to failure load
Dial locations are shown in the sketch above

FIG. 4.4 LOAD-DEFLECTION RELATIONSHIPS FOR STRUCTURE F6

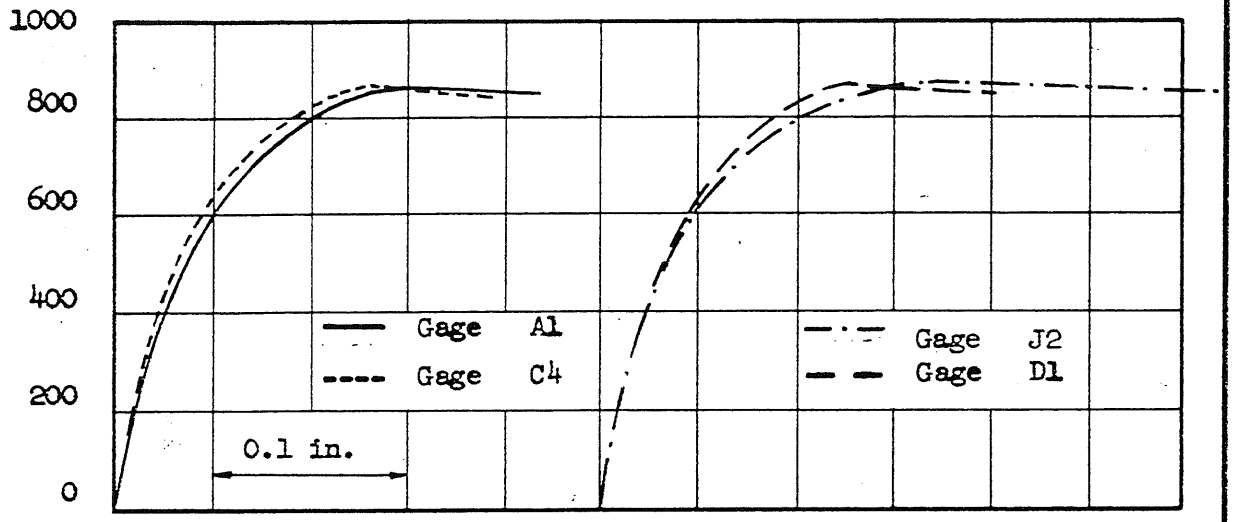

a. Above: Deflection of outer span inside and outside column centerlines

Deflection at midspan of the column centerline. Load to failure

Dial locations shown by sketch

b. Below: Deflection of inner span inside and outside column centerlines

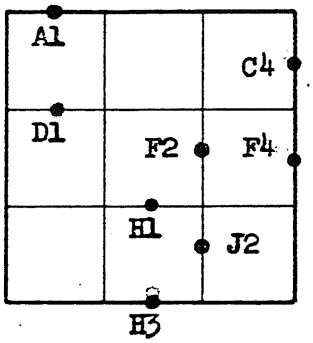

Applied Load, psf

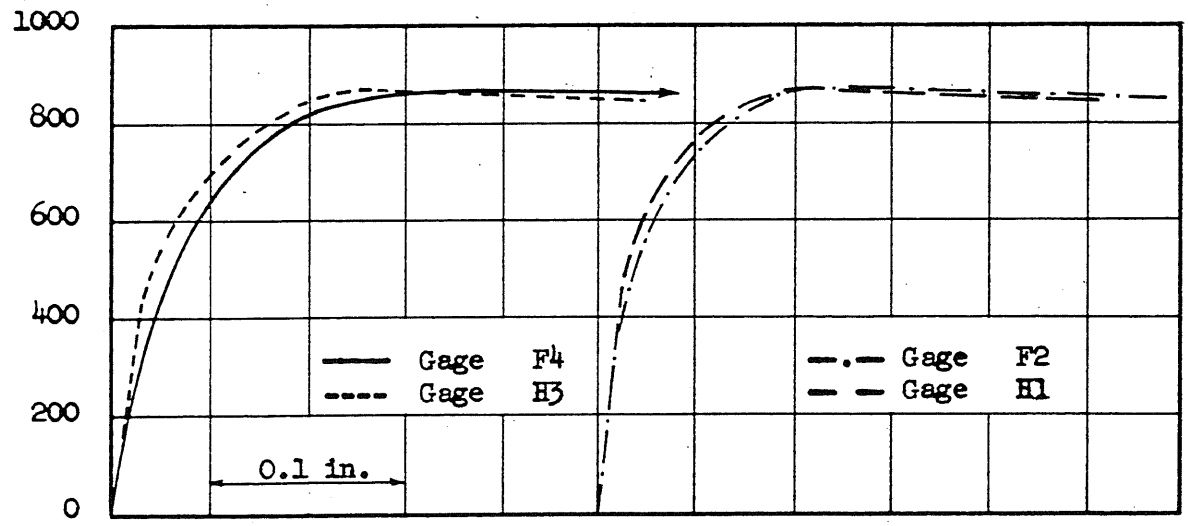

FIG. 4.5 LOAD-DEFLECTION RELATIONSHIPS FOR STRUCTURE F6

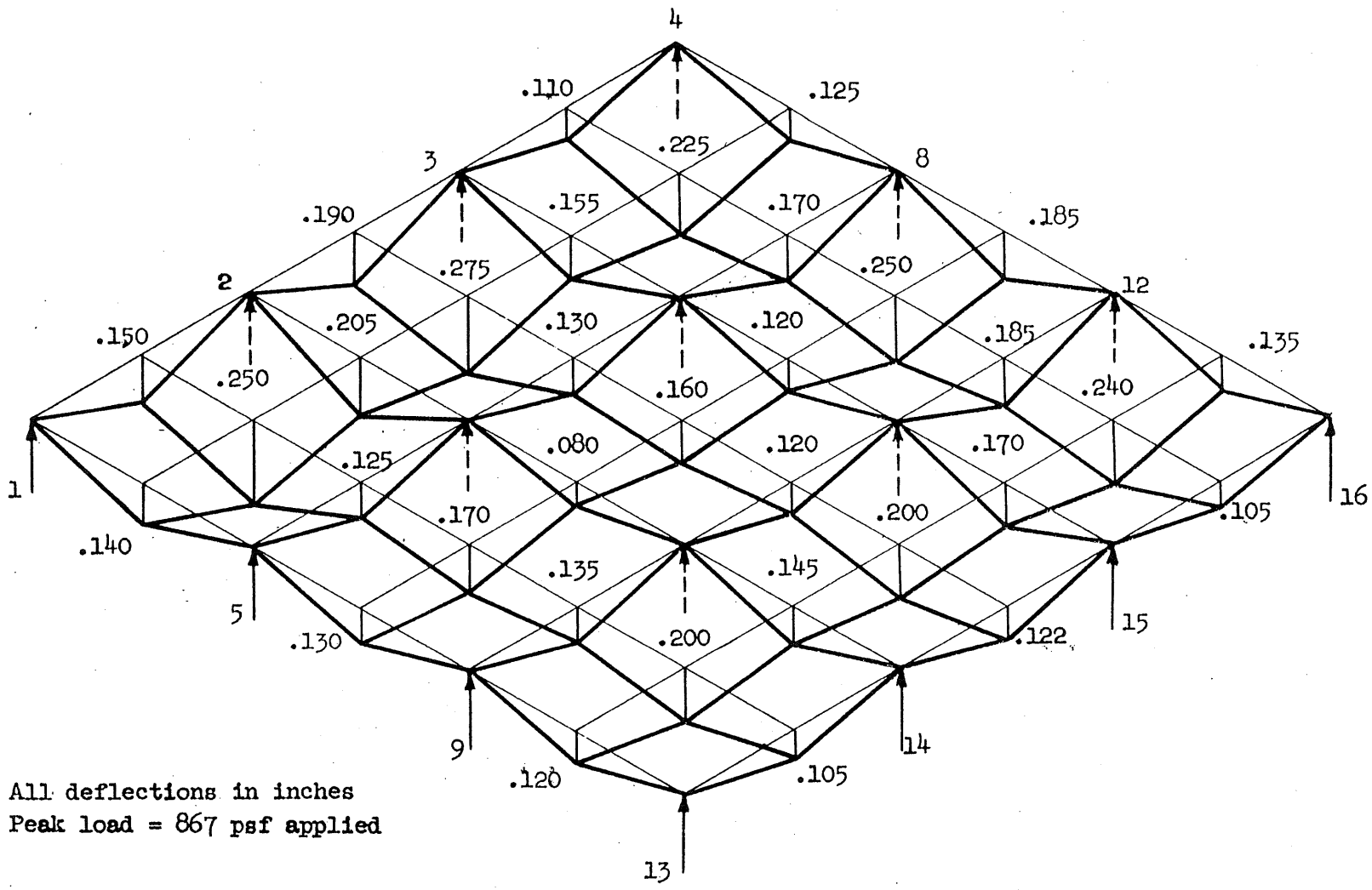

All deflections in inches
Peak load = 867 psf applied

FIG. 4.6 SCHEMATIC DEFLECTION DIAGRAM AT PEAK LOAD OF STRUCTURE F6

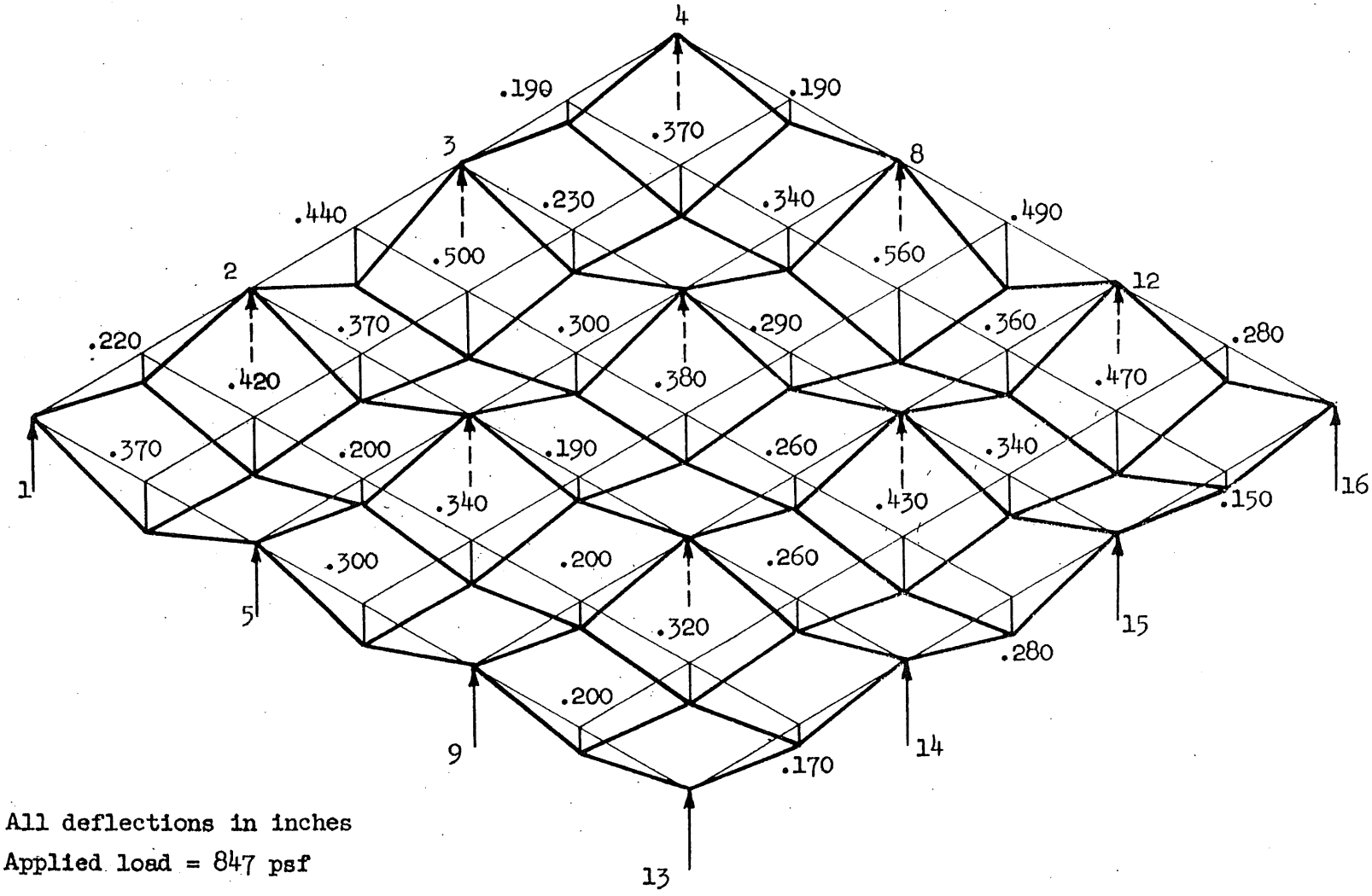

All deflections in inches

Applied load = 847 psf

FIG. 4.7 SCHEMATIC DEFLECTION DIAGRAM AT LARGEST DEFLECTIONS OF STRUCTURE F6

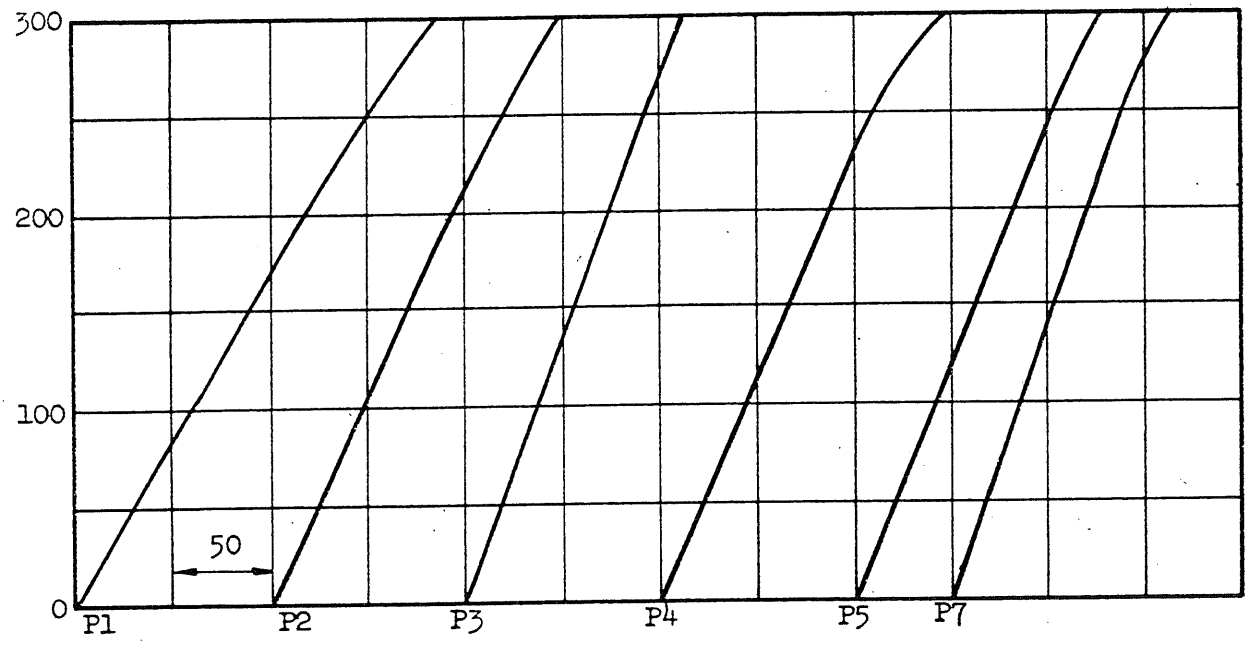

Strain x 10^6

Applied Load, psf

Strains, at locations shown on diagram, during early stages of loading. Design load = 263 psf applied

All gages located in positive moment regions (P)

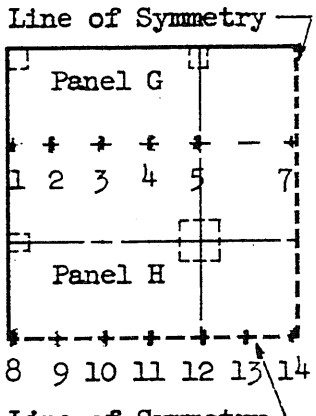

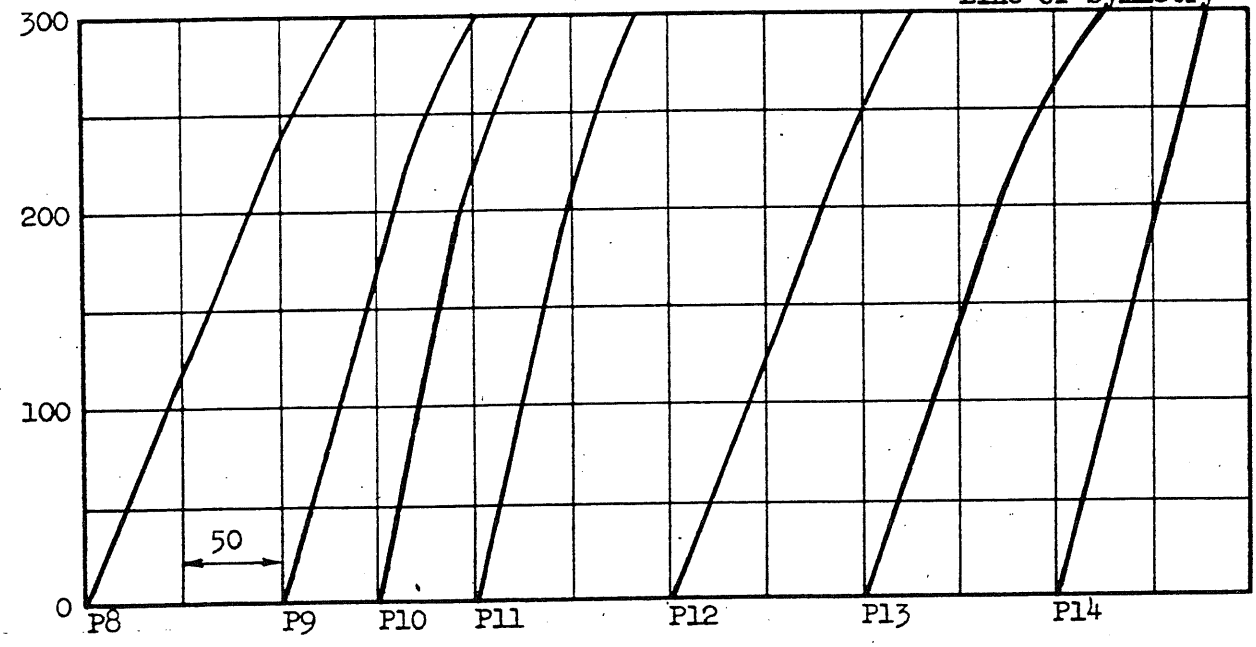

Strain x 10^6

FIG. 4.8 LOAD-STRAIN RELATIONSHIPS MEASURED IN STRUCTURE F6

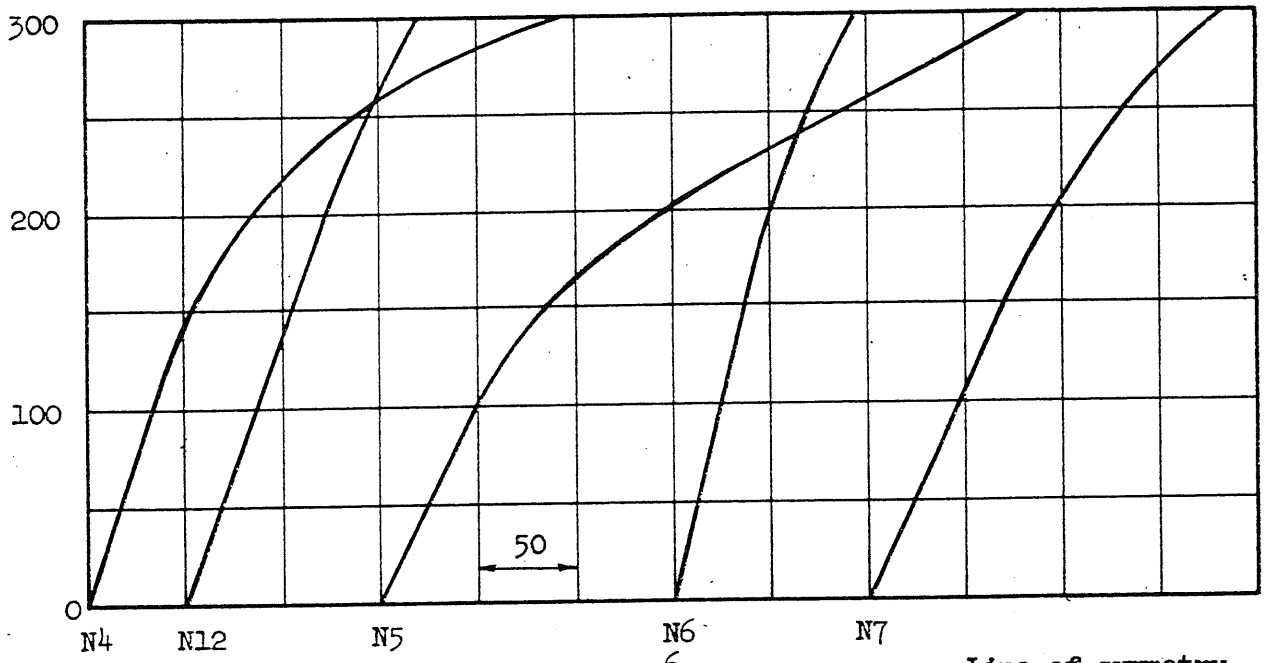

Applied Load, psf

Strains, at locations shown on diagram, during early stages of loading. Design load = 263 psf applied

All gages located in negative moment regions (N)

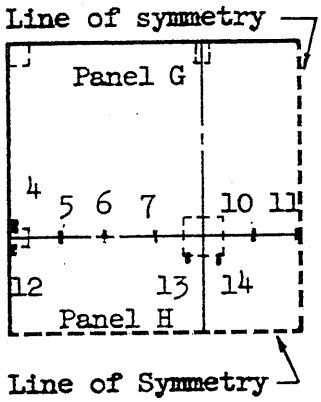

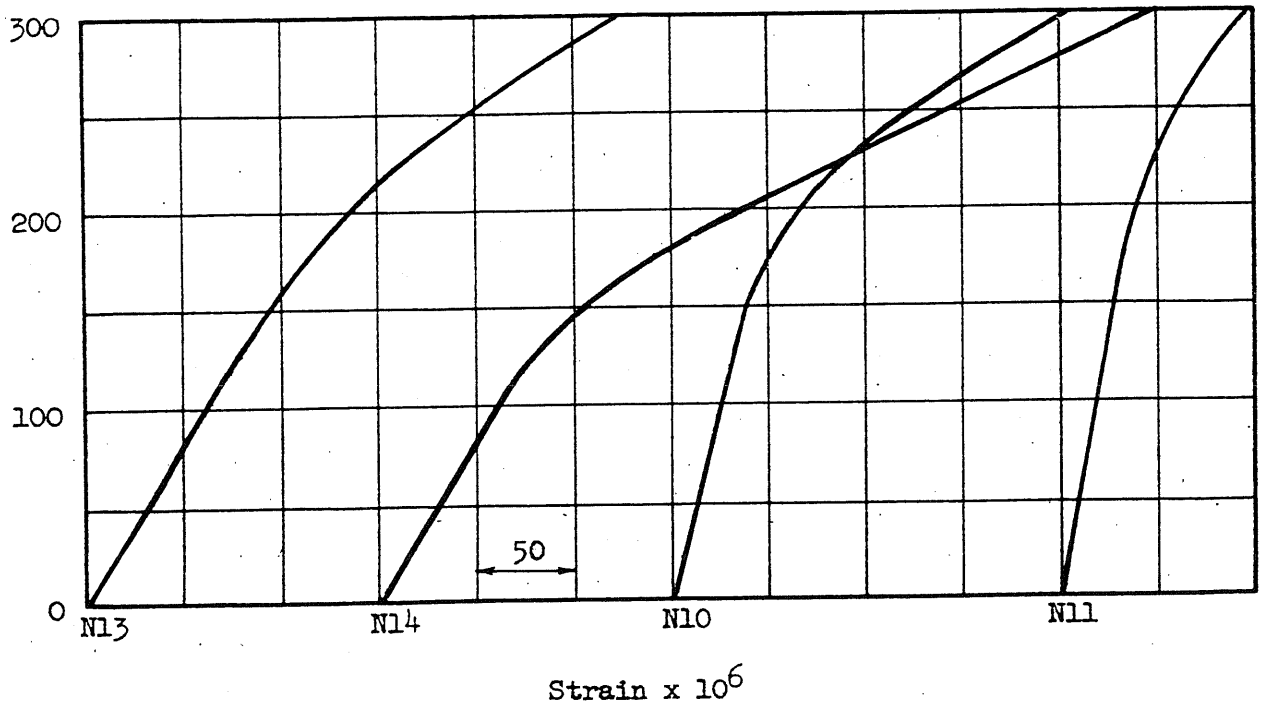

FIG. 4.9. LOAD-STRAIN RELATIONSHIPS MEASURED IN STRUCTURE F6

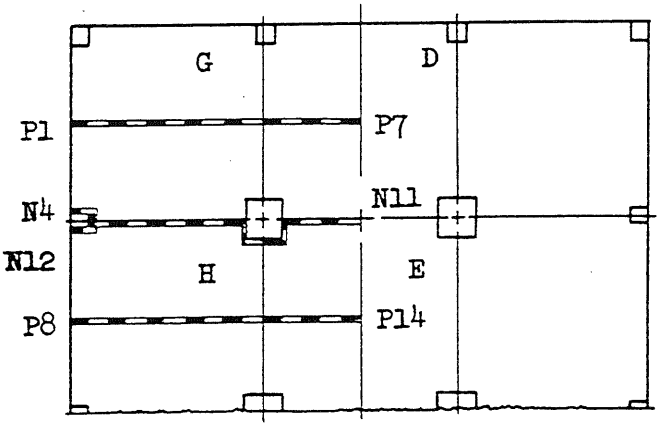

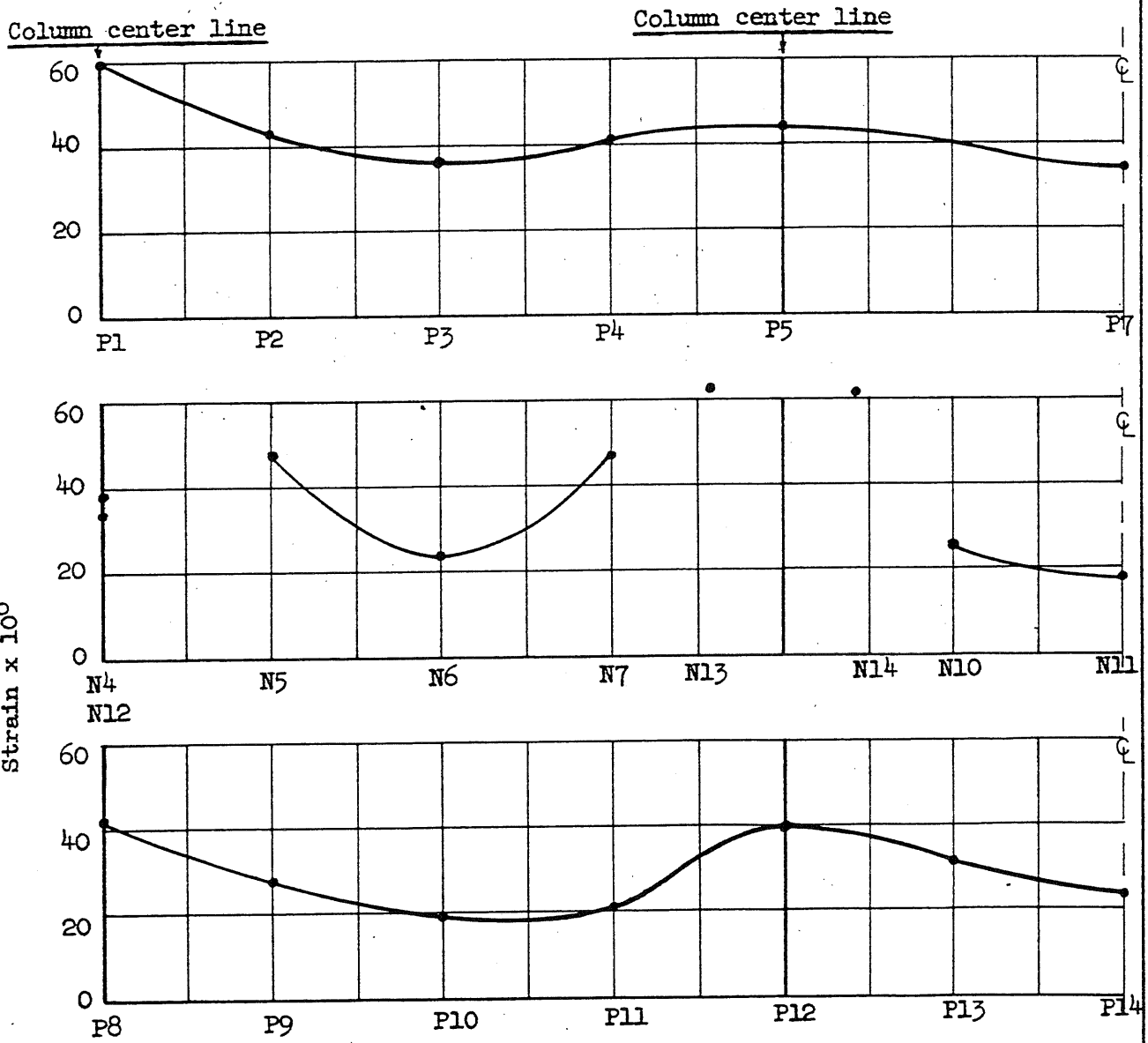

Gage Positions

"Elastic" Strains at 100 psf Load

FIG. 4.10 MEASURED STRAIN PROFILES FOR STRUCTURE F6

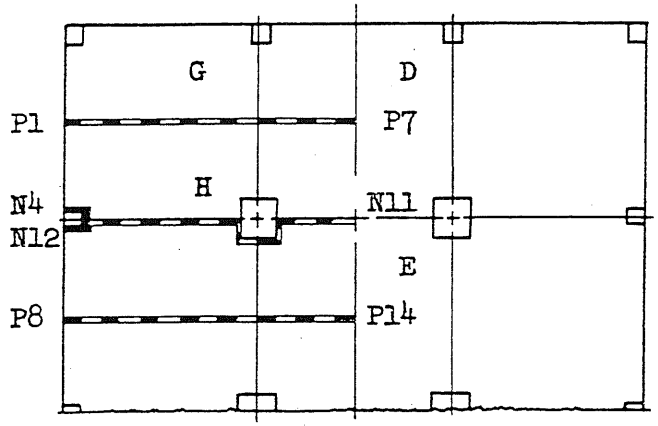

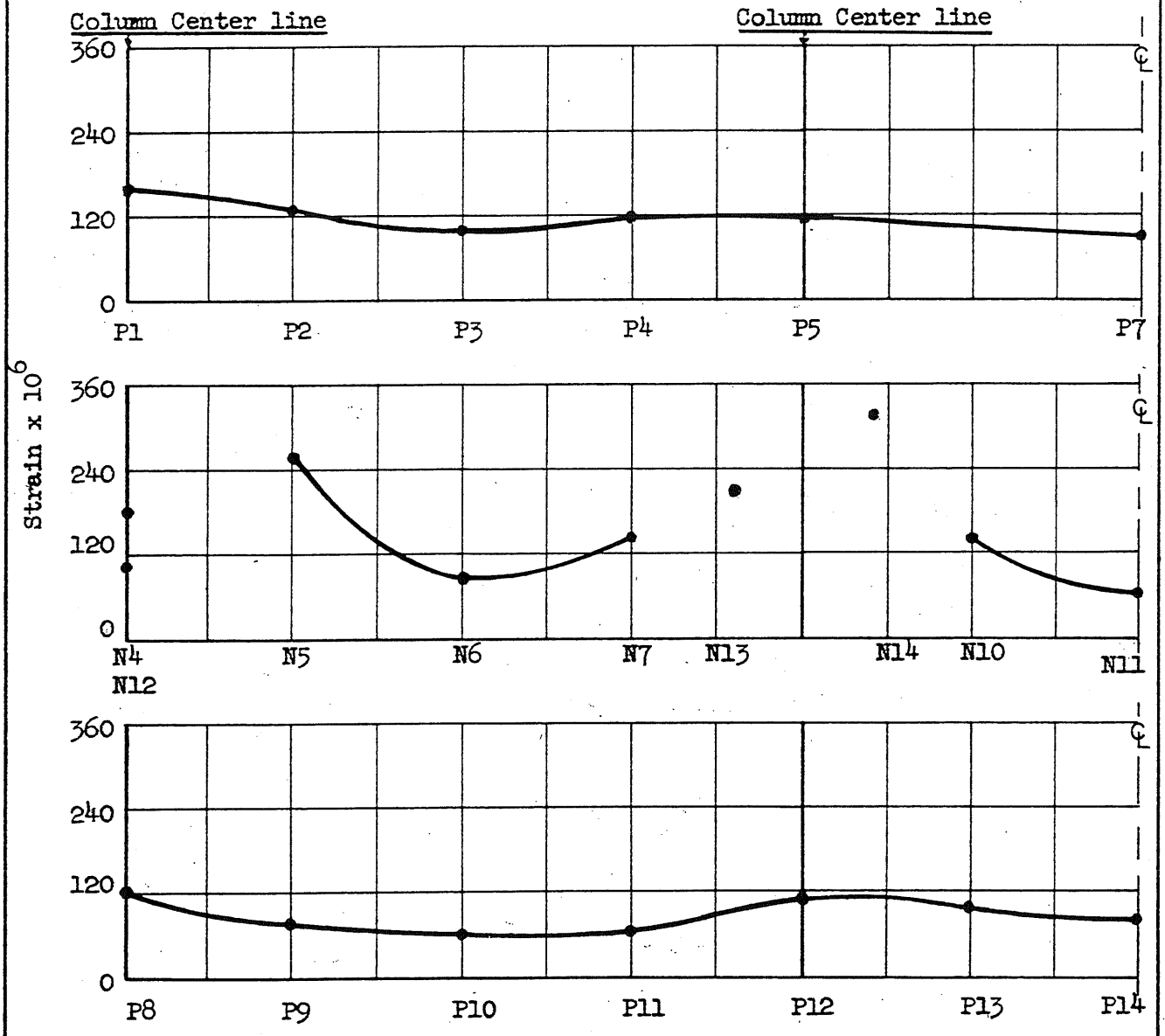

Gage Positions

Strains at Design Load: 263 psf applied

FIG. 4.11 MEASURED STRAIN PROFILES FOR STRUCTURE F6

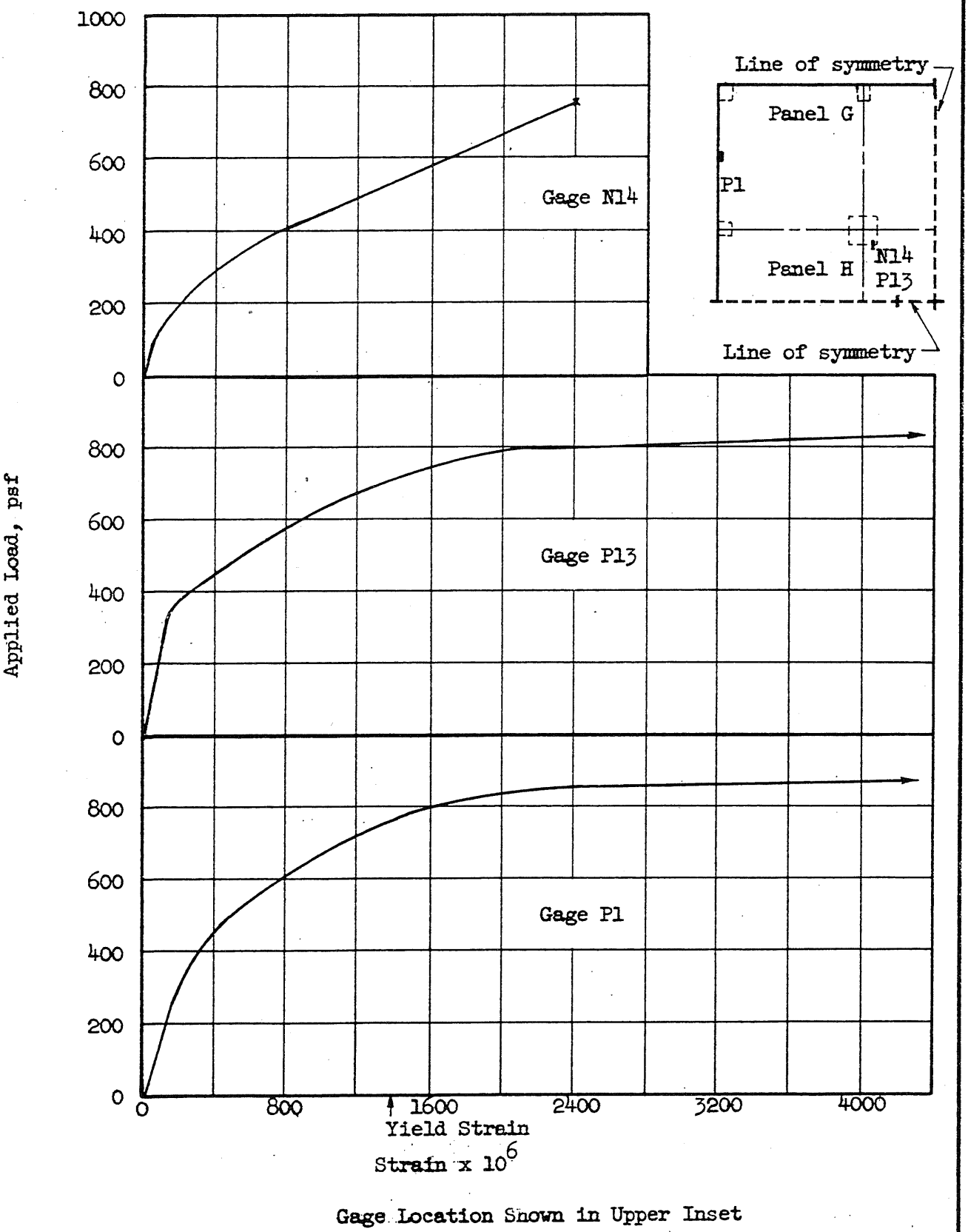

FIG. 4.12 LOAD-STRAIN RELATIONSHIPS MEASURED IN STRUCTURE F6

(a)

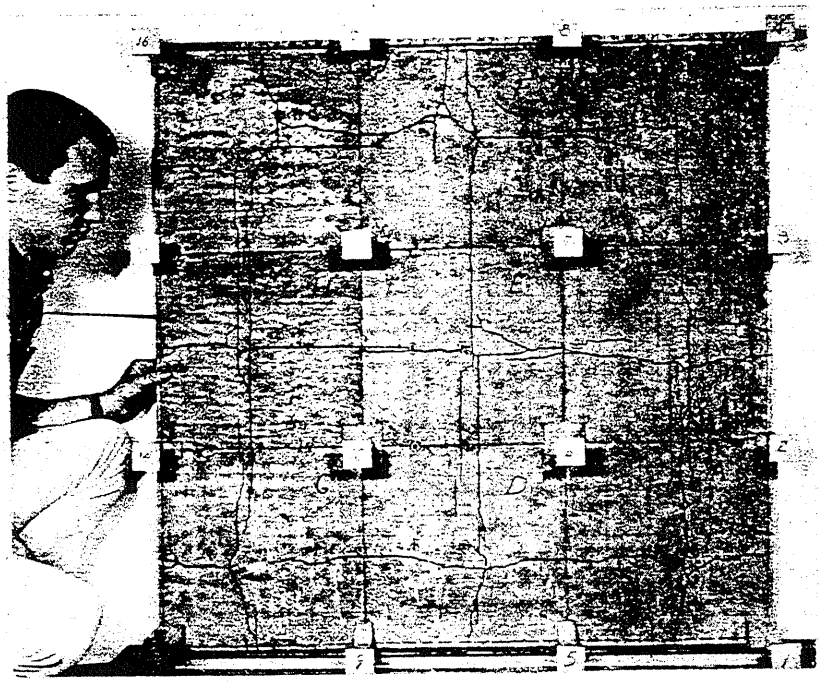

View of positive moment cracks at the bottom of slab F6 after removal of the load.

(b)

View of negative moment cracks at the bottom of slab F6 after removal of the load. Note the tensile membrane cracks in the middle of panels B, D, E, F and H, crossing the interior span.

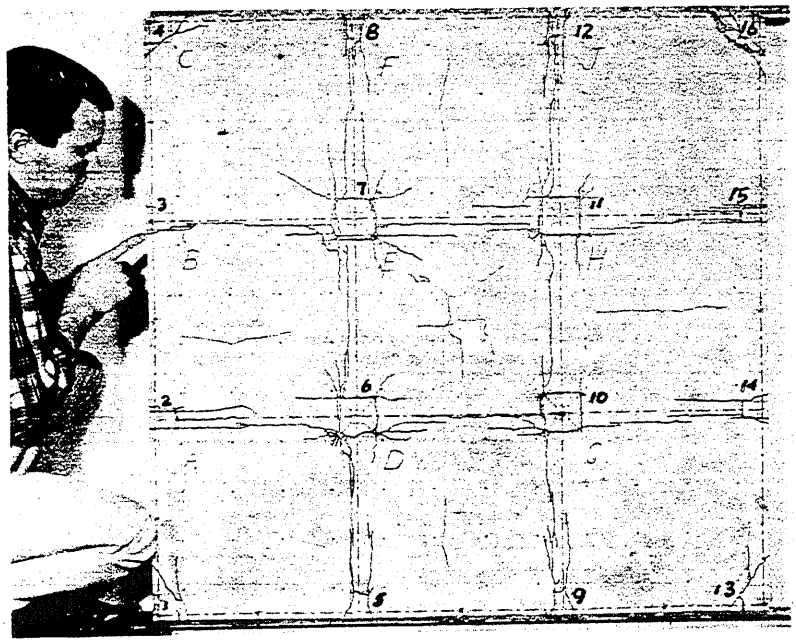

FIG. 4.13 CONDITION OF THE TEST STRUCTURE AFTER THE TEST TO FAILURE

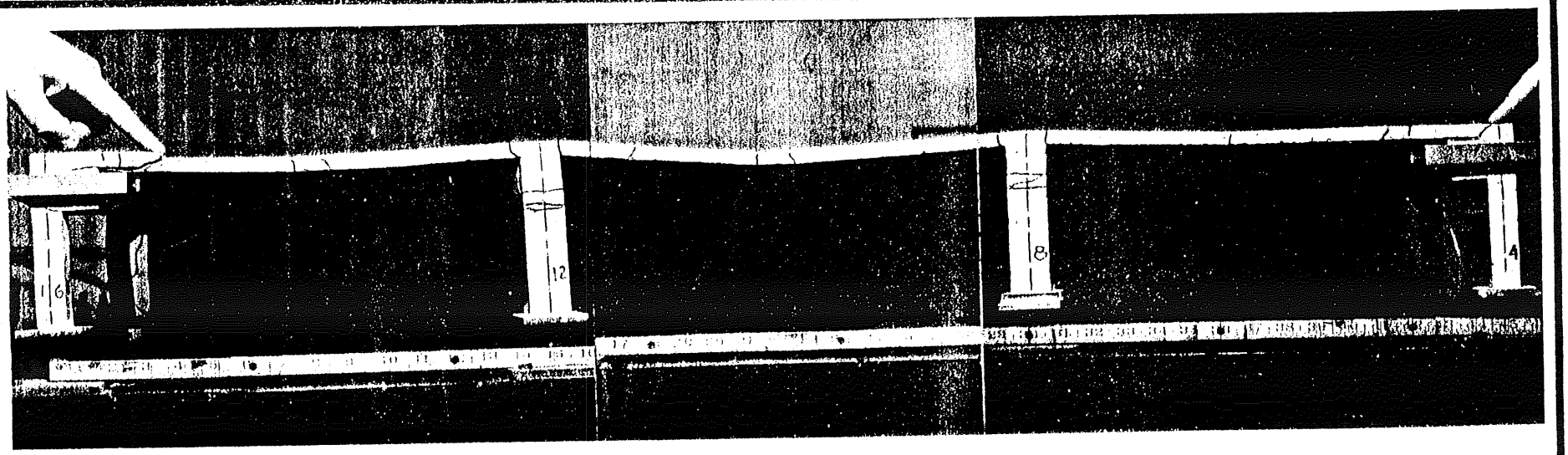

(a) Composite view of slab profile showing how the interior span yielded more severely than the rest.

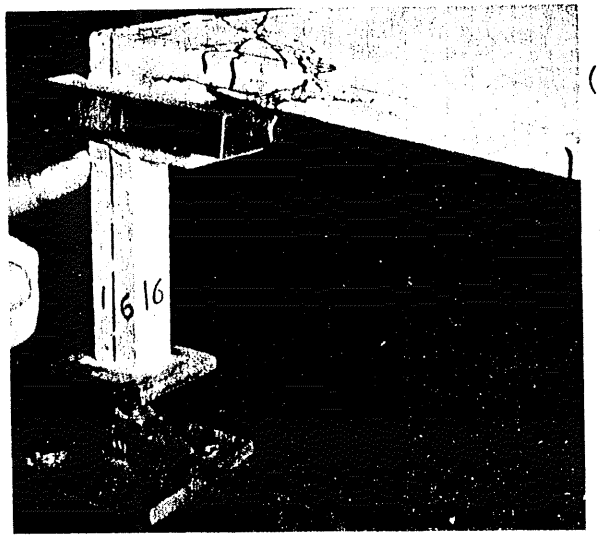

(b) Close up of punching failure at Column 16. Note the exposed reinforcing bars.

(c) Punching failure of Column 16 seen from the top of the structure.

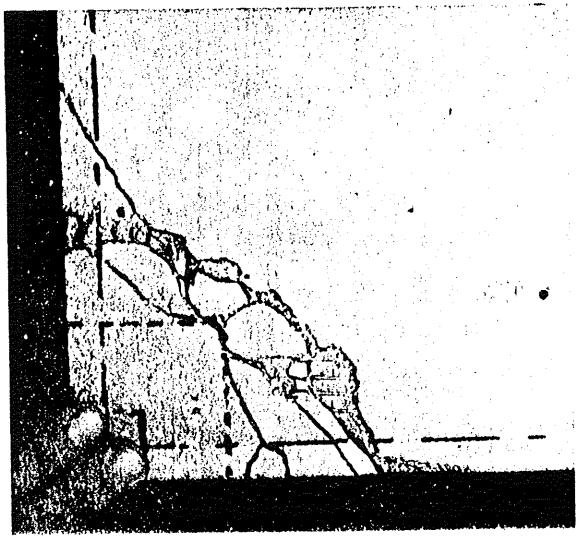

FIG. 4.14 CRACKS IN THE TEST STRUCTURE AFTER TEST TO FAILURE

(a) View from below of Column 16 area showing punching failure. Note that the prestressing clamp has been removed from the capital.

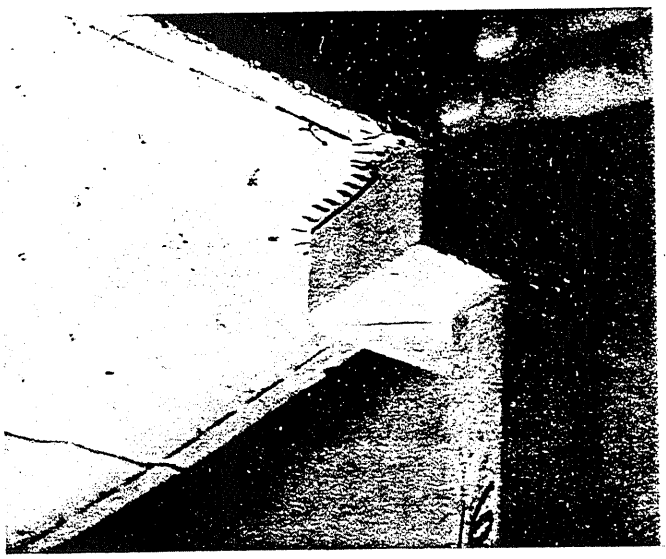

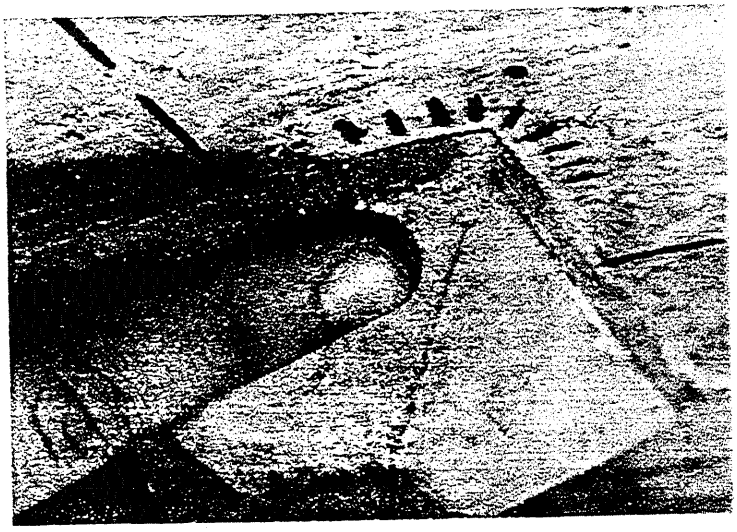

(b) Distress at the bottom of the slab at an interior column showing the initiation of a punching failure.

(c) View of a side column showing the initiation of a punching failure.
Note crushing of concrete at the bottom of the cap and the wide crack at the column side.

Slab after test to failure and removal of load

FIG. 4.15 SIGNS OF DISTRESS AT COLUMN-TO-SLAB CONNECTION

(a) Slab above an interior column showing a crack which indicates the initiation of a punching failure. Negative moment cracks radiate from the column.

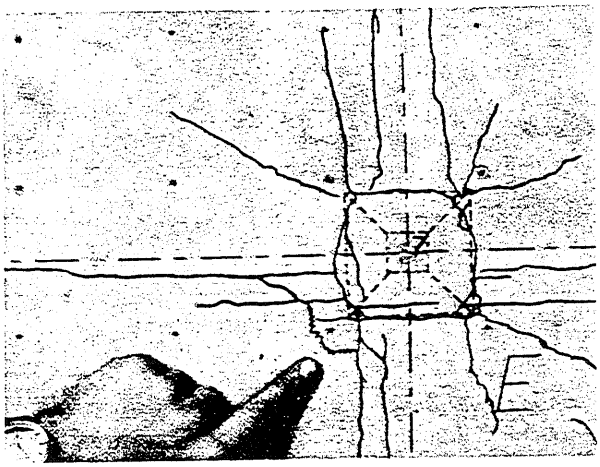

(b) View of slab top over a side column showing a typical arrangement of yield lines.

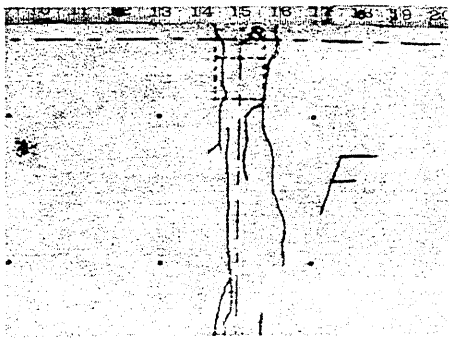

(c) View at a corner column. Negative steel extends from the edge of the slab to where the crack crosses the capital outline. Note how crack extends parallel to the edge of the slab.

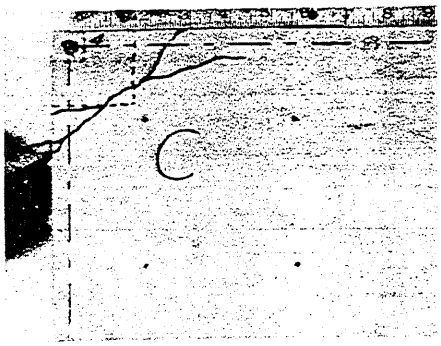

Slab after the test to failure and removal of load.

FIG. 4.16 VIEW OF SLAB TOP OVER THE COLUMNS

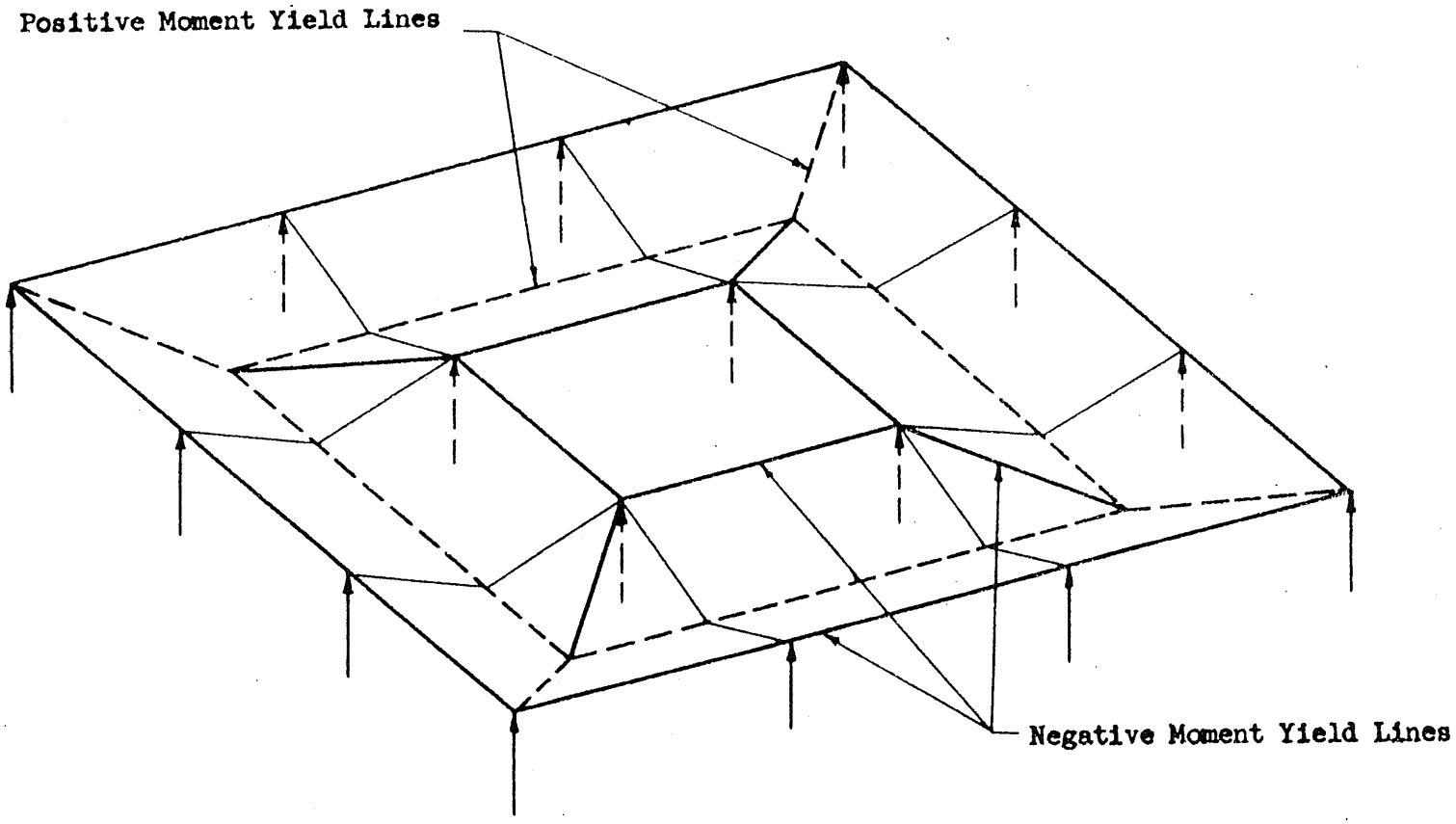

FIG. 5.1 "SLAB FAILURE" MECHANISM OF THE EXTERIOR SPANS

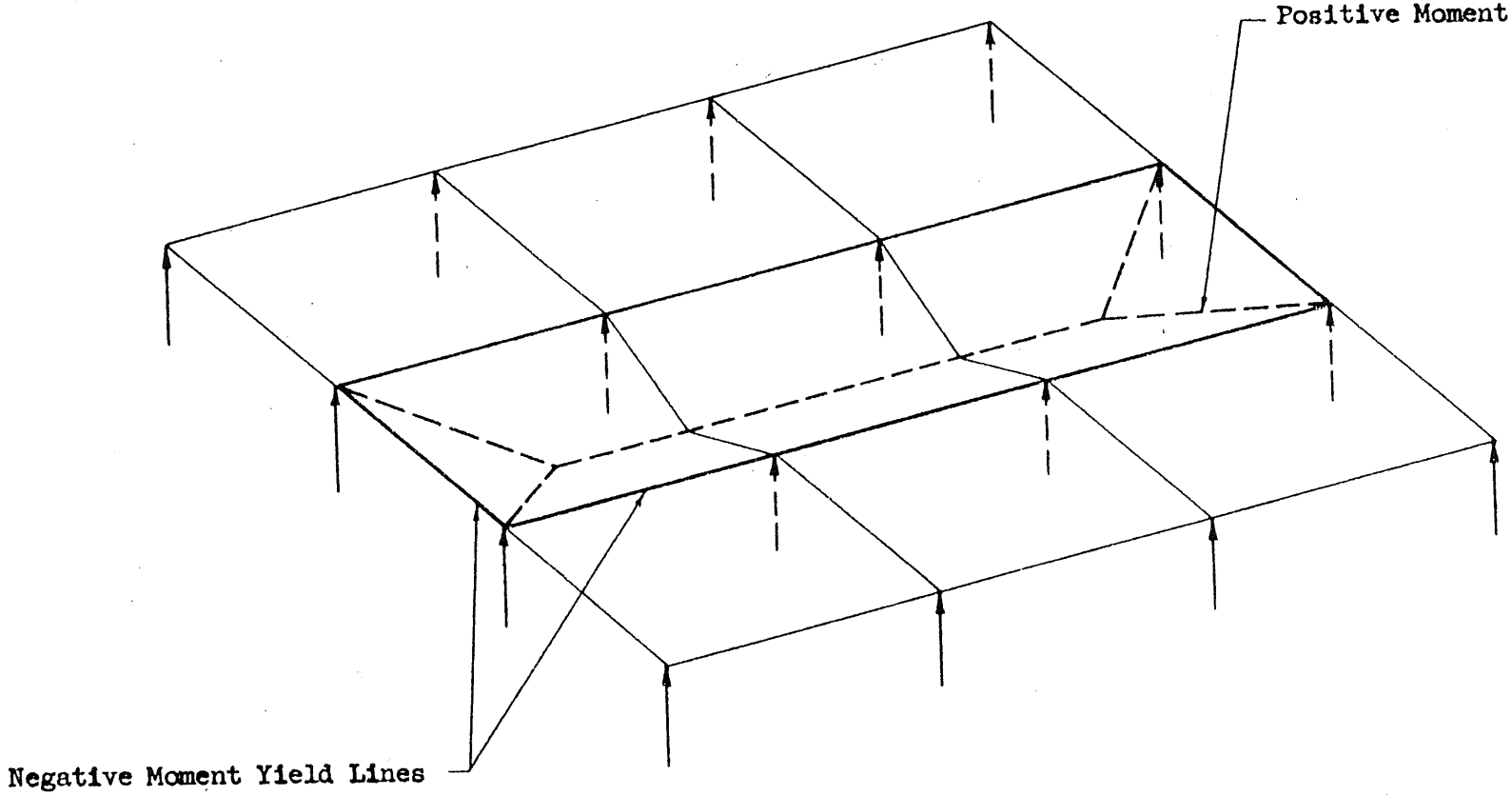

FIG. 5.2 "SLAB FAILURE" MECHANISM OF THE INTERIOR SPANS

Note: The formation of a mechanism in the interior spans does not require the formation of one in the exterior spans and vice versa.

The exterior span mechanism is shown with local negative yield lines over the outside columns.

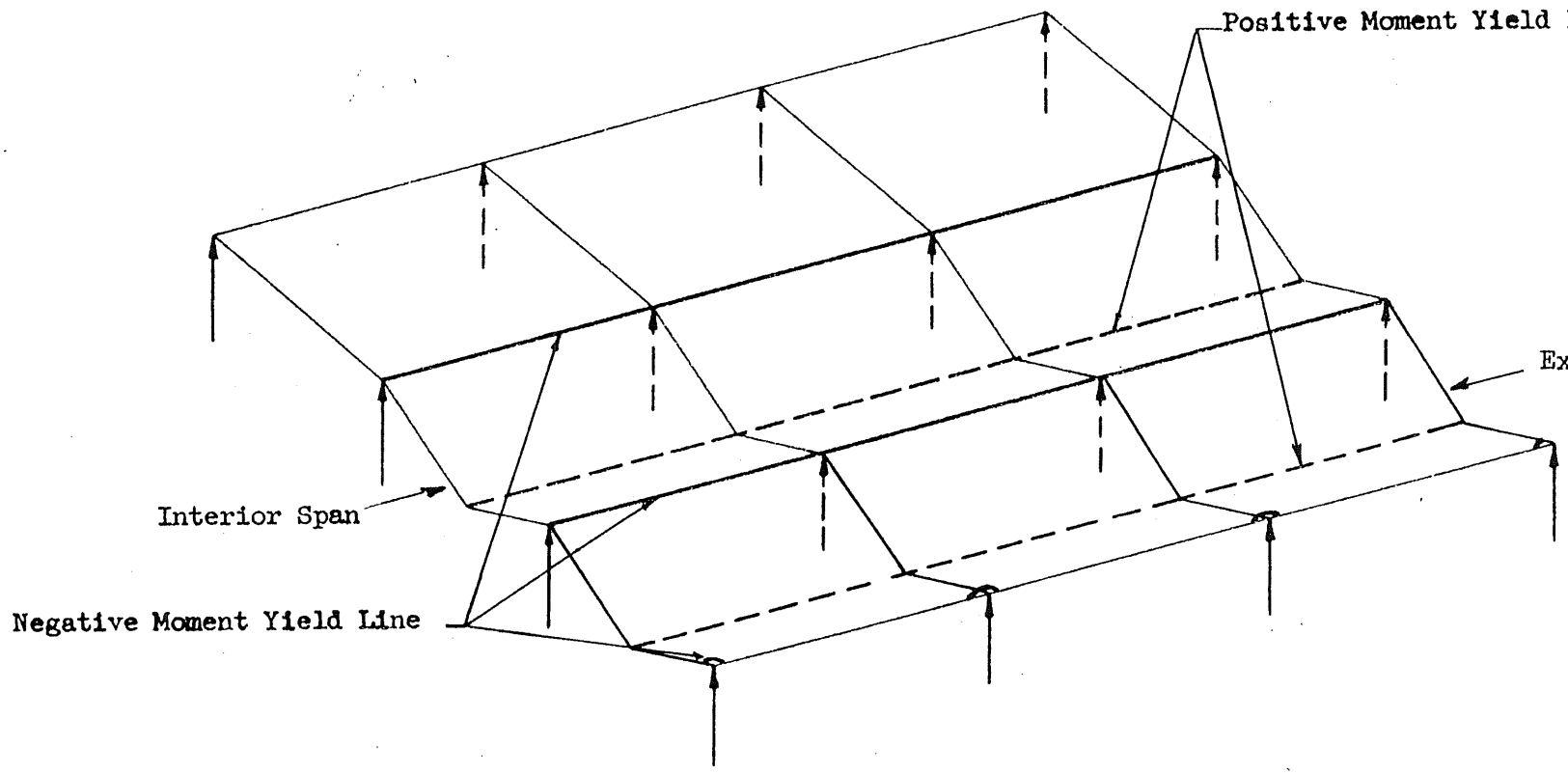

FIG. 5.3 "STRUCTURAL FAILURE" MECHANISM IN EXTERIOR AND INTERIOR SPANS

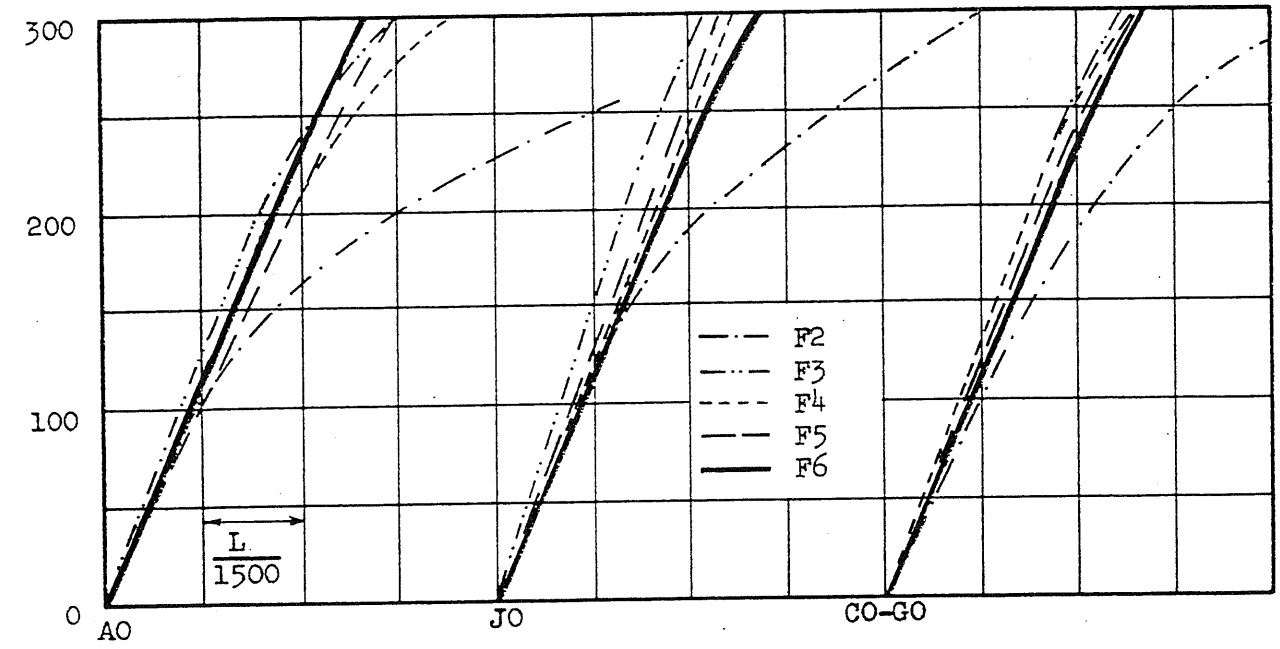

Total load, psf

Above: Comparison of corner panel deflections. Curves F6 are identical since the average of the corner panels is used.

Sketch shows location of dials with respect to the beams in structures F2, F3, F4 and F5.

L = bay span

Below: Comparison of side and center panel deflection. Curves F6 of locations BO, DO, HO and FO are identical.

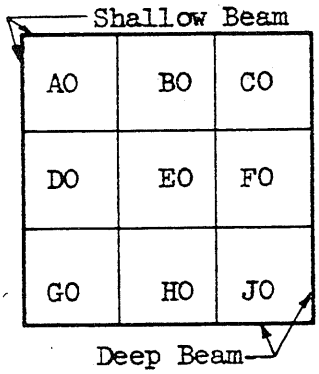

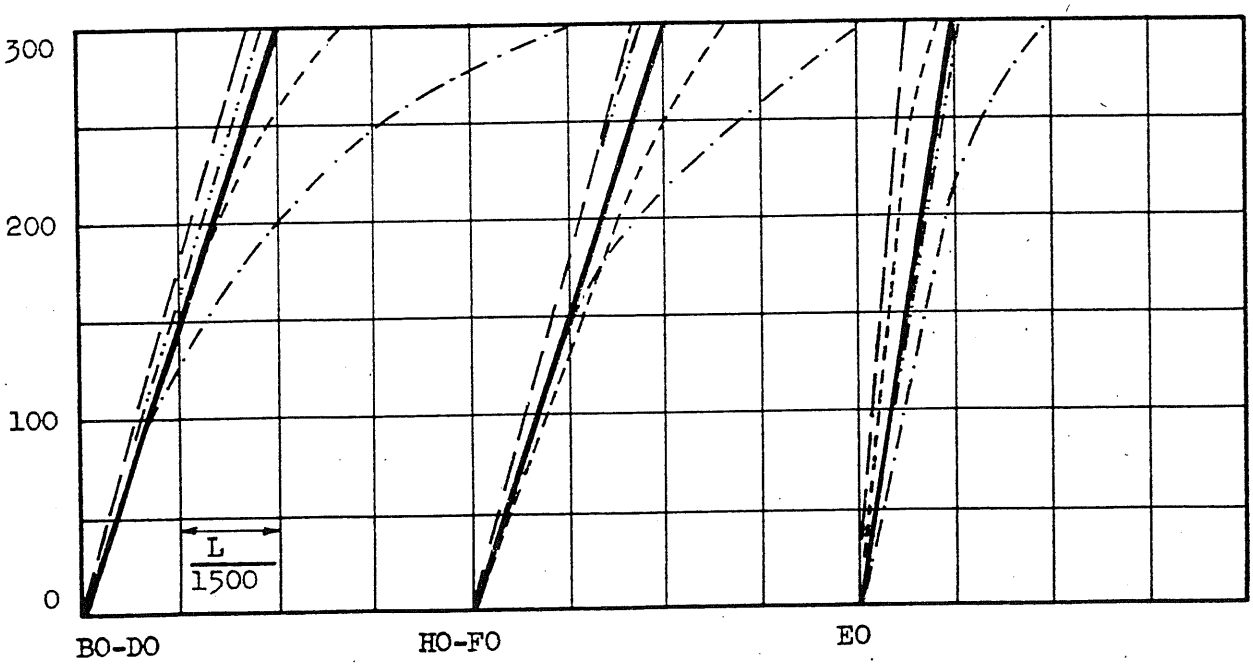

FIG. 6.1 COMPARISON OF MID-PANEL LOAD-DEFLECTION CURVES

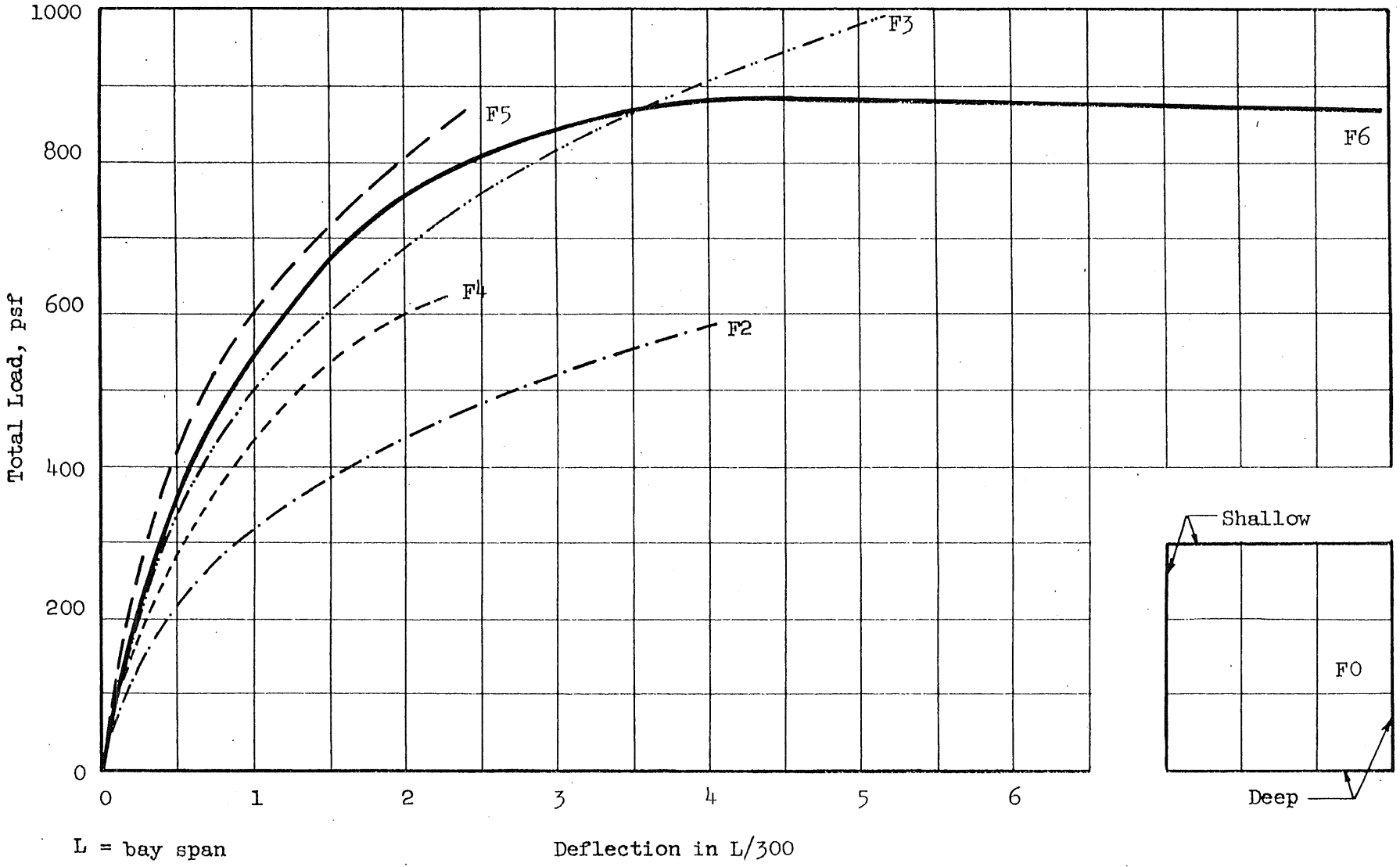

FIG. 6.8 COMPARISON OF LOAD-DEFLECTION CURVES TO FAILURE AT MID-PANEL

Note: The values of structure F5 are not shown since they were not reliable in this panel (see Ref.4)

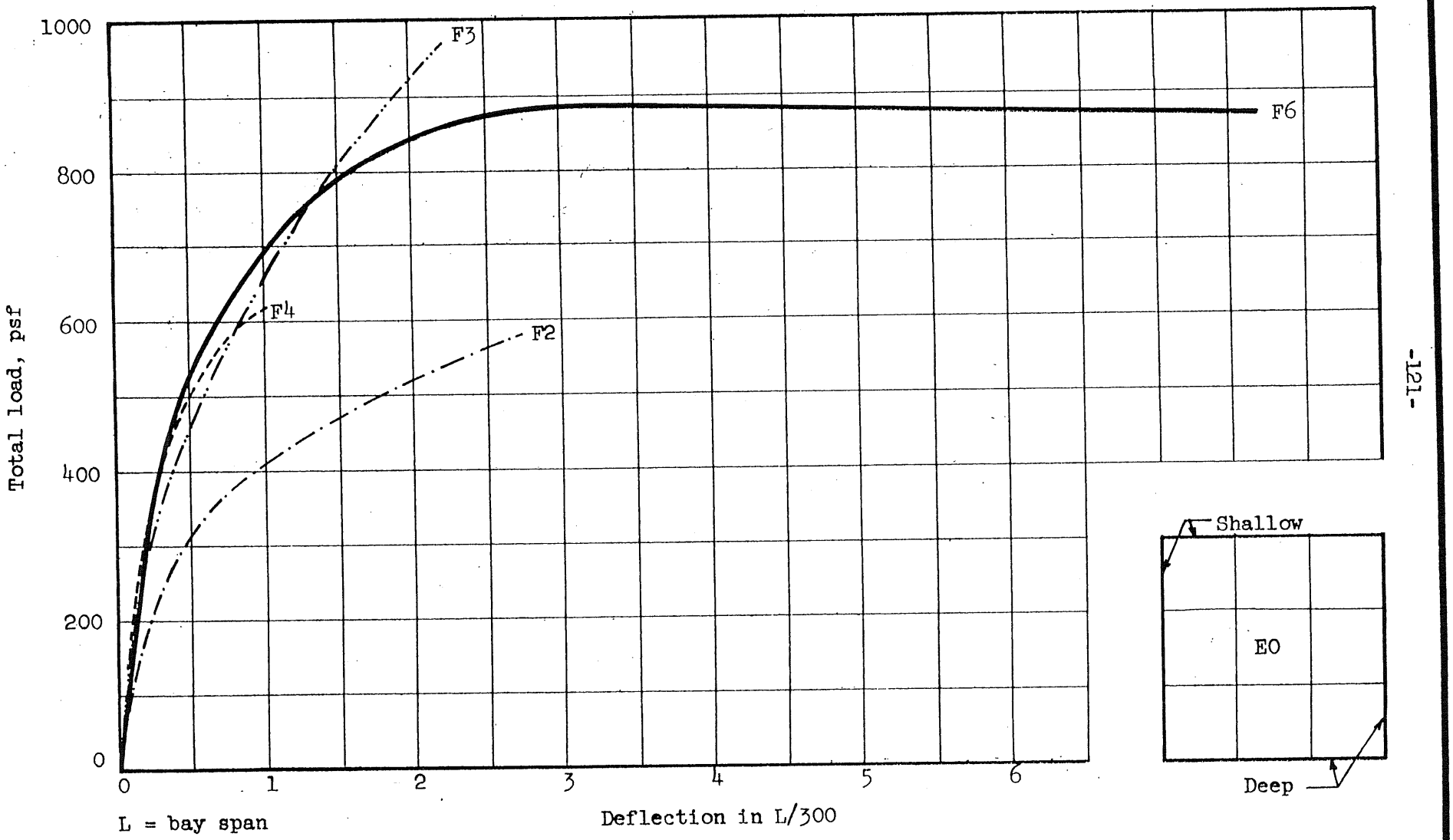

FIG. 6.9 COMPARISON OF LOAD-DEFLECTION CURVES TO FAILURE AT MID-PANEL

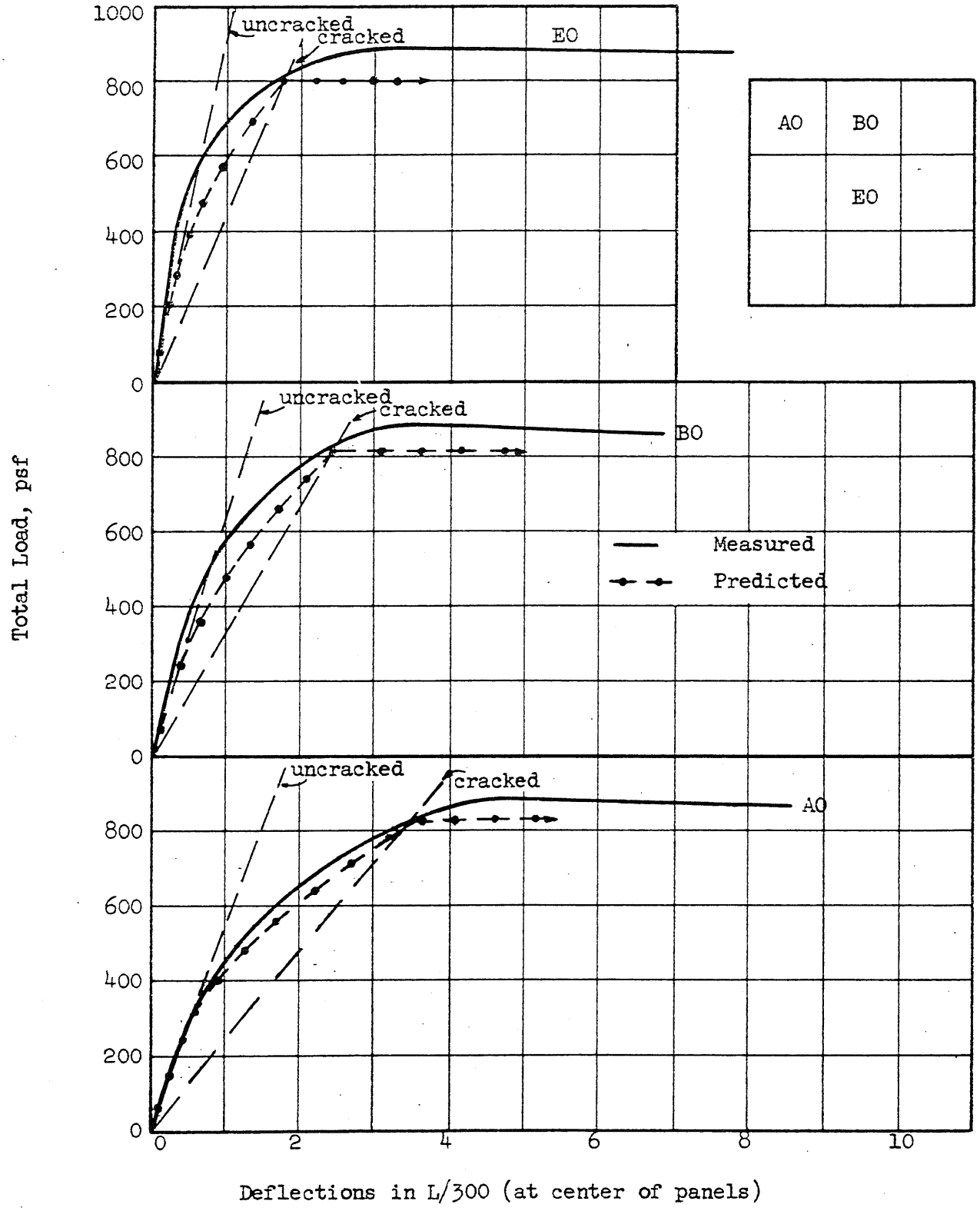

L = span length

FIG. 6.10 MEASURED AND PREDICTED LOAD-DEFLECTION CURVES

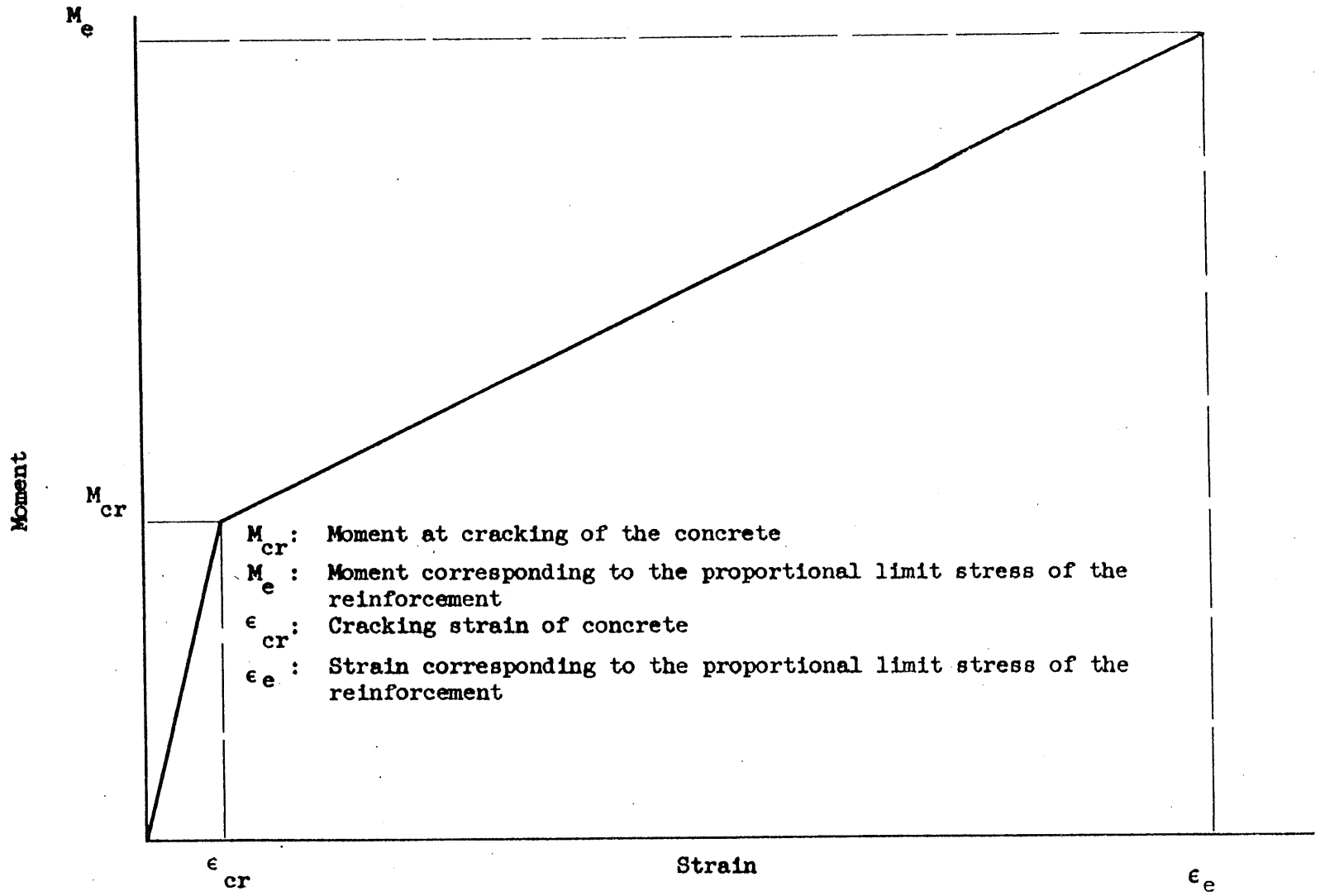

FIG. 6.11 TYPICAL MOMENT-STRAIN RELATIONSHIP FOR THE SLAB SECTIONS

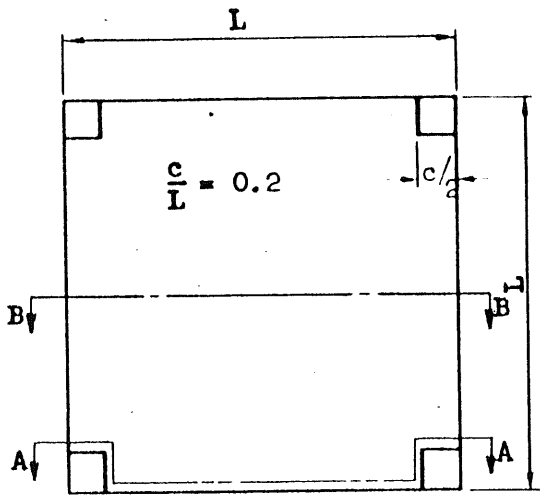

Plan View of Panel

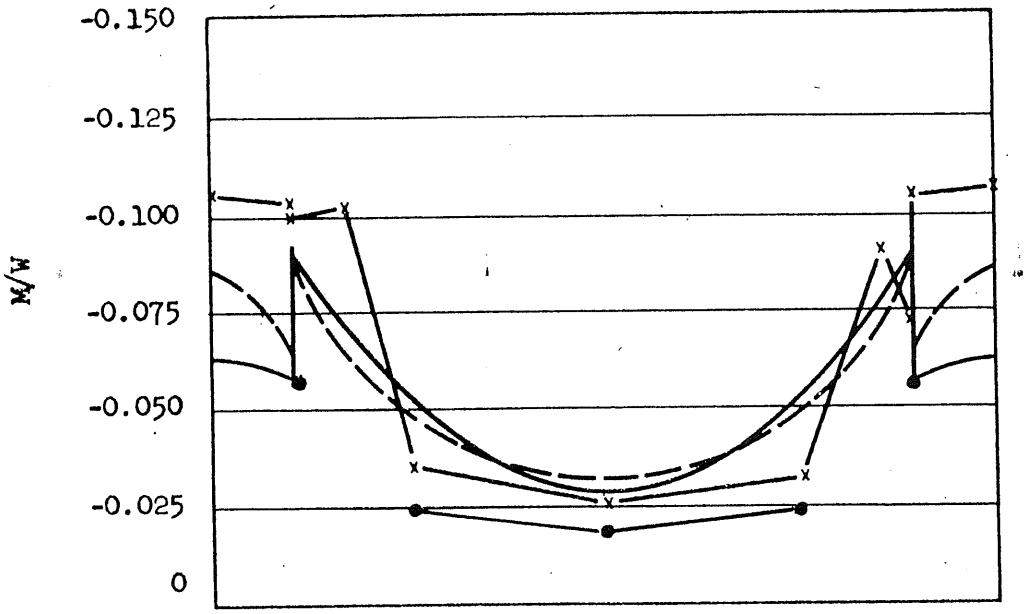

Moment Across Section AA

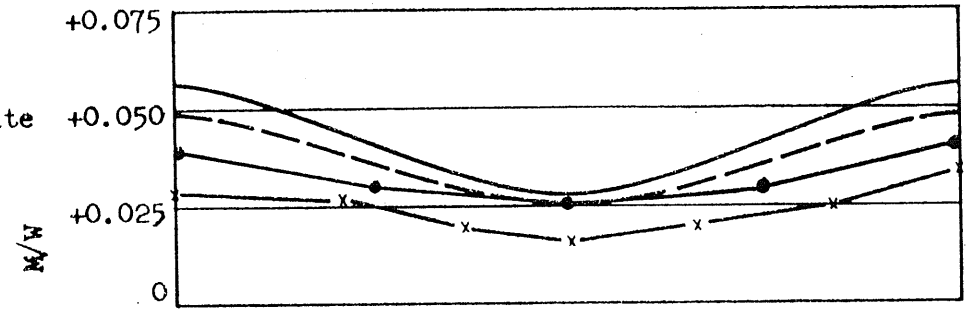

——— Theoretical Moment based on uniform distribution of reaction over capital area

– – – – Theoretical moment based on infinite stiffness of capital at midpoint

—●— Measured moment of F6

—x— Measured moment of F3

M = unit moment (lb.)
W = total load on the panel (lb.)

FIG. 6.12 COMPARISON OF MEASURED MOMENTS WITH THEORETICAL MOMENTS IN THE INTERIOR PANEL - SOLUTION BY NIELSEN

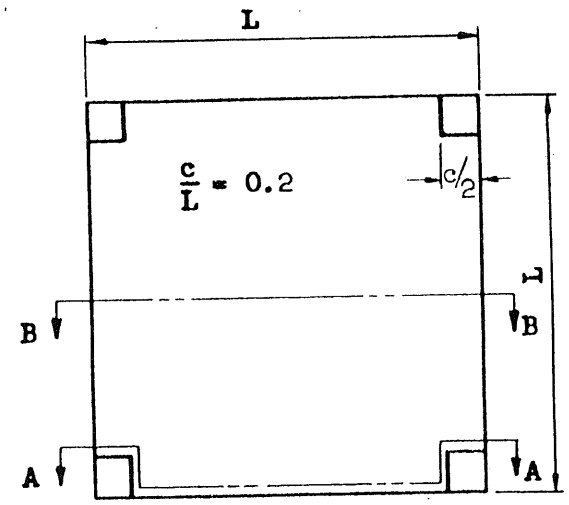

Plan View of Panel

Theoretical Moments

x Measured Moments of F3

Measured Moments of F6

M = unit moment (lb.)

W = total load on panel (lb.)

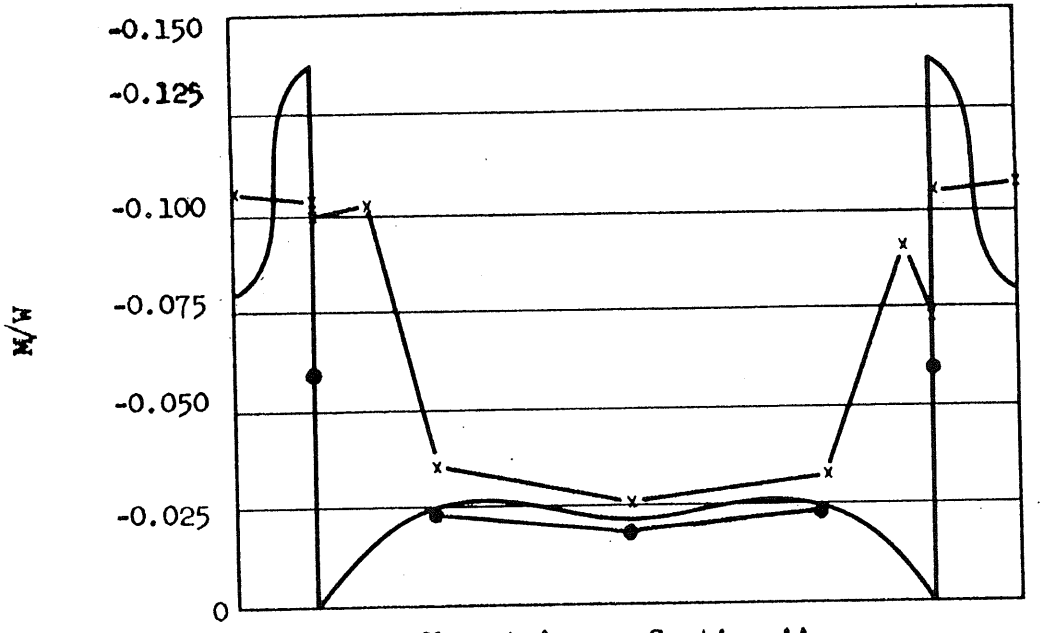

Moment Across Section AA

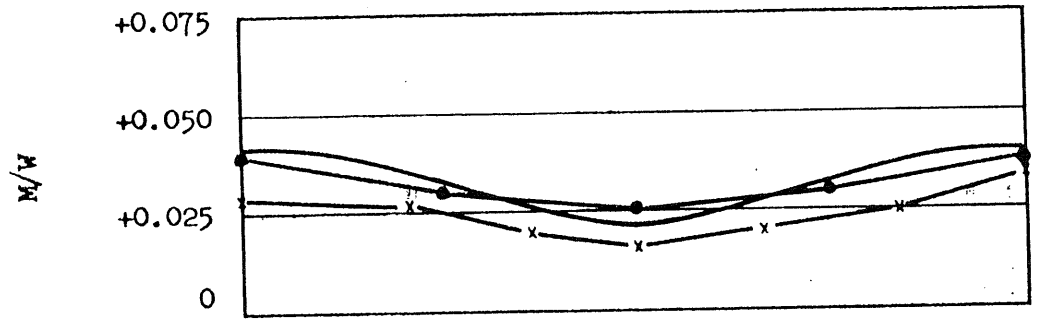

Moment Across Section BB

FIG. 6.13 COMPARISON OF MEASURED MOMENTS WITH THEORETICAL MOMENTS IN THE INTERIOR PANEL - SOLUTION BY CORLEY

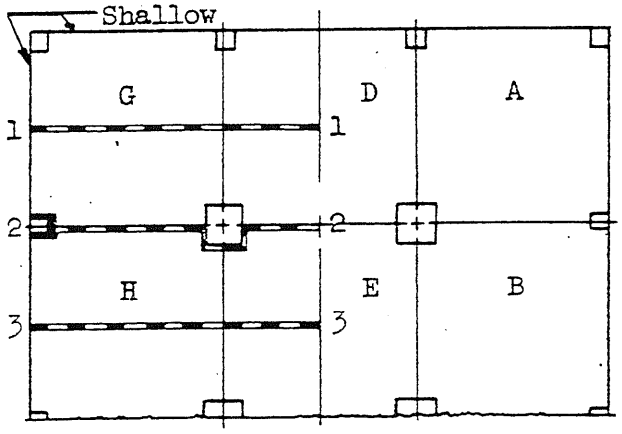

Note:
Size of beam refers to F3

F6 ——
F3 —·—

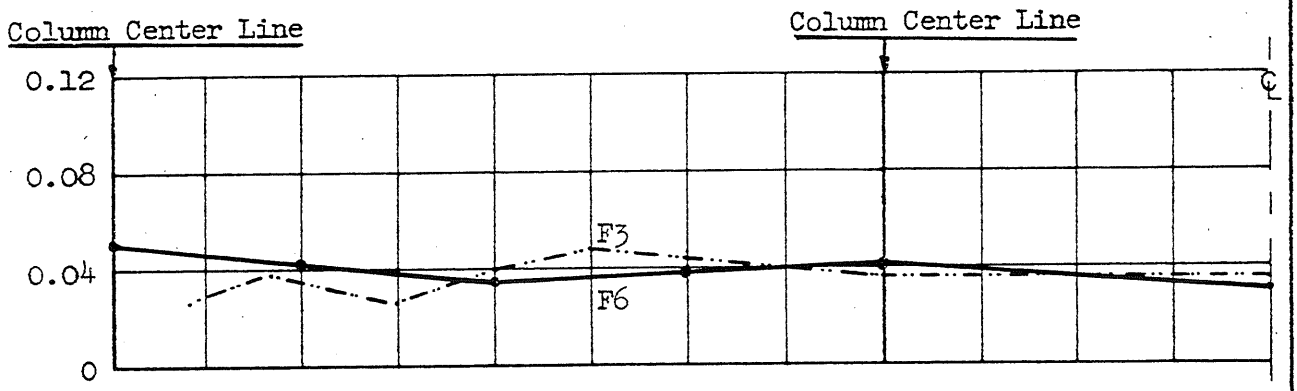

Section 1-1

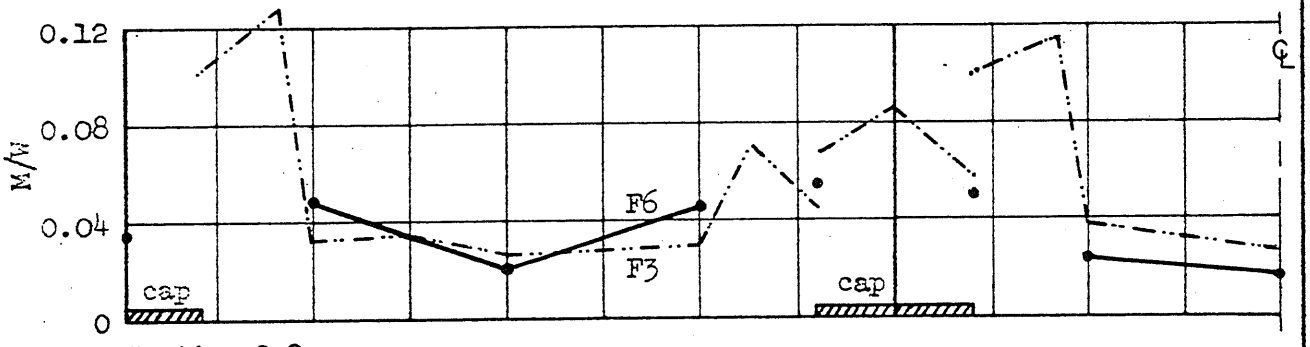

Section 2-2

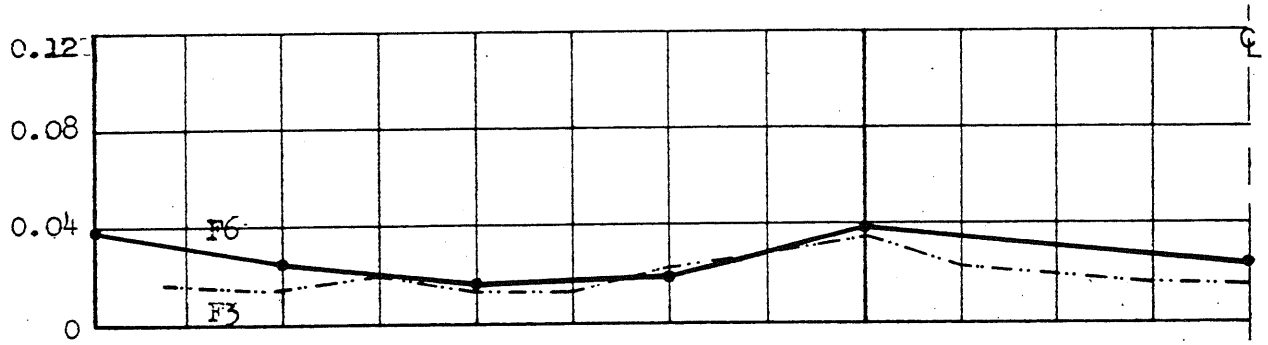

Section 3-3

Load on slab: 100 psf

M = Unit Moment
W = Total load on panel

FIG. 6.14 MOMENT DISTRIBUTION MEASURED AT LOW STAGES OF LOADING

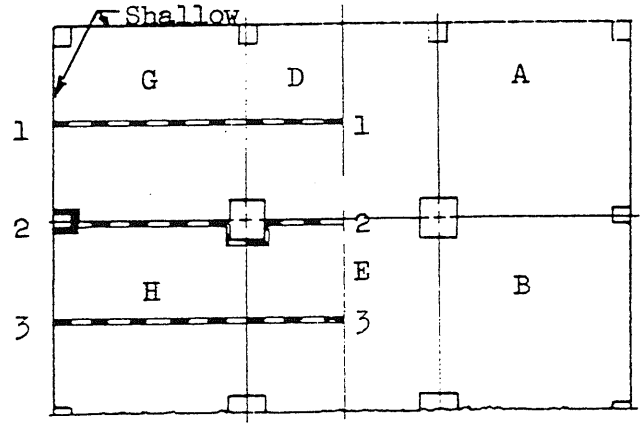

Note:

Size of beam refers to F3

F6 ——

F3 —·—

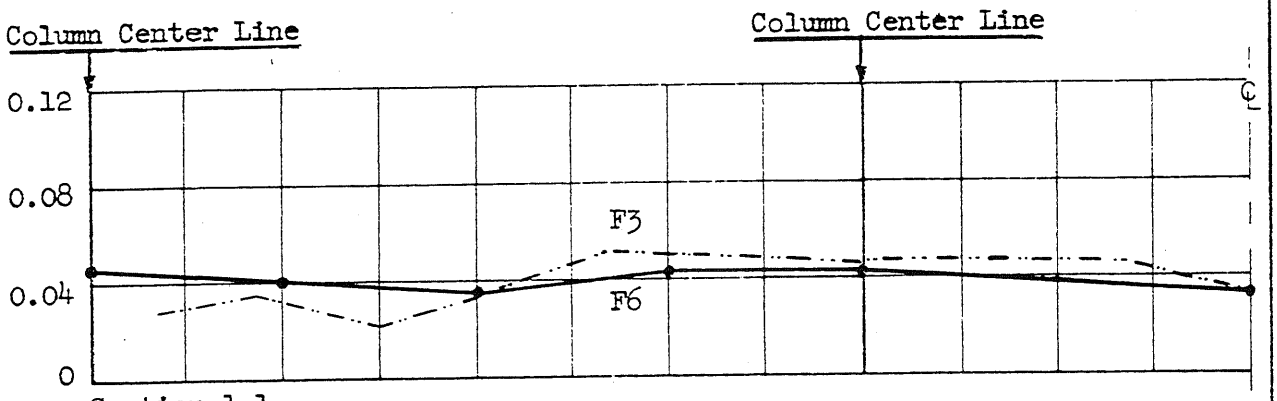

Section 1-1

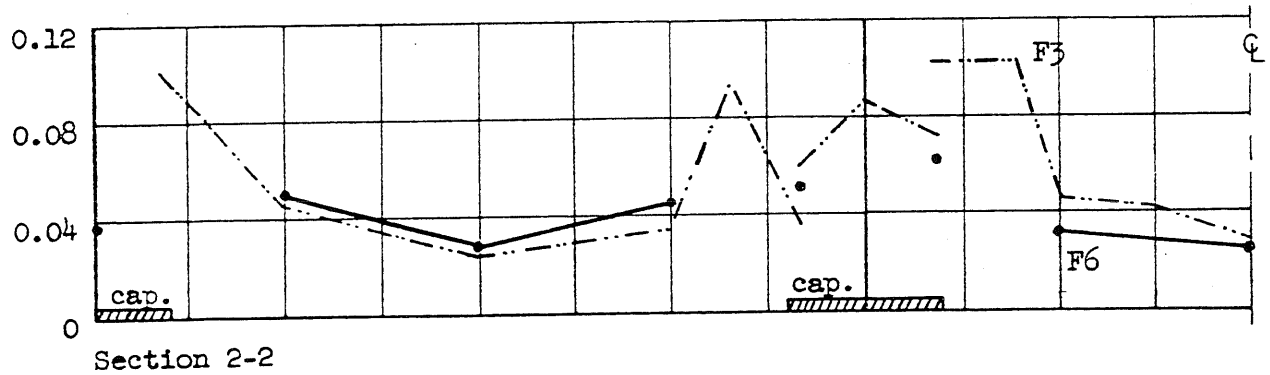

Section 2-2

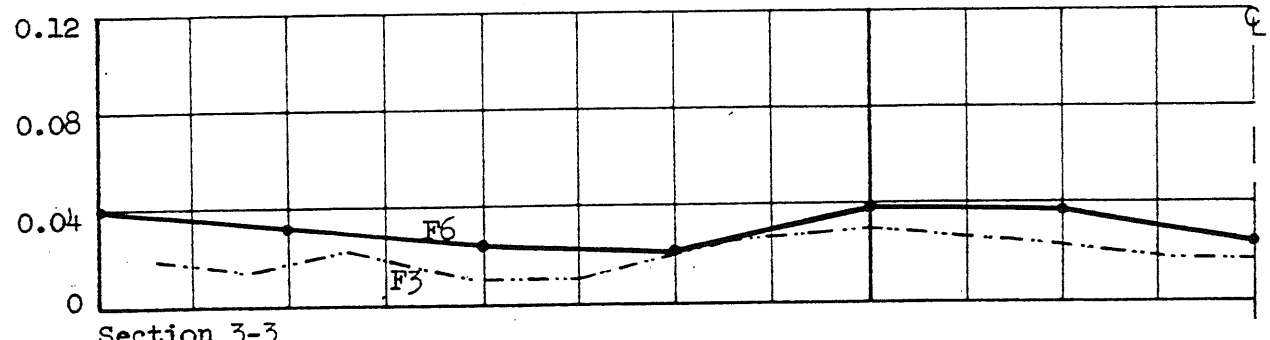

Section 3-3

Total load on slab: 285 psf

M = Unit moment
W = Total load on panel

FIG. 6.15 MOMENT DISTRIBUTION MEASURED AT DESIGN LOAD

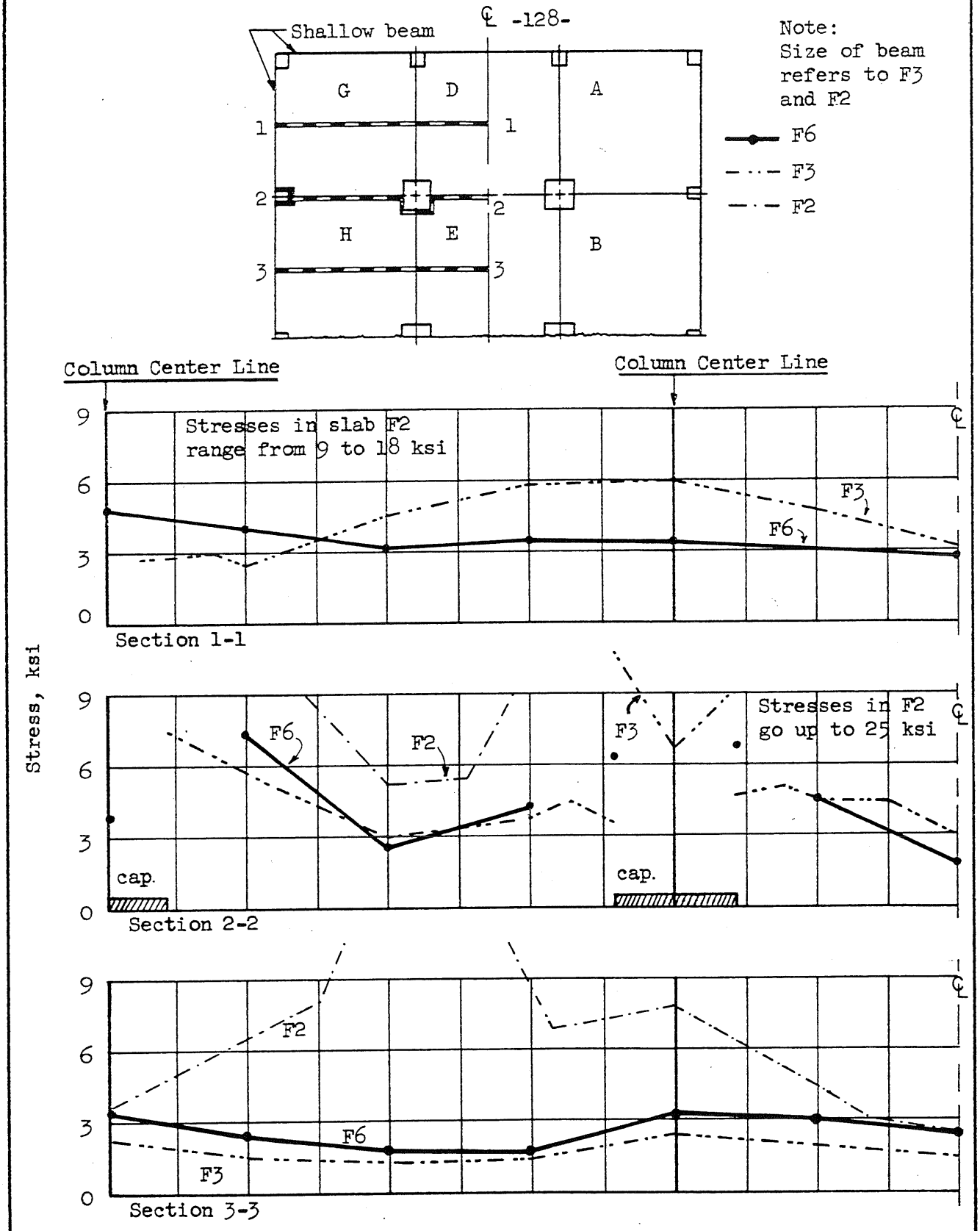

FIG. 6.16 DISTRIBUTION OF SLAB STEEL STRESSES AT DESIGN LOAD

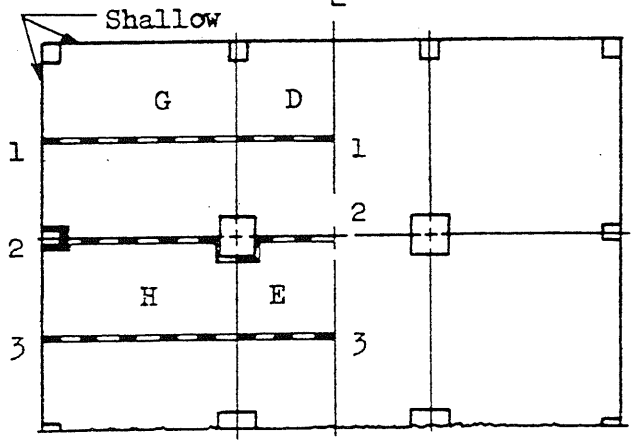

Note:
Size of beam refers to F3 and F2

F6
F3

Column Center Line

Column Center Line

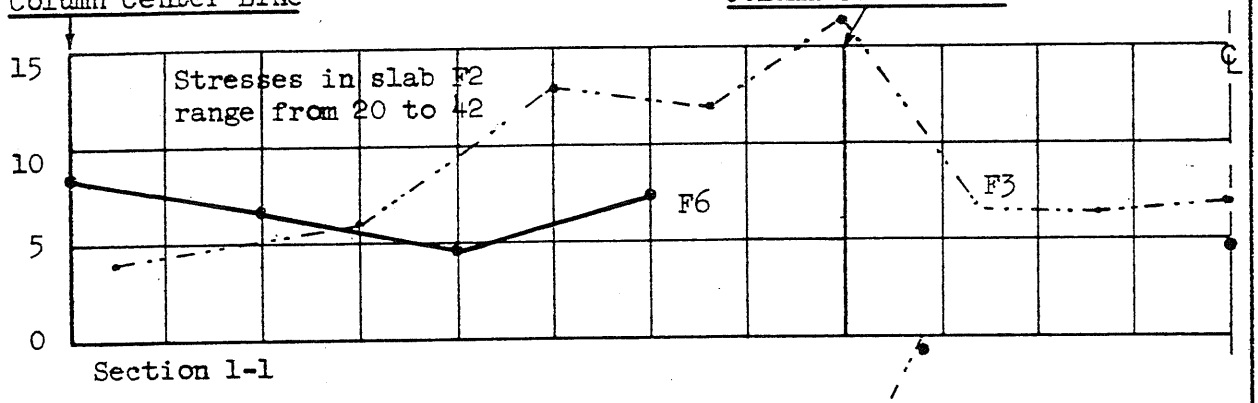

Section 1-1

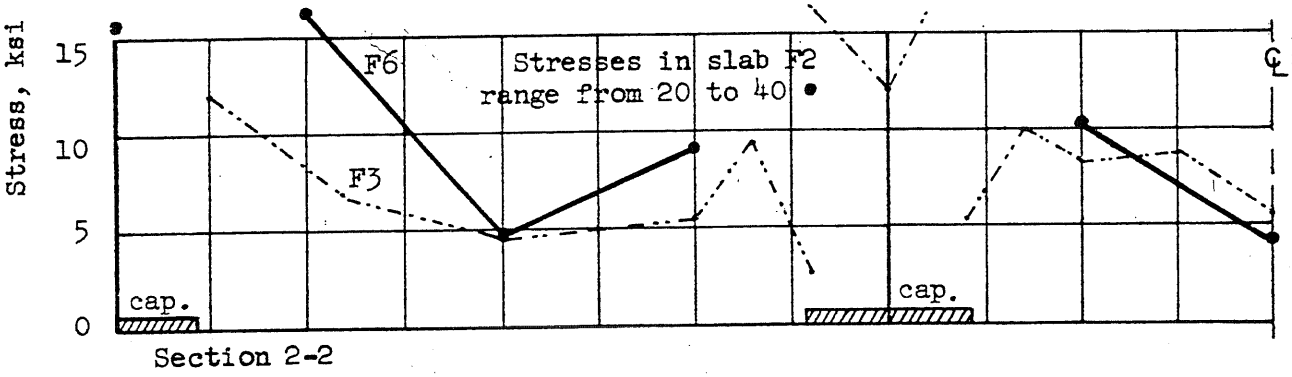

Section 2-2

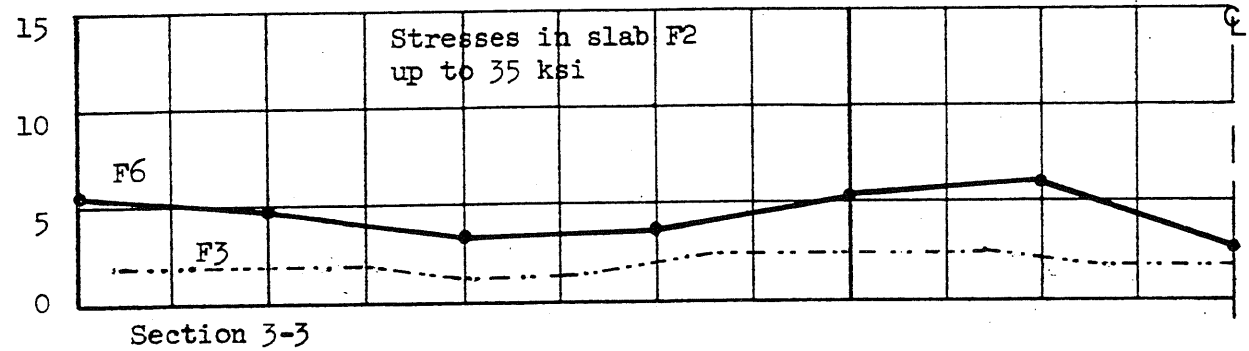

Section 3-3

Load: 1 Dead Load + 1.5 Live Load = 385 psf

FIG. 6.17 DISTRIBUTION OF SLAB STEEL STRESSES AT OVERLOAD

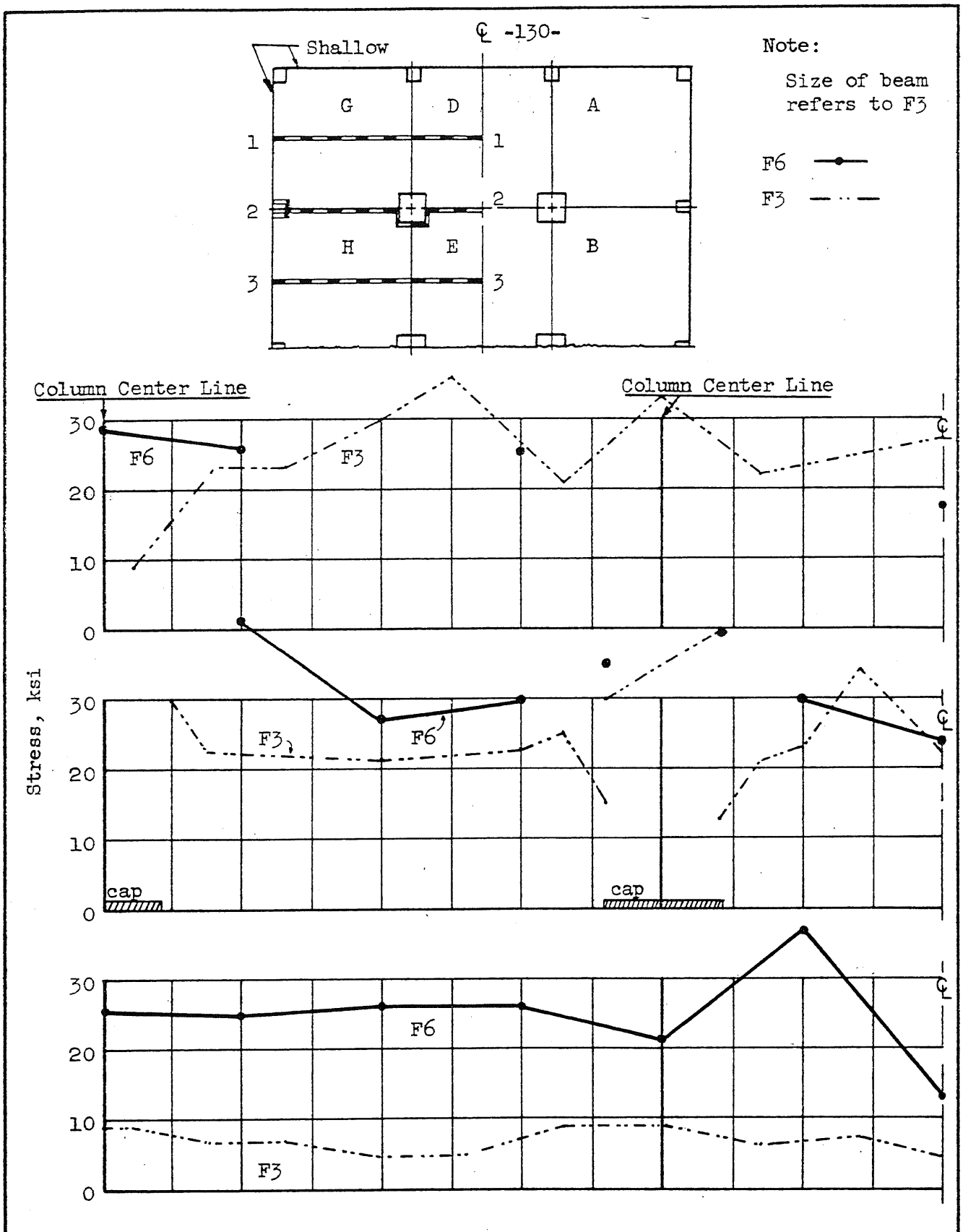

Load: 1 D. L. + 3 L. L. = 685 psf

FIG. 6.18 DISTRIBUTION OF SLAB STEEL STRESSES AT OVERLOAD

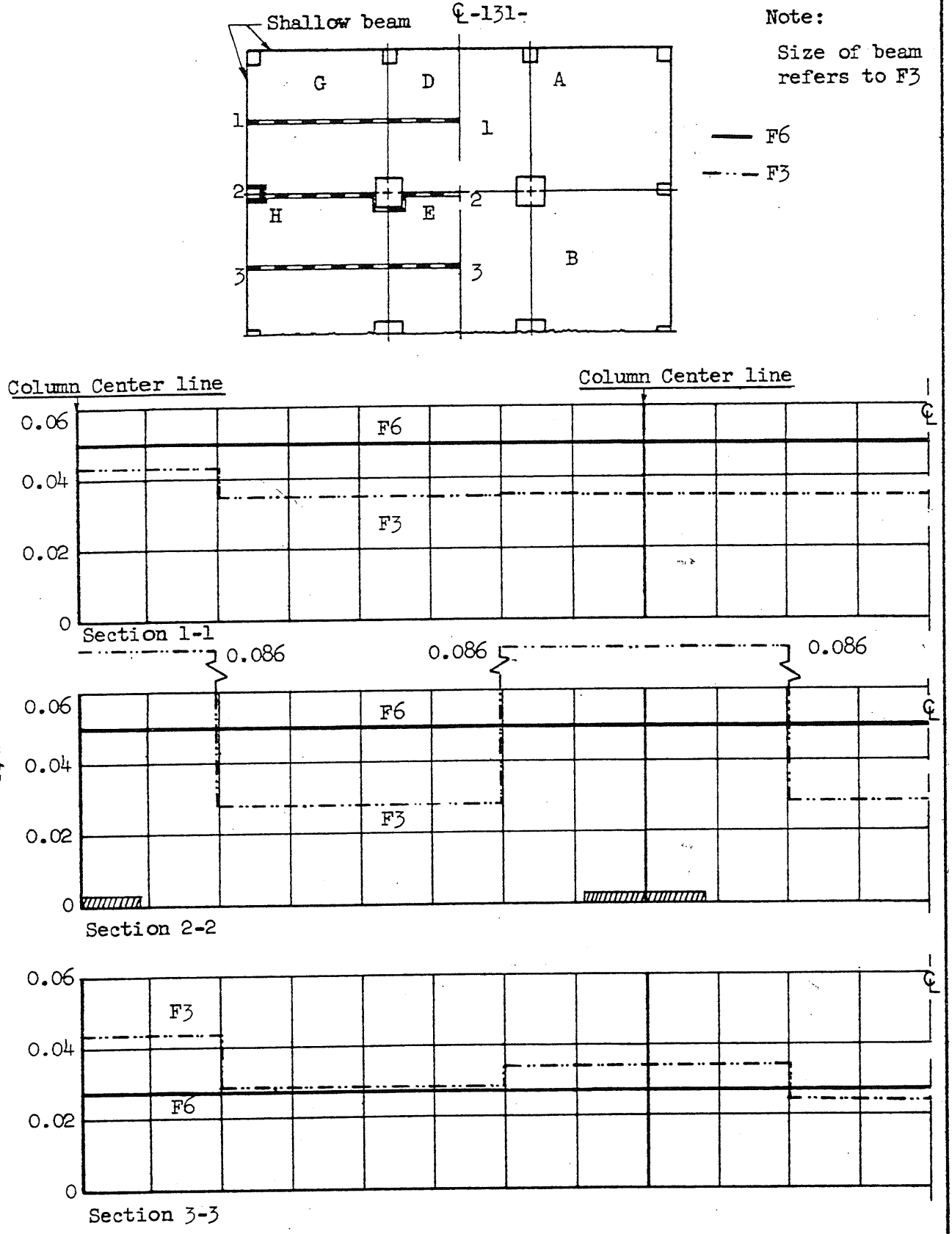

Failure loads: F3: 980 psf
F6: 890 psf

M = Unit moment
W = Total load on panel

FIG. 6.19 MOMENT DISTRIBUTION AT FAILURE OF SLABS

xxxxxx Indicates crushing

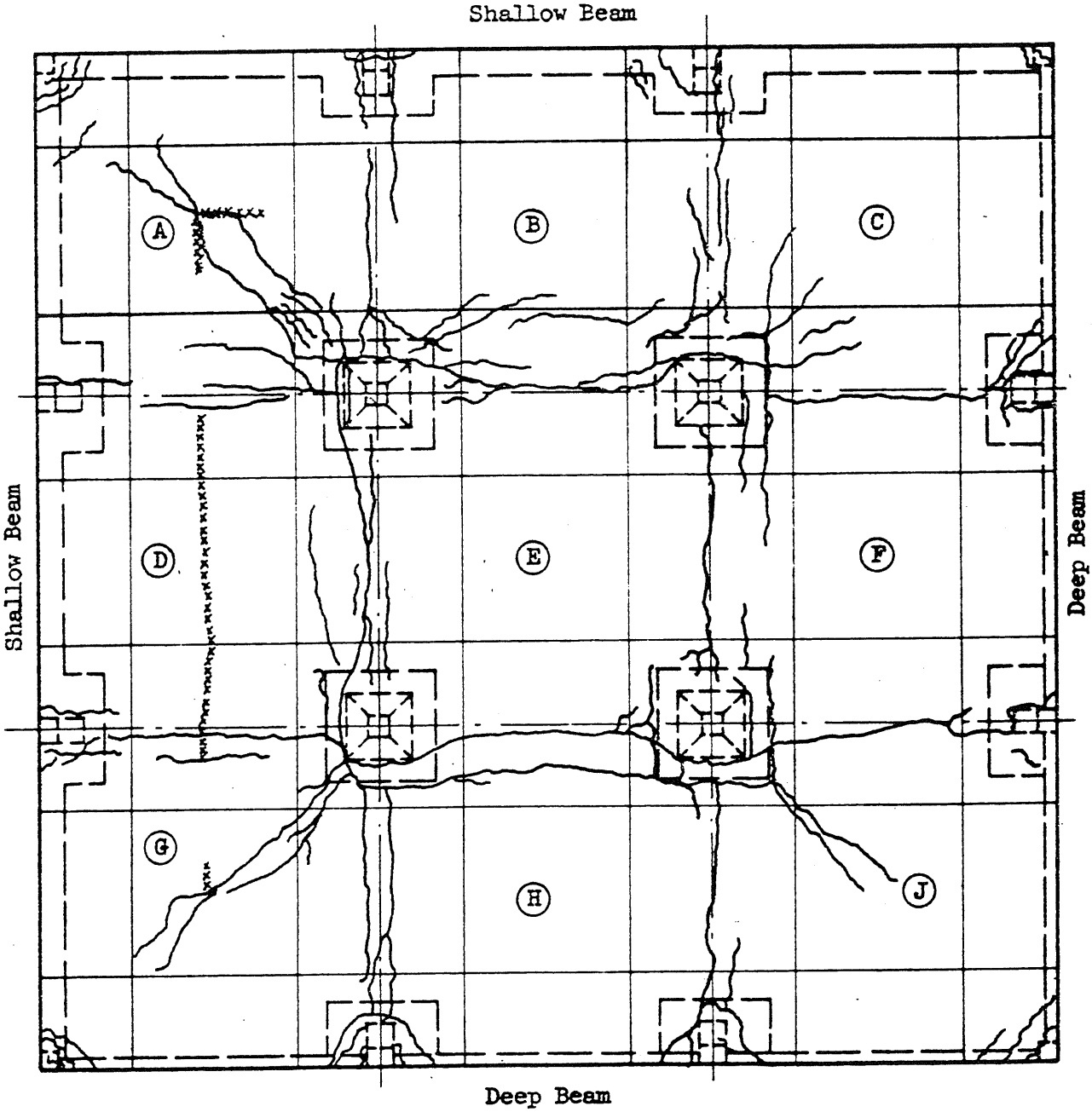

FIG. 6.22 CRACK PATTERN ON TOP OF SLAB F4 AFTER TEST TO FAILURE

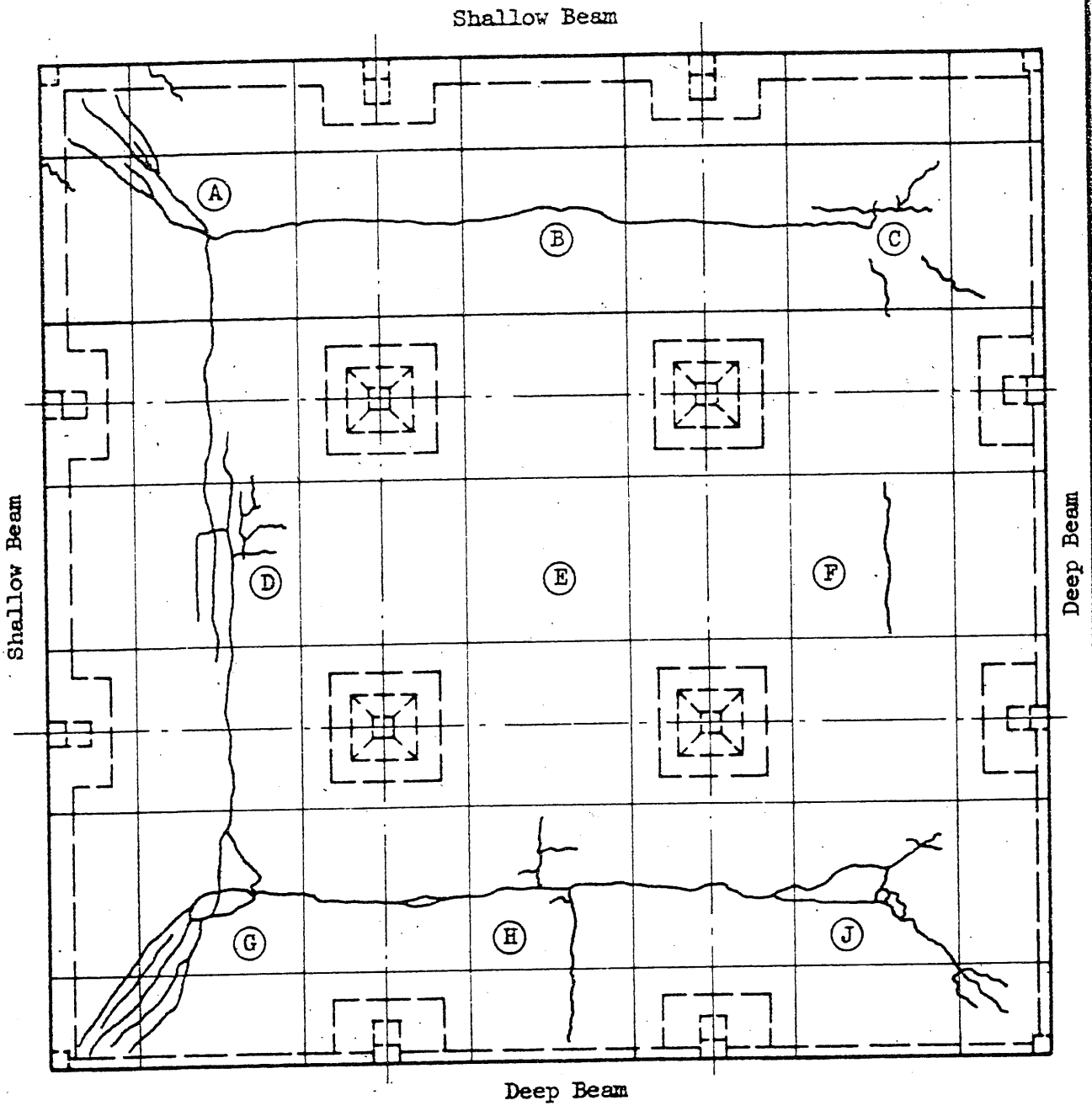

FIG. 6.23 CRACK PATTERN ON BOTTOM OF SLAB F4 AFTER TEST TO FAILURE

Tensile membrane cracks

Cracks related to imminent combined bending and shear failure

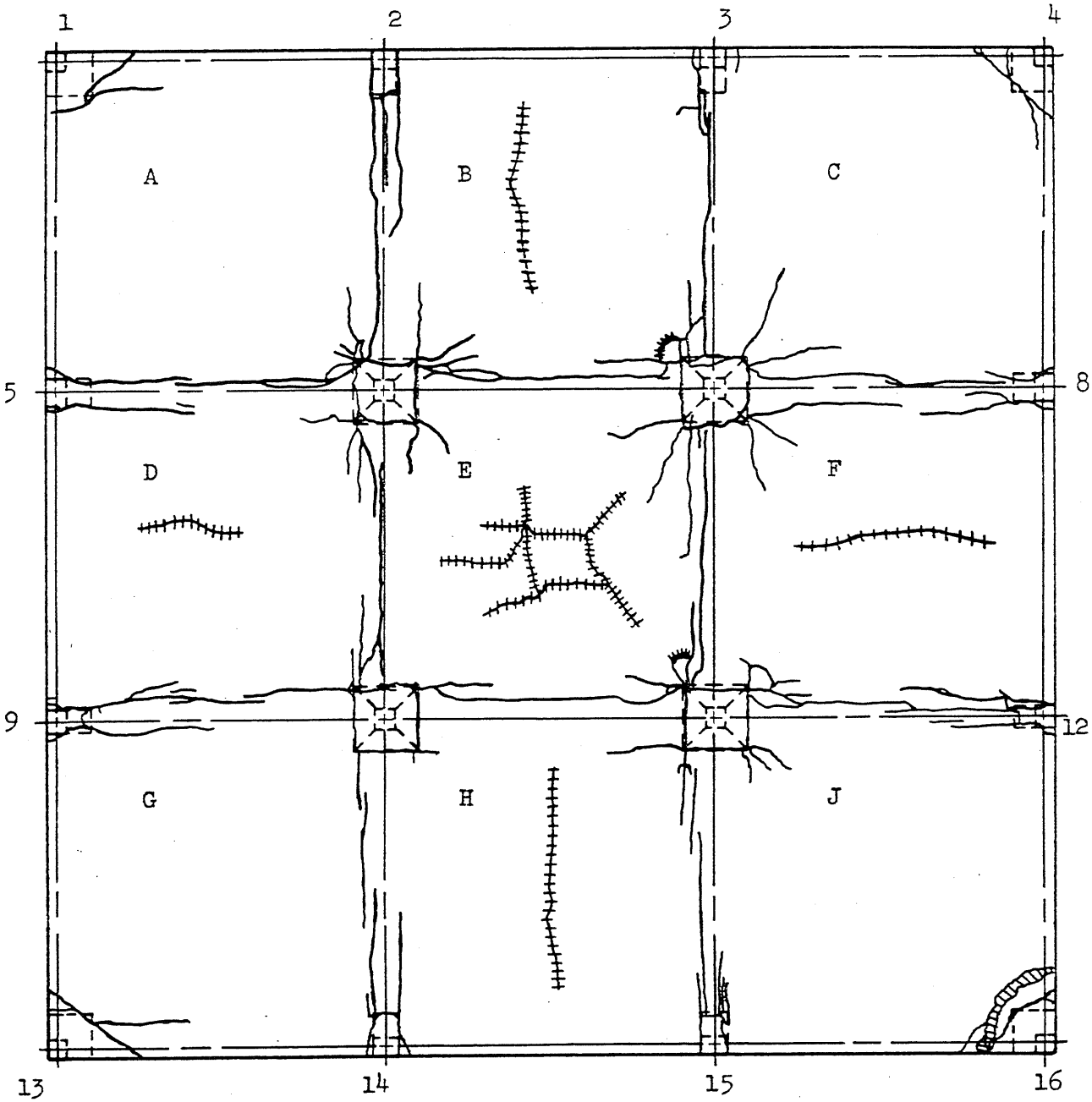

FIG. 6.20 CRACK PATTERN ON TOP OF SLAB F6 AFTER TEST TO FAILURE

Initiation of spalling related to a combined bending and shear failure.

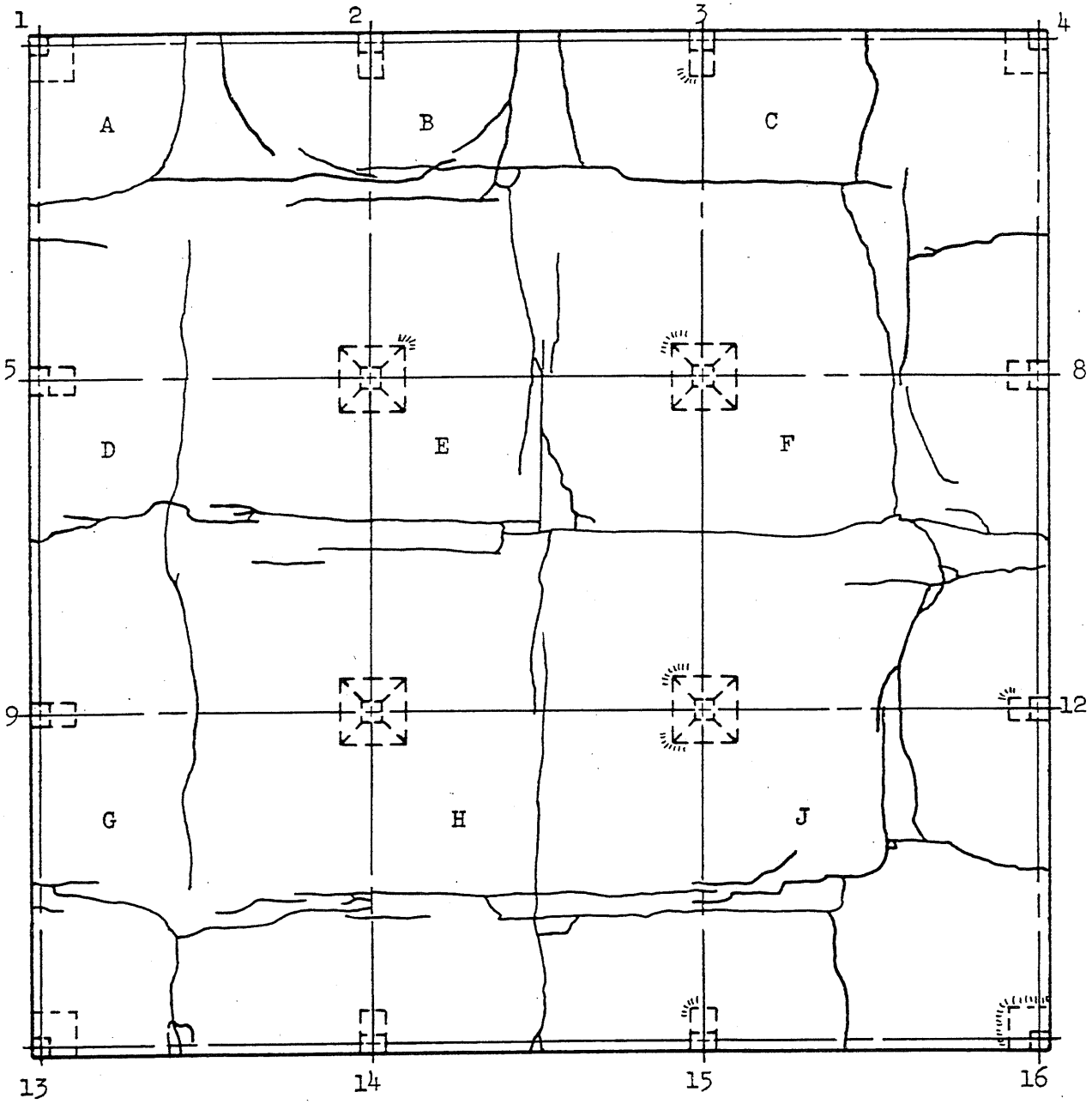

FIG. 6.21 CRACK PATTERN ON BOTTOM OF SLAB F6 AFTER TEST TO FAILURE

APPENDIX A

CONSTRUCTION AND MATERIALS

A.1 Introductory Remarks

This appendix describes in detail the construction procedure and the materials used in the fabrication of the test structure. Essentially the procedure follows that of structure F5, reported in Chapter 4 of Reference (4).

Since structure F6 was a 1/16-scale model with a slab thickness of 7/16 in., great importance must be given to the tolerance in the dimensions of the structure and to the placement of the reinforcement. The description of the construction is thus included to give the reader a means of evaluating the accuracy with which this experiment was carried out. This accuracy must be maintained at a high level if the model is expected to predict the behavior of a full size floor slab.

A.2 Formwork

The structure was cast upon the test frame in the same position which would be used in testing the structure. The test frame consists of a gridwork of 6 WF 12.0 steel beams arranged at 15 in. centers as shown in Fig. 3.1. The bearing points upon which the columns were pinned were adjustable through the base shown in Fig. 3.3 to provide for movements due to shrinkage in the concrete.

The slab formwork was designed in nine separate units (one per panel) fabricated from 1/2 in. plywood faced at the edges with 1/4 in.

balsa wood. The balsa wood was used to facilitate in the close fitting of the panels, as well as to provide a material that would allow some compression of the forms which would be caused by shrinkage of the concrete during the curing period.

The panel forms were supported by a system of wood stringers and cross members which in turn rested on the test frame as shown in Fig. A.1. One-inch clearance was provided between the bottom of the slab forms and the top of the framing system in order to facilitate the form removal and the leveling of the slab forms. The clearance was filled with shims. The form for each panel was then bolted to the framing system by seven bolts which could be loosened to insert or remove shims. Once the slab had cured and the columns supports raised to contact the columns, the bolts could be removed and the framing system slipped out from under the slab, after removing the shims.

The edge of the slab was formed by a steel frame of 1/4 by 2-in. plate enclosing the perimeter of the structure (see Figs. A.1 and A.2). The steel frame, which was fastened to the wooden framing system and to the plywood forms, was used as an exact screed guide.

The placement of the column and capital Plexiglas forms for the interior columns consisted of positioning the column-capital form in the corresponding hole in the formwork, lining the column through a system of plumb-bobs hanging from a nylon thread grid stretched across the peripheral steel plate, and gluing the Plexiglas column-capital form to the 1/4 in. balsa trim of the slab forms (see Fig. A.3). The exterior columns were fastened directly to the peripheral steel frame by machine screws, making the steel plate part of the column form (see Fig. A.2).

Weep holes of 1/8 in. diameter were drilled through the Plexiglas forms to aid in placing the concrete in the columns.

After the construction of the formwork, the slab depth was checked to within ± 0.01 in. by means of a feeler gage and a 7/16 in. calibrated steel prism. The thickness was checked against a nylon thread stretched between opposite screed guides. If the error exceeded the above quantity the forms were shimmed. After completion of the checking, the form was shaken vigorously to test its rigidity. The form measurements were checked again and no deviations were discovered. Two coats of "Slippit", a paraffin base form-lubricant, were applied to ease form removal. Figure A.4 shows a view of the formwork after completion.

A.3 Manufacture of Reinforcement

The reinforcement was made from high strength bright basic wire of 0.0355 in. diameter with no well-defined yield stress. The wire came in rolls of 18-in. diameter. Thus it was necessary to straighten and anneal this wire. A stressing rack 18 in. long was built to hold 200 lengths of wire. The wire was strung on the rack and enough tension was applied to keep the wire straight. The rack was then placed in a small industrial oven with the temperature maintained at 1175° F. for four hours. The rack was then removed, the wires relaxed from the end anchor and allowed to cool in the air. Figure A.5 shows the rack with wire before annealing.

After cooling the wire was placed in a bath of one part hydrochloric acid and two parts of water in order to remove all the mill scale.

The wire was left in the bath for about five minutes; then it was thoroughly rinsed and dried.

A similar procedure was followed in manufacturing the column steel.

A.4 Slab Reinforcing Mats and Column Cages

For ease in placing the reinforcement it was fabricated in mats of convenient size. The wires were placed in grooves of the correct spacing, machined onto a Plexiglas guide, and clamped down. Another orthogonal group of wires was clamped on the former wires and then connections were welded at staggered intersections at intervals of about one inch. This insured a relatively stiff mat which could resist handling and the casting operation. A Weldmatic, Model 1016C, resistance welder was used at 10 wattseconds heat output for these welds.

The effect of a weld was to reduce the yield stress by about 4 percent, but since in each cross section of a mat only one out of six wires was welded, the over-all reduction in yield stress was considered negligible.

Column reinforcement cages were fabricated using 16-gage annealed wire for vertical steel and slab reinforcement for ties. The ties were welded to the vertical reinforcement at 20 wattseconds heat output.

A.5 Placement of Reinforcement

The first reinforcement to be placed was the column cage steel. To insure proper and firm positioning of the cage, 20 gage wire was welded to the outside of the cage and bent outward so as to establish bearing

against the form. The longitudinal column steel was welded to the steel plate and shear connectors shown in Fig. 2.5.

The positive moment slab reinforcement was placed next. Adequate cover was achieved by resting each mat (which covered the whole panel) on short lengths of wire of the necessary diameter. The mats were then tied directly over this spacer by means of thin copper wire passing through small holes drilled through the forms. The system was extremely rigid since over 200 tie downs were used per panel.

Placement of the negative reinforcement mats was preceded by the attachment of chairs to the mats. These chairs were made of 20-gage wire welded perpendicular to the plane of the mats as shown in Sketch A.

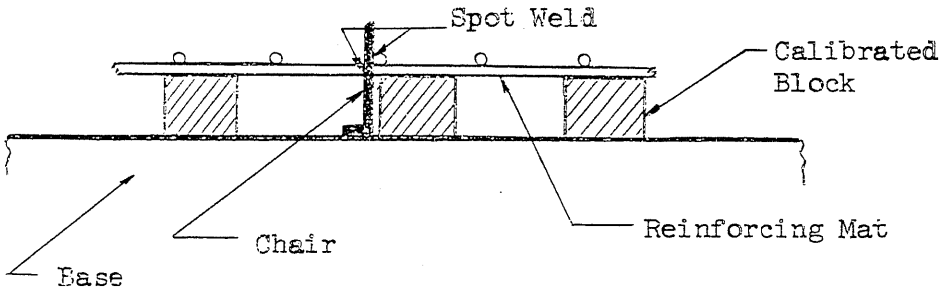

Sketch A

These chairs were placed at approximately one inch intervals. The mats were then placed in their corresponding locations and tied to the form at each chair position.

Figure A.6 shows a detail after the placement of the reinforcement was completed. Figure A.7 shows another view of the reinforcement. The negative steel and the chairs that held it in place may be seen at the left hand side. The gentleman seen in the picture is pointing to one of the 144 plastic lugs used to pre-form the holes in the slab through which the loading cables would pass. Figure A.8 shows a complete view of the

structure before casting. The small arrows point to the locations of the electrical steel strain gages. At Column 5, the clearance between the negative reinforcement and the screed edge is being checked by means of a feeler gage.

At the completion of the placement of the reinforcement, careful checks were made to insure that sufficient tie downs had been made and that the elevation for all the steel was correct. The rigidity of the mats was such that by pressing on them with the open palm the whole formwork could be jarred without displacing the reinforcement.

A.6 Casting

The aggregate used in the concrete mix consisted of two types of sand. The coarse portion was a Wabash River Sand which was sieved through a No. 14 U. S. Sieve Size screen. Only the material passing this sieve was used as a coarse aggregate. The fine portion was a Lake Sand. One day prior to casting the aggregate was oven dried.

The cement used was Type I Lehigh Portland Cement.

The desired mix was one that would minimize shrinkage, that is, a rather stiff mix. However the narrow space available through which the concrete had to pass to fill the column forms dictated some workability requirements. The mix used was one that would flow only when vibrated.

Casting began at 2:30 p.m. on the 27th of March 1963. The mixing was accomplished in a 2.0 cubic foot Lancaster Mixer. Mixing time was three minutes, care being taken to insure that all the constituents were well blended. The batch proportions were:

Coarse Sand	145 lbs.
Fine Sand	40 lbs.
Cement	37 lbs.
Water	27.5 lbs.
w/c (by weight)	0.74

Casting of the structure began at a corner column (No. 13). Concrete was piled over the column and the steel edge of the form was vibrated until the concrete filled the Plexiglas form and began flowing from the weep holes in the column form. Additional vibration was applied directly to the concrete over the column to insure proper filling of the form, care being taken not to disturb the steel with the vibrator. The operation was continued until all the columns were full, and then the slab itself was vibrated from the bottom and on the surface. During the casting operation, the negative reinforcement mat over Column 1 was bent and some bars were displaced. The mat was partly removed, straightened, rewelded, and replaced in its correct position. It was then covered with concrete which was vibrated.

After the concrete was in place it was screeded with a 2 by 4-in. planed wood screed which rode on the steel edges of the slab form. The test cylinders and companion beam specimens were cast at this time. The entire operation was completed in two hours.

The surface was troweled lightly one hour after the screeding was completed. Six hours after casting, the structure, cylinders, and companion specimens were covered with wet burlap and a plastic moisture barrier on top. Two days later the cylinders were removed from the molds

and maintained under wet burlap and plastic. Curing was continued for seven days after the completion of casting during which time the burlap was maintained saturated, and then the burlap was removed. Variation of ambient temperature during curing varied from 75 to 85° F.

A.7 Form Removal

Form removal began April 4, 1963 with the removal of the steel edge form. Subsequently the plastic forms of the columns were removed. During this operation, extreme care was exercised in the removal of the forms from the corner columns, since they were very susceptible to damage from moments different from the design moments of the slab. However, Column 4 was damaged as described in Section 2.5, and precast capitals had to be added to the corner columns (see Fig. 2.15).

After the column forms were removed, the column base plates were adjusted to insure proper bearing, and the supporting wood framework was removed. The balsa wood trim of the slab panel-forms was stripped, and the plywood sections were removed, after cutting the reinforcement tie-down wires, by lightly prying the edges of each form. Five strain gage leads were severed during the removal of the forms of panels G and D.

After the slab forms were removed, the plastic lugs that formed the holes in the slab were pulled out, leaving 144 holes at the load point locations, through which the loading cables were to pass.

The operation was completed on April 6. No voids of serious magnitude could be seen. The structure after form removal and after the placement of the loading plates and cables, and precast corner column capitals is shown in Fig. A. 9.

No shrinkage cracks could be detected in the structure.

APPENDIX B

RELATED TESTS

The purpose of this Appendix is to describe to a limited extent some control tests which were conducted in relation to this investigation.

B.1 Behavior of Small Scale Models

Reference (4) describes the construction and testing of structure F4. The sole purpose of this structure was to determine if a very small scale reinforced concrete model could be used to predict the behavior of a full scale structure. Since structures F2 and F3 were 1/4-scale structures identically proportioned in geometry and steel cross sectional areas, it was decided to construct F4 as a 1/16-scale structure with identical proportions to these two 1/4-scale structures. There existed some differences, however, in the material properties of the structures. These properties have been tabulated in Table 6.1. The behavior of the three structures can be compared by looking at curves F2, F3 and F4 in Fig. 6.4. It may be seen that the limit load on each structure is within two to three percent of being in direct proportion to the yield stresses of the respective structures. The behavior at initial stages of loading is related to the concrete strength, and the behavior of F4 is close to that of F3 since their concrete strengths are similar.

It was concluded in Reference (4) that the behavior of a 1/16-scale structure could predict the flexural behavior of 1/4-scale

structures at all stages of loading. Any differences could logically be accounted for by considering the properties of the materials measured through standard tests.

The behavior of the 1/4-scale structures was compared with the behavior of a 3/4-scale structure tested at the Portland Cement Association's laboratories. The correlation indicated that the behavior of the 1/4-scale model did not differ substantially from that of the near full-scale structure.

It can be stated then, that very small scale structures can accurately predict the flexural behavior of full scale structures when suitable materials are used. The properties of the materials used in this investigation, measured through standard ASTM tests, have shown good similitude with the properties of the materials used in full scale structures insofar as the properties important in flexural behavior are concerned.

B.2 Strength of the Test Slab in Combined Bending and Shear

In order to investigate the possibility of designing the test structure without drop panels, it was necessary to investigate the shear capacity of the slab. For this purpose it was decided to conduct some punching tests on slab samples identical to the slab sections over the columns of the test structure.

The proportions of the slab specimens were chosen such that the span would be long enough to allow the development of yield lines across the load point, before the shear capacity was reached. This would be the expected behavior of the test structure. The dimensions of the samples

are shown in Fig. B.1. Figure B.2 shows a specimen after the load to failure was applied. Figure B.3 shows the top and bottom views of two specimens.

The concrete mix for the specimens had the same proportions as the mix described in Appendix A.4, except that high early strength cement was used. Two specimens were tested after one week of moist curing; another specimen was tested after one week of moist curing and one week in the laboratory. Computing the nominal shear strength at a section d/2 from the face of the loading lug, the results were:

Specimen	Age at Test	f'_c	Failure Load	v	$v\sqrt{f'_c}$
1	1 week	2750 psi	555 lb.	420 psi	8
2	1 week	2750 psi	550 lb.	420 psi	8
3	2 weeks	4200 psi	655 lb.	500 psi	7.6

B.3 Calibration of Dynamometers

Since the loading system used in the test structure was determinate and suspended by flexible cables 3 ft. long, no eccentric load of substantial magnitude could be induced on the dynamometer which was bearing on a 1/2 in. ball bearing (see Fig. 3.2). It was thus deemed advantageous to calibrate the dynamometers using a setup which could simulate the actual operating conditions.

The apparatus used is shown in Fig. B.4. The four legs rested on the testing machine base and the load was applied by pumping the jack against the machine head. The load was then recorded to the nearest pound from the testing machine reading. Strain readings from the dynamometer

were recorded at each load increment. The load was increased up to 2,000 lb. in 15 increments and then removed while readings were being taken, thus providing a calibration curve for loading and unloading. When the load was completely removed the dynamometer was rotated 90° and recalibrated. This procedure was repeated four times. Then an eccentricity was induced by raising the adjusting nut under one of the beams and another calibration was performed. Throughout these tests, the calibration curves remained within ±7 lbs. of each other. The procedure was identical for the nine dynamometers used. The dynamometers have been briefly described in Section 3.1.

The applied load on the structure could thus be recorded to within ±5 psf.

B.4 Flexural Specimens

Part of the mix that was used in casting the test structure was also used for the companion flexure specimens. The dimensions of the beams and the manner of testing are shown in Fig. B.5. Figure B.6 shows a reinforced specimen after the test to failure.

A total of 14 beams were tested, four of which were plain concrete beams. The other 10 beams had steel spacings and depths representative of the two different spacings used in the slab and the two different depths imposed by the different levels of the bars in a given reinforcement mat. The testing of the beams was not carried out until 40 days after the testing of the slab. During this time the beams remained fastened to their plastic forms.

The average modulus of rupture of the four plain concrete beams was about 780 psi with a range of 680 to 820 psi, while the average of the ten reinforced beams was 750 psi with a range of 620 to 800 psi.

The yield moments measured in the reinforced beams were on the average about five percent higher than the moments computed from equation 5.1. The discrepancy can be ascribed to a slight load arching in the loading system.

One reinforced concrete specimen was instrumented with electrical strain gages of the type used in the slab reinforcement. The moment-strain curve computed by means of the method of Fig. 6.11 was in good agreement with the measured moment-strain relationship from the beam test.

All the reinforced beams showed satisfactory ductility since the midspan deflections were on the order of L/10 (L = span).

These tests showed that the classical methods of flexural behavior and capacity computations can be used to predict the behavior and strength of very small scale models.

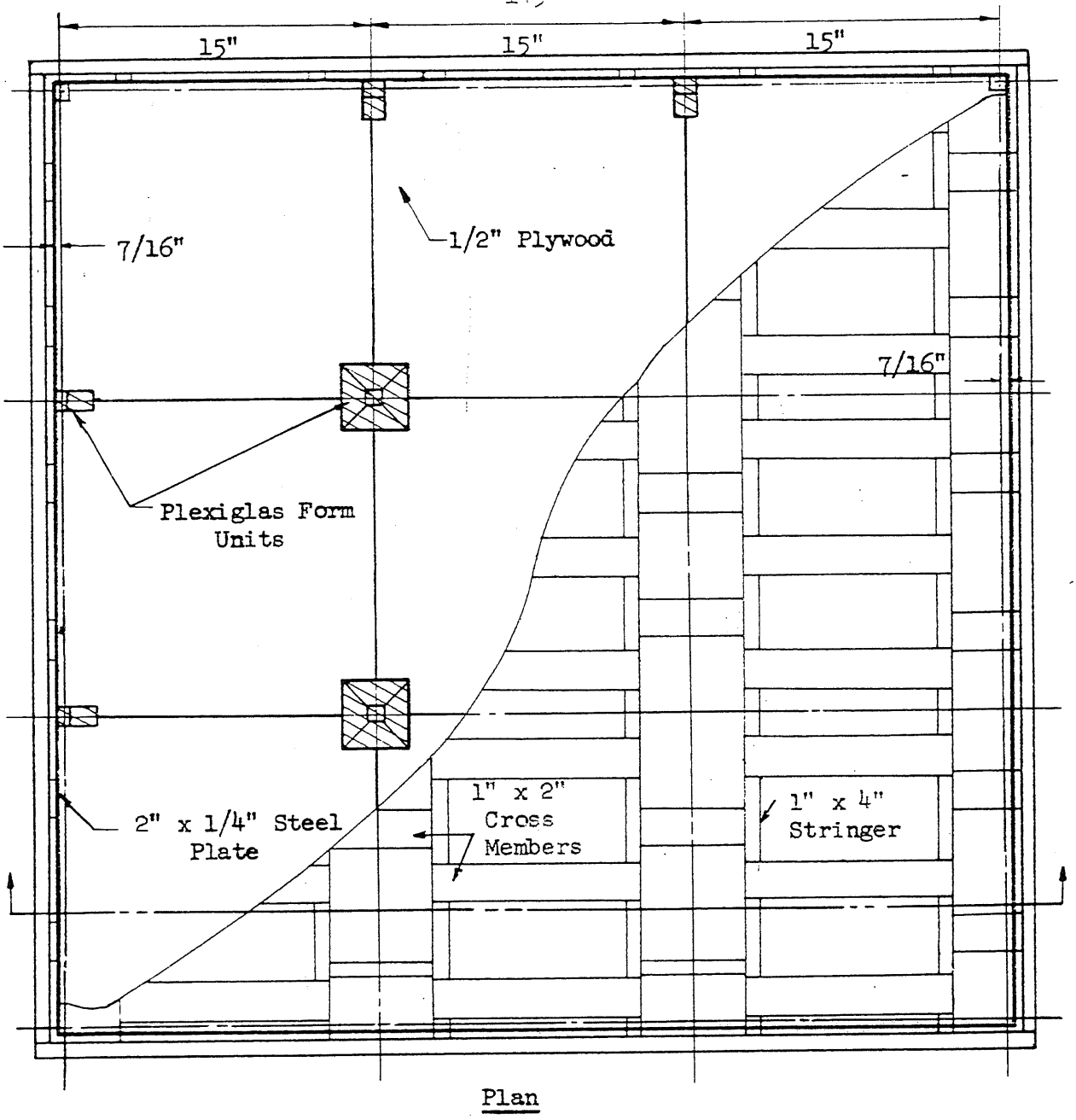

FIG. A.1 PLAN AND SECTION OF FORMWORK

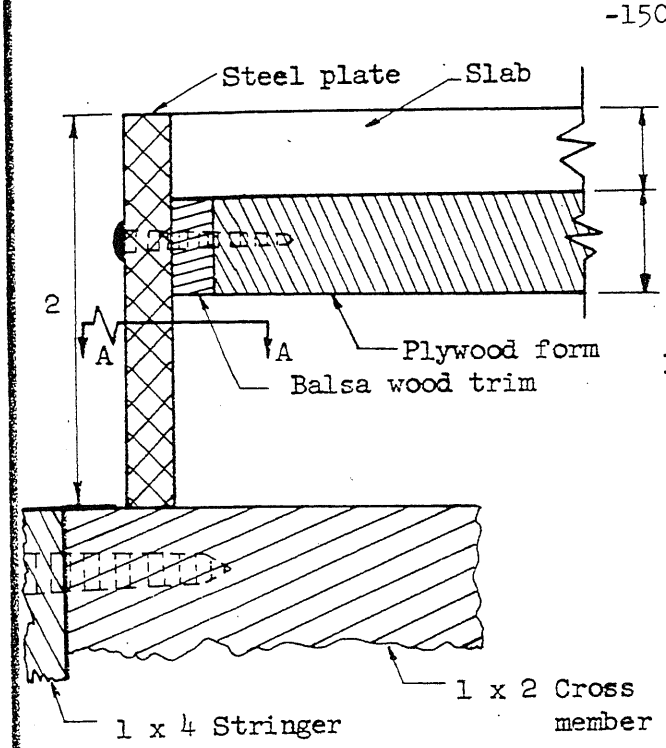

Above: Elevation - Section C-C

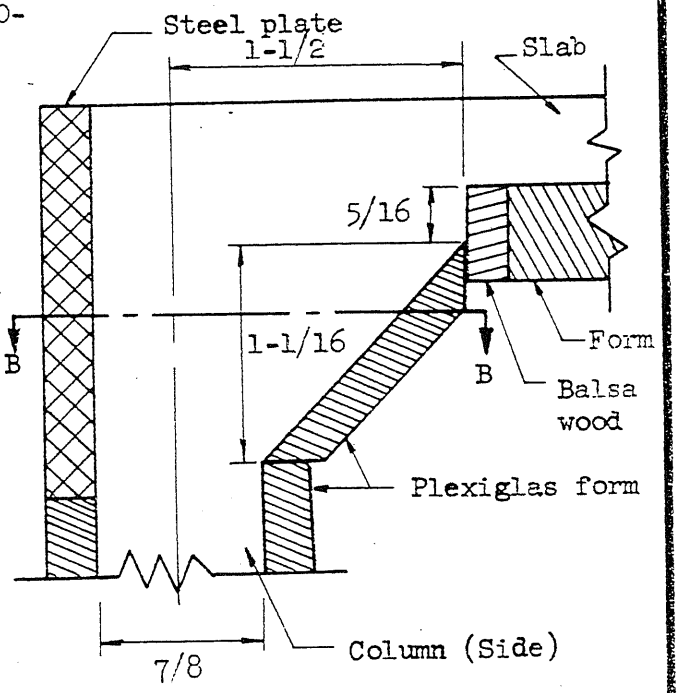

Above: Elevation - Section D-D

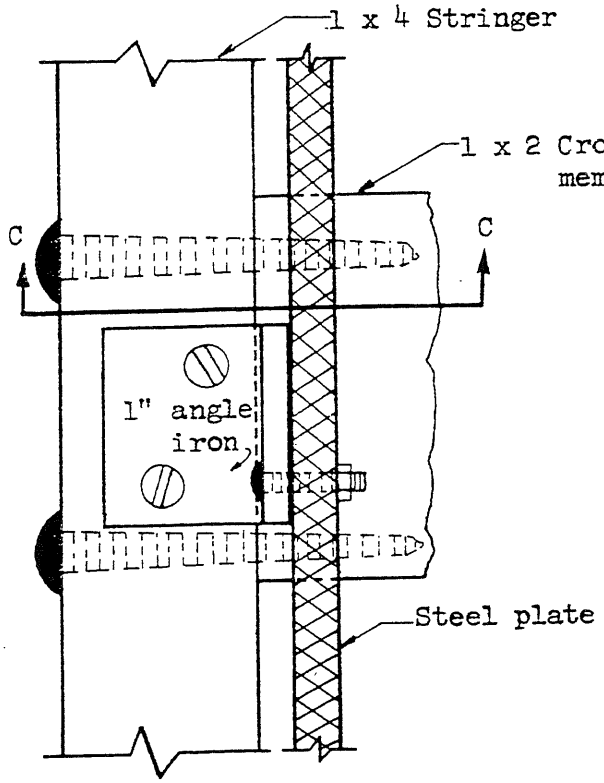

Above: Plan - Section A-A

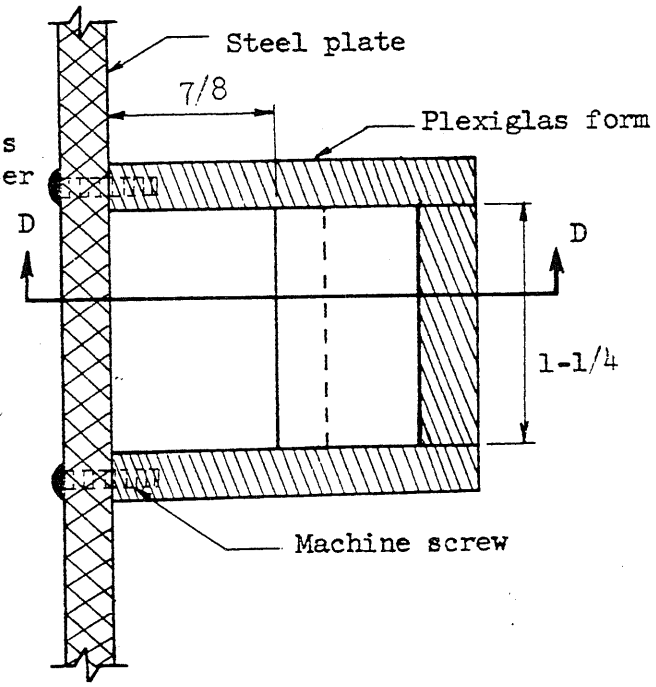

Above: Plan - Section B-B

Note: All dimensions in inches

FIG. A.2 DETAILS AT EDGE OF FORMWORK

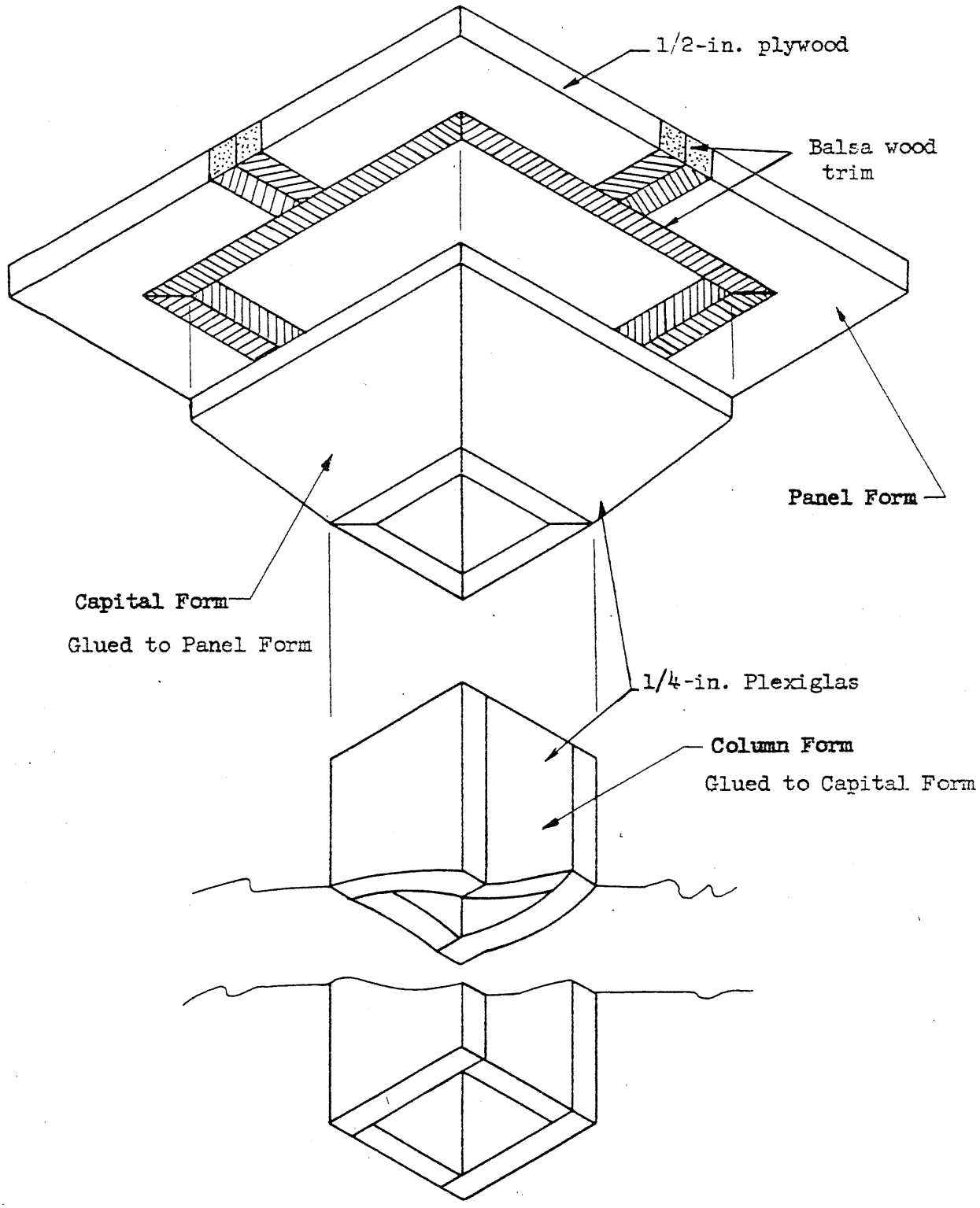

FIG. A.3 CONNECTION OF COLUMN AND CAPITAL FORMS TO SLAB FORM (INTERIOR COLUMN)

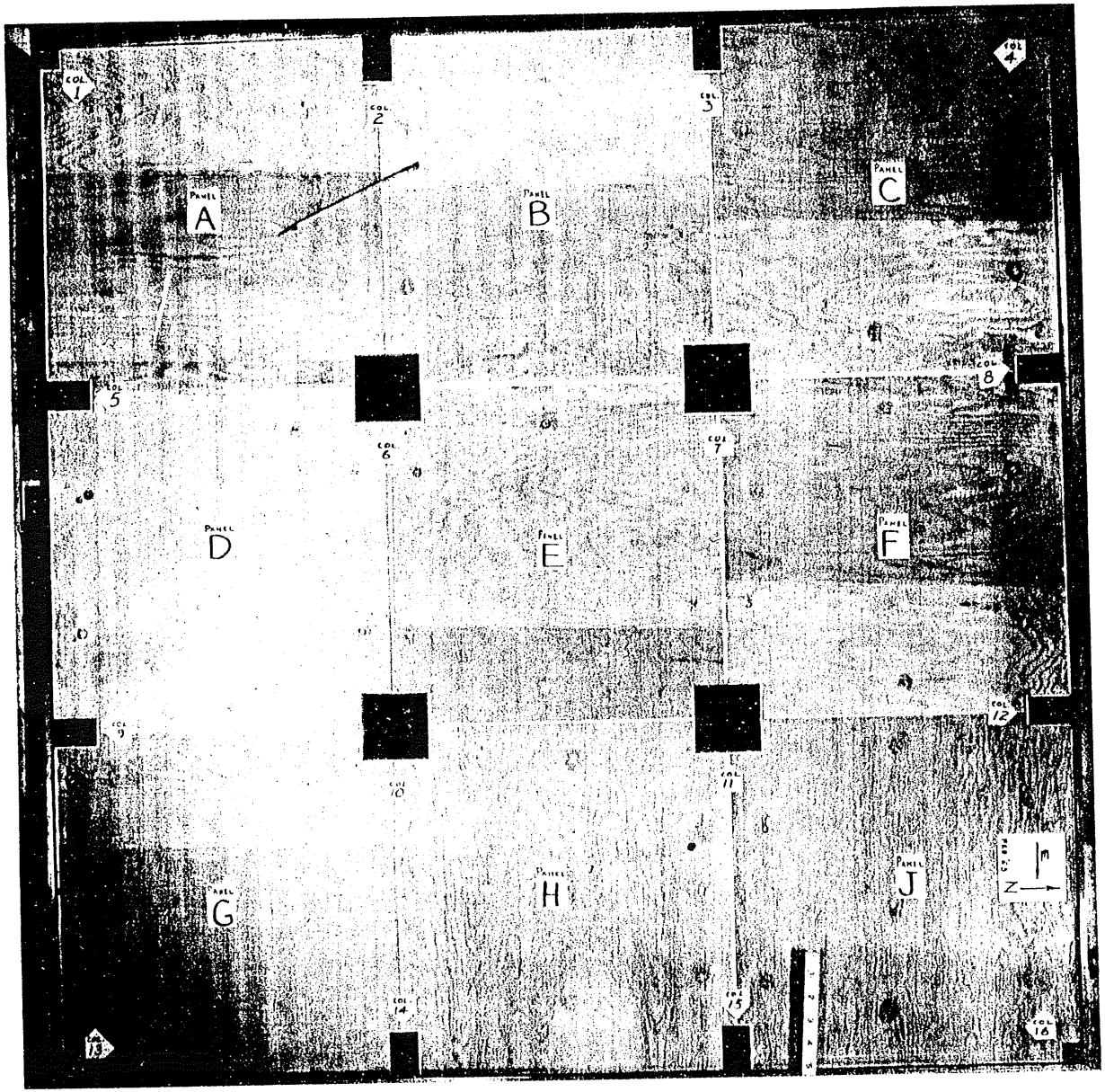

FIG. A.4 FORMWORK AFTER ITS COMPLETION

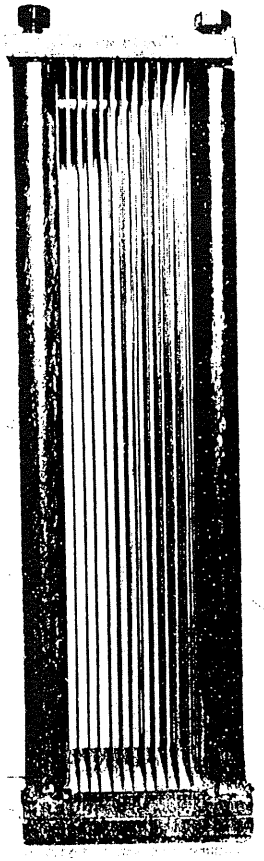

FIG. A.5 STRESSING AND ANNEALING RACK

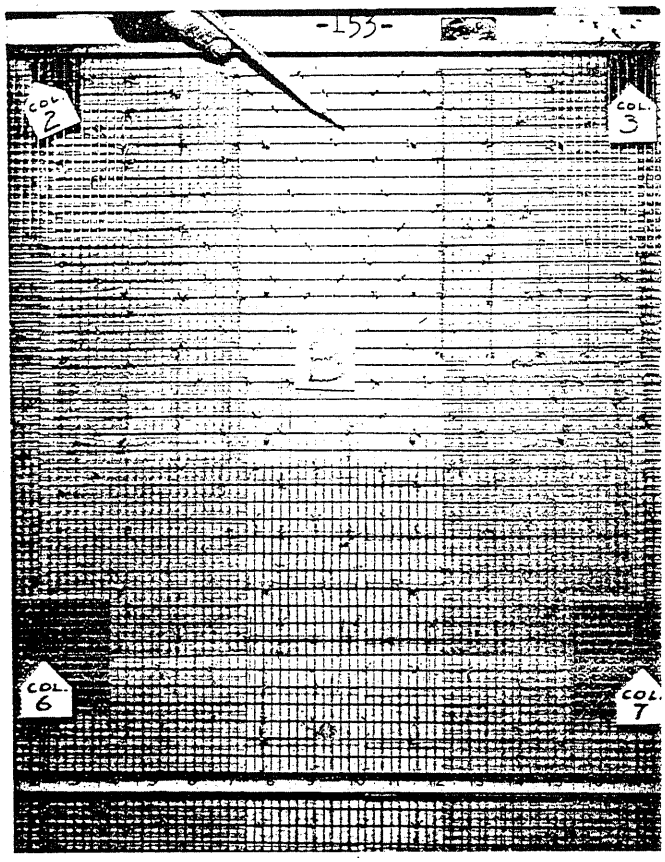

FIG. A.6 DETAIL OF REINFORCEMENT IN PLACE

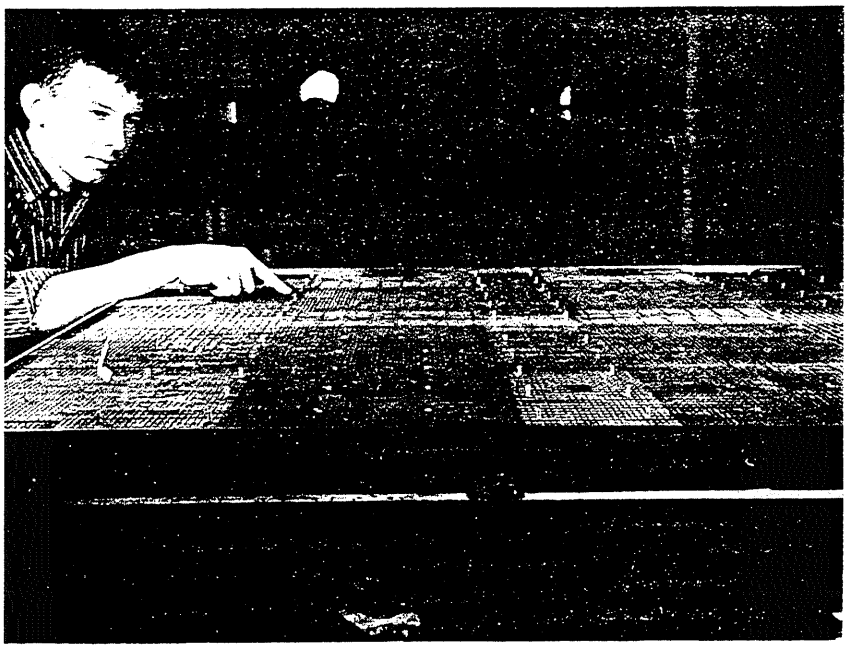

FIG. A.7 VIEW OF THE REINFORCEMENT IN PLACE

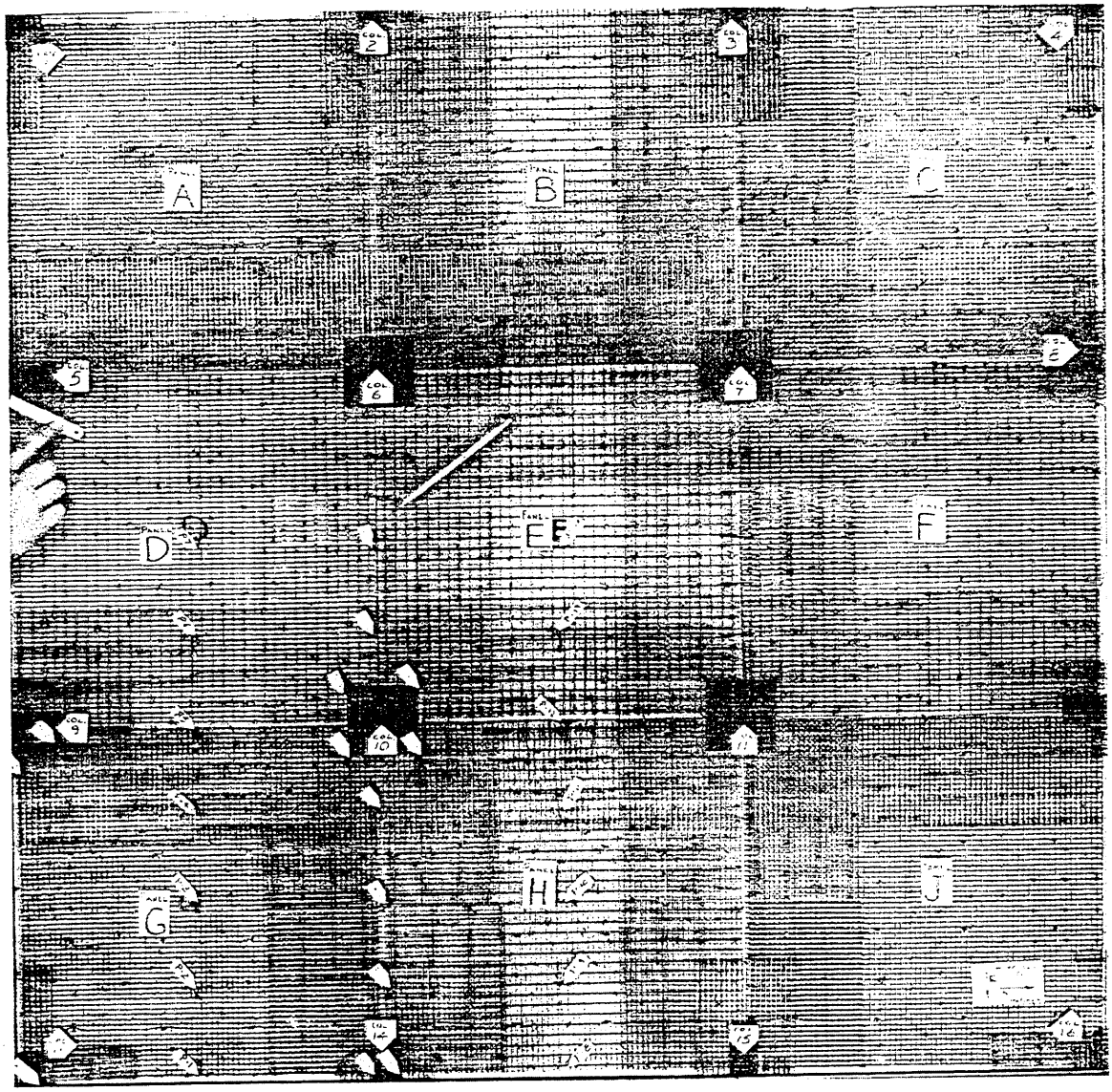

FIG. A.8 OVER-ALL VIEW OF REINFORCEMENT

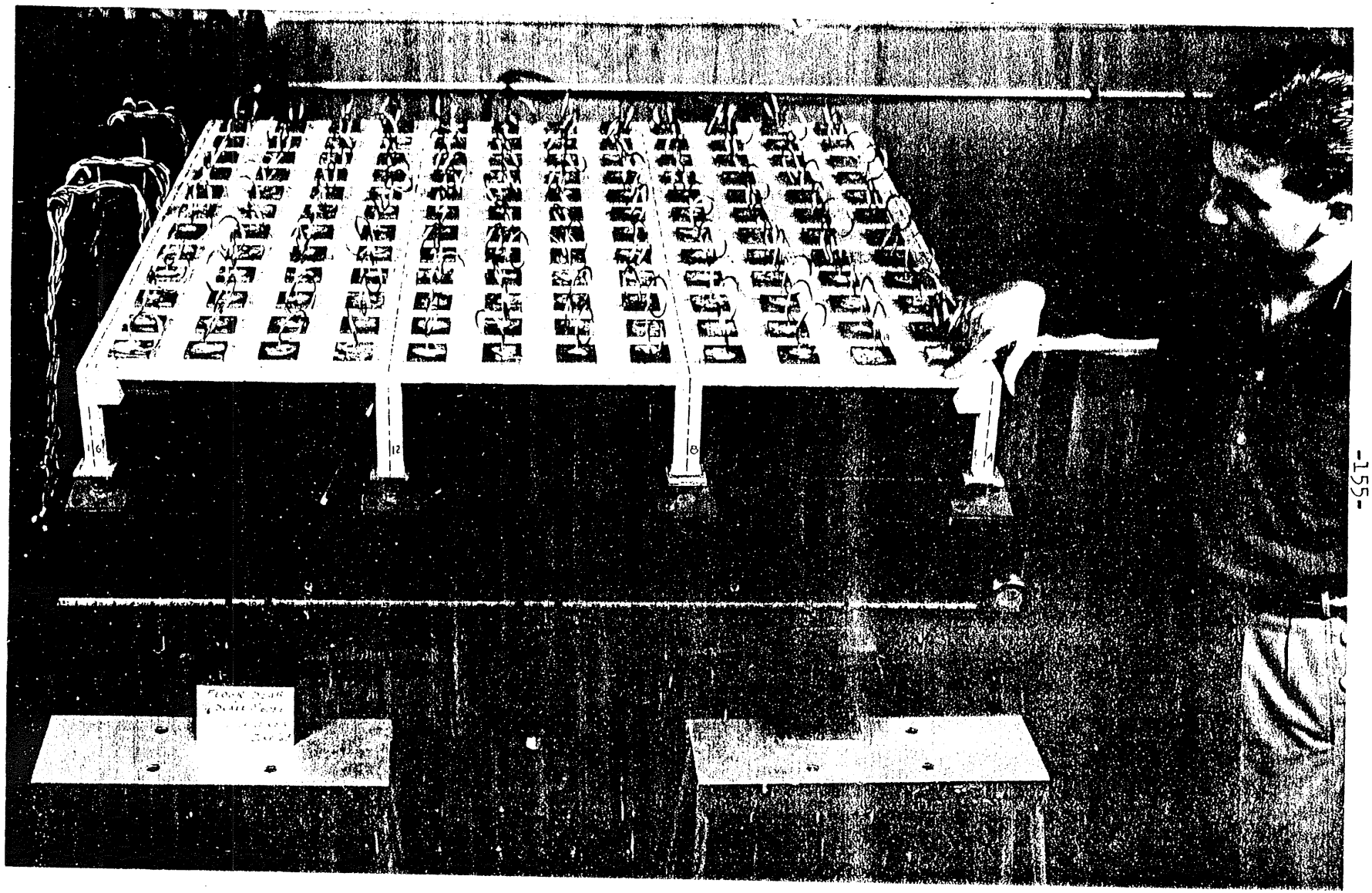

FIG. A.9 STRUCTURE AFTER CASTING (PRECAST CAPITALS AND PART OF THE LOADING EQUIPMENT IN PLACE)

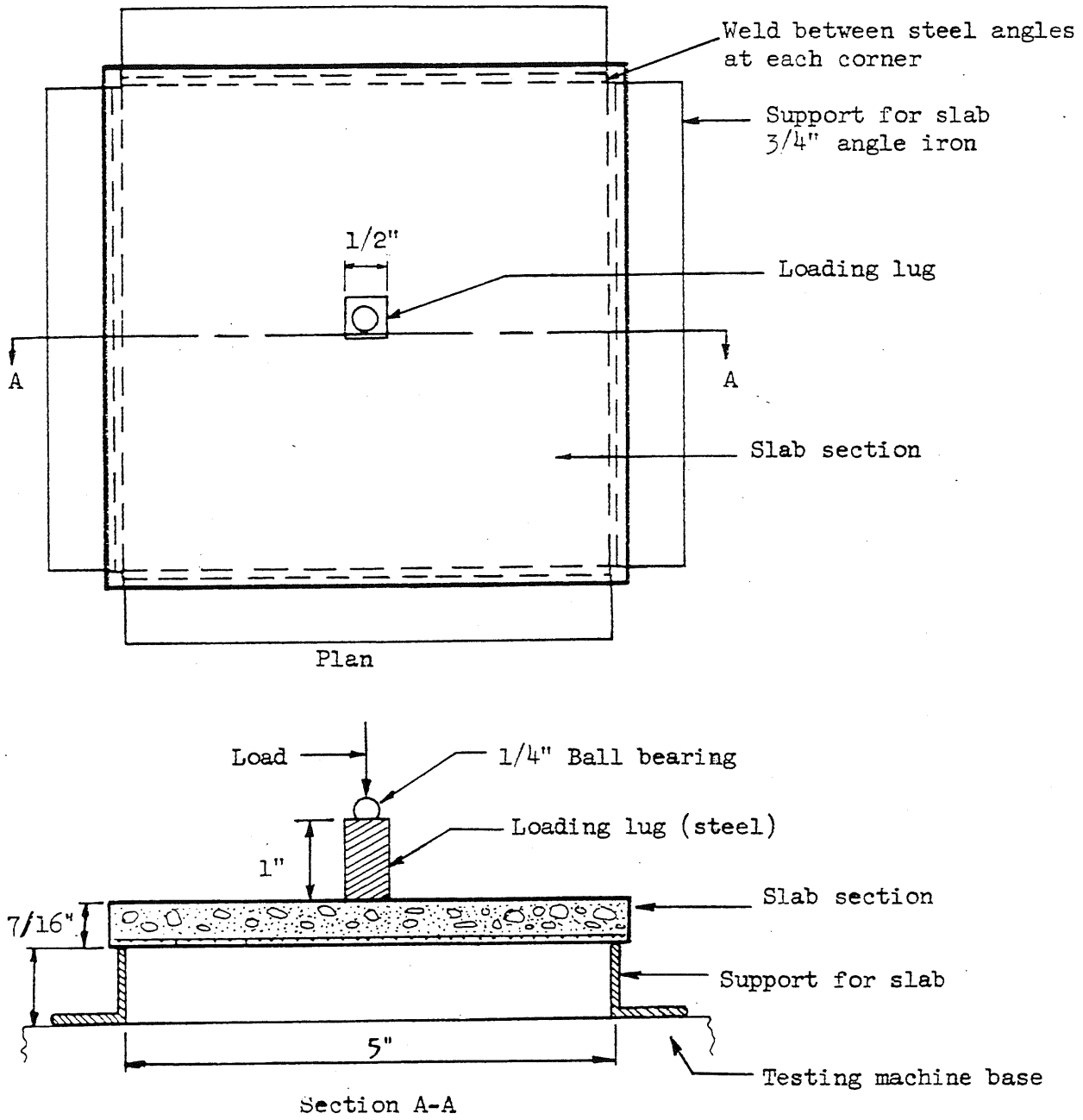

Note: All specimens reinforced with 0.0355 in. dia. bars, at 7/32 in. spacing in both directions.

No negative reinforcement provided since support could not exert a downward force at the corners.

FIG. B.1 PUNCHING SHEAR TEST SLABS

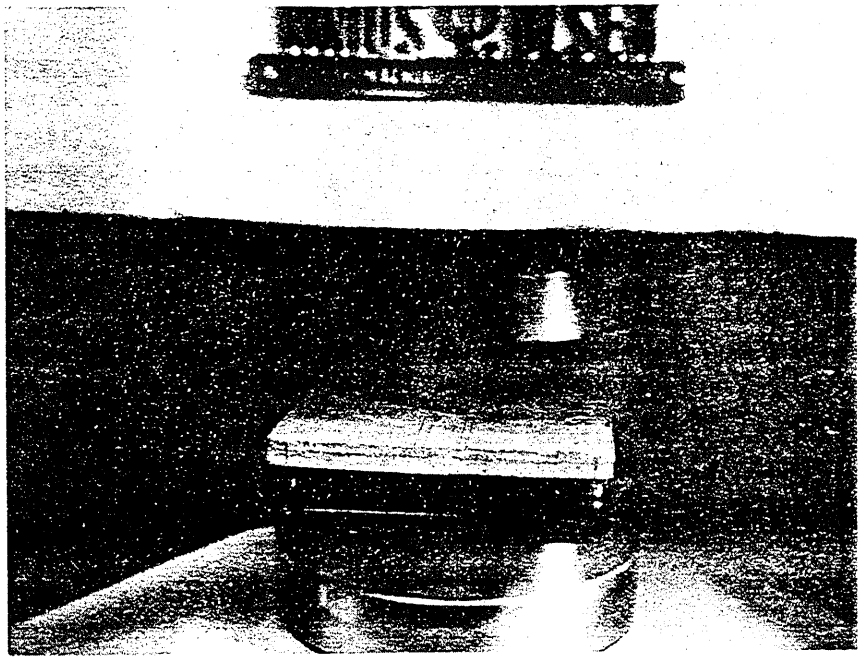

FIG. B.2 PUNCHING SHEAR TEST ON SLAB SPECIMEN

FIG. B.3 SLABS AFTER THE LOAD TO FAILURE

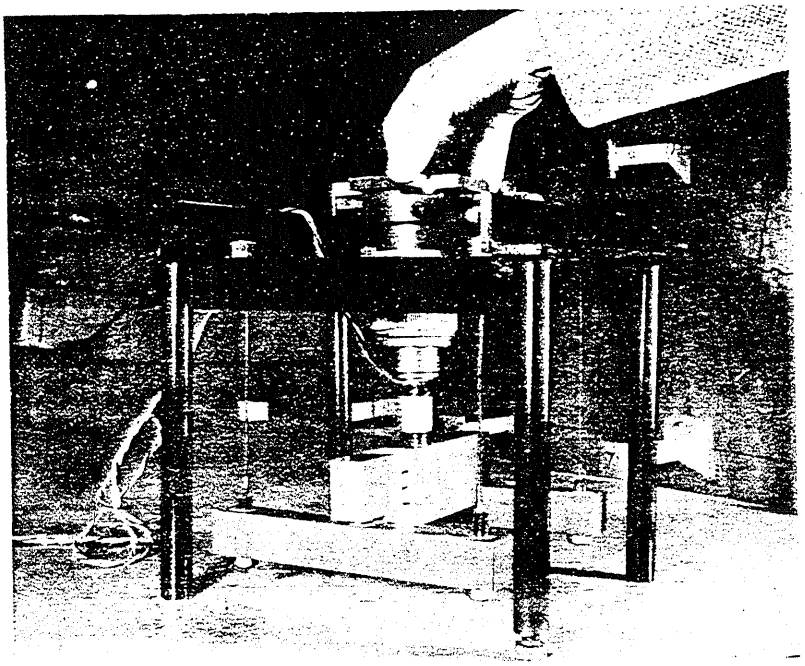

FIG. B.4 APPARATUS USED FOR DYNAMOMETER CALIBRATION

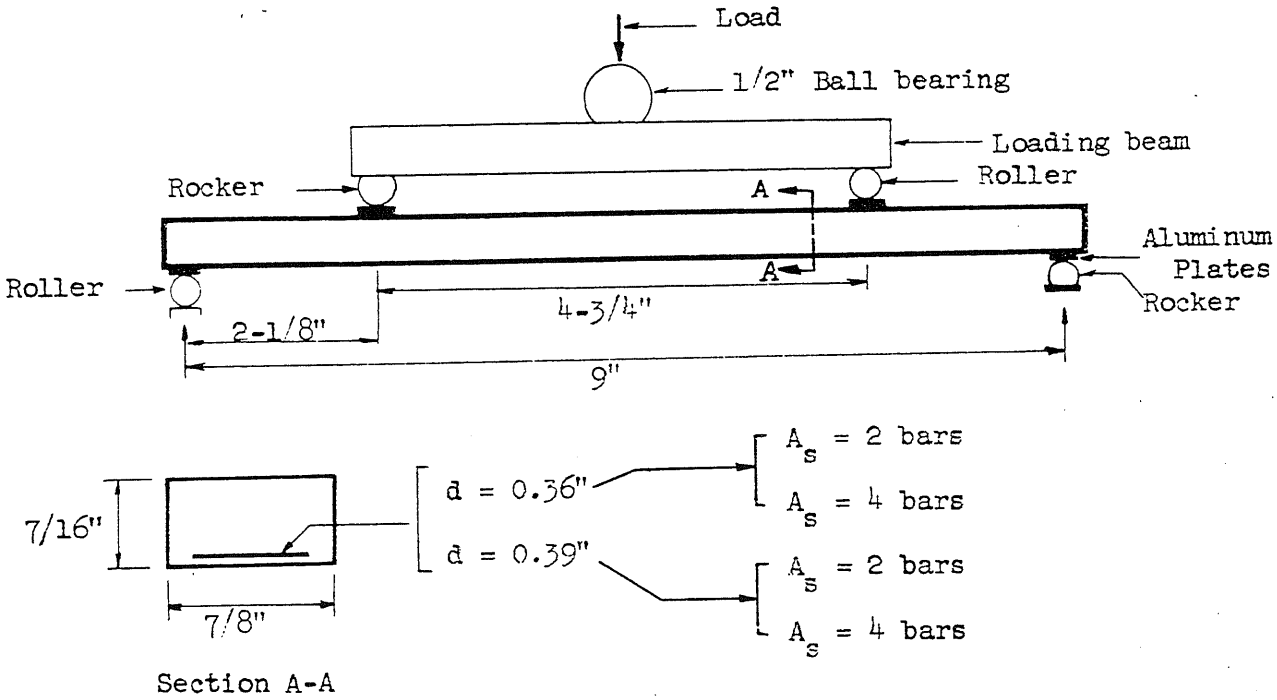

Section A-A

Note: All reinforceing bars: 0.0355 in. diameter

FIG. B.5 DIMENSIONS OF FLEXURAL SPECIMENS

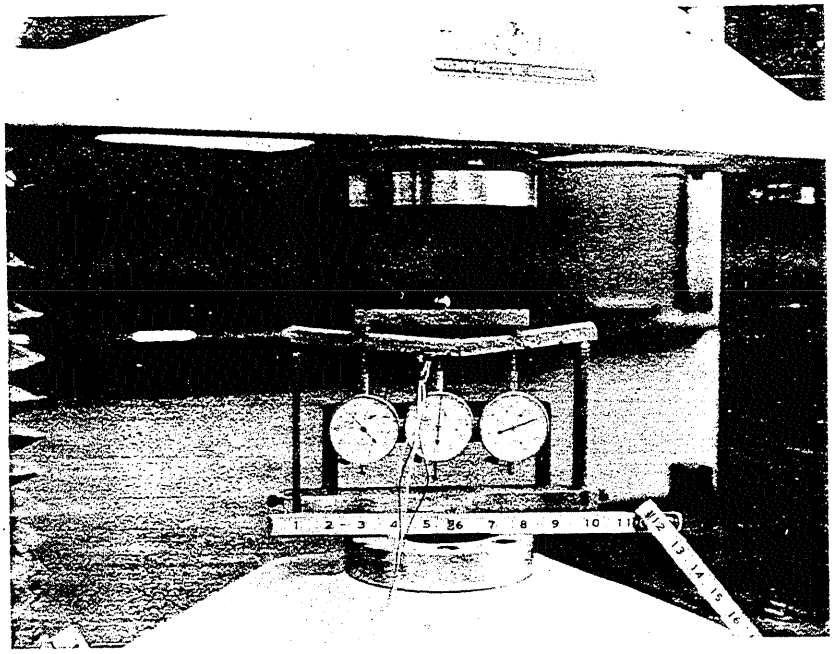

FIG. B.6 BEAM SPECIMEN AFTER TEST TO FAILURE